Role of Polarity on the Interfaces of Binary Combinations

by

Nusrat Ahmad

A thesis submitted in partial fulfillment of the requirements for the degree of

Master of Science

Department of Mechanical Engineering
University of Alberta

Abstract

Owing to a large number of applications, starting from pharmaceutical packaging to advancement in nanotechnology and microfluidic devices, wetting characteristics has always been regarded as an essential prerequisite for many phenomenal processes. In the present time, the term 'wetting' is not limited to spreading of a liquid on a solid but also portrays displacement ability of a gas over a liquid. To quantify wetting of a solid surface by a liquid, numerous established theories argue that interactions between polar–polar, polar–non-polar and non-polar–non-polar components of surface tension or equivalently, surface energy dictate the final equilibrium contact angle.

In this work, the extent to which individual phases of binary liquid−vapor and solid−liquid system interacts, and how such interactions are influenced by the polar and the dispersive components of the surface tension is examined. For liquid−fluid systems, the effect of the polarity of the surrounding (saturated) vapor medium on the equilibrium surface tension, γ_{eq} is critically investigated. Such measurements being prone to inaccuracy for highly volatile liquids, a standard protocol to obtain γ_{eq} with reasonable accuracy has been developed. A wide range of fluids covering polar−polar, polar−nonpolar and nonpolar−nonpolar liquid-vapor combinations, are studied and results confirm that the influence of molecular weight of both of the phases (drop and surrounding saturated vapor) must be accounted for in addition to the interactions (polar-polar, polar-nonpolar etc.) that occur therein. For the case of polar-polar and nonpolar-nonpolar combination, observations suggest that the liquid drop interface becomes active only if the molecular weight of vapor is lower than the liquid phase. Further, it is observed that γ^{p} of drop (for polar liquid) influences the interaction between γ_{eq} and Fowkes' dispersive interaction. Similar influence of the polar component of the surface tension has been observed for the solid–liquid systems where the percentage polarity of the (gold) substrates are varied by means of functionalization with mixed self assembled monolayer, SAM. Moreover, the surface characterization using X-ray photoelectron spectroscopy (XPS) proved that the mole fraction of the chemicals on the surface is different than that of the immersion solution.

Preface

This dissertation is an original work by Nusrat Ahmad. Here, all the summarized work are my own except the experiment involving X-ray Photoelctron Spectroscopy (XPS), which was conducted by Dr. Shihong Xu (application/research analyst, nanoFAB, University of Alberta). However, I am familiar with the experimental conditions and procedures that were followed for the measurement. It was my sole responsibility to conduct rest of the experiments, analyze all the results, develop theoretical frameworks and to write the manuscripts. Dr. Aleksey Baldygin and Dr. Raymond Sanedrin designed the experiments and reviewed the manuscripts. Dr. Raymond Sanedrin and Dr. Prashant R. Waghmare helped with conceptual formulation of the problems and by revising the manuscripts. Dr. Prashant R. Waghmare supervised the research.

A version of Chapter 2 of this thesis has been prepared for submission in Journal of Americal Chemical Society (JACS) as: Nusrat Ahmad, Aleksey Baldygin, Raymond Sanedrin and Prashant R. Waghmare, "Role of polarity on interface: Liquid−fluid binary combination".
Parts of this work has also been presented (virtually) in Droplets Conference 2021 (Droplets 2021), Darmstadt, Germany, August 16-18, 2021.

A version of Chapter 3 of this thesis has been prepared for submission in Langmuir as: Nusrat Ahmad, Aleksey Baldygin, Raymond Sanedrin and Prashant R. Waghmare, "Role of polarity on interface: Solid−liquid binary combination".

"A river cuts through rock not because of its power, but because of its persistence."

- Jim Watkins

To my family:

Nasir Ahmad and Abeda Nasir, my parents

Asif Ahmad, my younger brother

and Muhammad Rizwanur Rahman, my life partner

- their love and support inspires me to aim for the sky.

Acknowledgments

First of all, I want to thank the one and only Almighty for guiding me and providing me with the strength to pursue my chosen path. My sincere gratitude towards my supervisor, Dr. Prashant R. Waghmare, without whom this thesis would not have been possible. He envisioned the project and guided me with his insightful suggestions throughout the program. Most importantly, his continuous encouragement and cooperation provided me with all the things that I needed to finish my thesis successfully. I would like to extend my special thanks to Dr. Aleksey Baldygin for his contributions in designing the experiments and providing me with valuable suggestions throughout this program. I am very grateful to Dr. Raymond Sanedrin for his conceptual suggestions and his time for reviewing the manuscript. I sincerely thank my defence committee : Professor Dr. Xuehua Zhang, Professor Dr. Peichun Amy Tsai and Professor Dr. Sina Ghaemi for their invaluable time and effort in reviewing my thesis work.

I acknowledge technical support from Krüss GmbH, without which the experimental investigation would not have been possible. I would also like to acknowledge nanoFAB- Fabrication and Characterization Centre, for training me and providing me with facilities to prepare solid substrates and perform surface characterization process.

Last but not the least, I would like to thank all the members of interfacial Science and Surface Engineering Lab.

Table of Contents

List of Tables

List of Figures

List of Symbols

$\Delta\gamma$	Difference between initial surface tension of pure liquid and equilibrium surface tension of binary combination with saturated vapor
γ^+	Surface tension component for electron acceptor by Van Oss and Good
γ^-	Surface tension component for electron donor by Van Oss and Good
γ^d	Nonpolar component of surface tension
γ^{LW}	Lifshitz or dispersive component by Van Oss and Good
γ^p	Polar component of surface tension
γ^{SR}	Short range or polar component by Van Oss and Good
$\gamma_{\mathrm{L_dL_m}}$	Liquid drop-liquid medium interfacial tension for Schultz method
$\gamma_{\mathrm{L_dV}}$	Liquid drop-vapor surface tension for Schultz method
$\gamma_{\mathrm{L_mV}}$	Liquid medium-vapor surface tension for Schultz method
$\gamma_{\mathrm{SL_d}}$	Solid-liquid drop interfacial tension for Schultz method
$\gamma_{\mathrm{SL_m}}$	Solid-liquid medium interfacial tension for Schultz method
γ_{12}	Interfacial tension between phase 1 and 2
γ_{1v}	Surface tension of phase 1
γ_{2v}	Surface tension of phase 2
γ_d^d	Nonpolar component of surface tension of drop

γ_d^p	Polar component of surface tension of drop
γ_{eq}	Equilibrium surface tension
γ_{exp}	Experimental surface tension of pure phase
γ_{LV}	Surface tension of liquid phase
γ_{LV}^d	Nonpolar component of surface tension of liquid phase
γ_{LV}^p	Polar component of surface tension of liquid phase
γ_m^d	Nonpolar component of surface tension of medium
γ_m^p	Polar component of surface tension of medium
γ_o	Initial surface tension of pure phase
γ_{SL}	Interfacial tension between solid and liquid phase
γ_{SV}	Surface tension of solid phase
γ_{SV}^d	Nonpolar component of surface tension of solid phase
γ_{SV}^p	Polar component of surface tension of solid phase
ϕ	Girifalco and Good's constant
τ	Completion time of experiment
θ	Contact angle of a liquid on a solid surface
$M_{w,d}$	Molecular weight of drop
$M_{w,m}$	Molecular weight of medium
M_w	Molecular weight
V_o	Initial volume
$x_{solution}$	Mole fraction of 11AUT/11MUA/3MPA with PFDT in solution
$x_{surface}$	Mole fraction of 11AUT/11MUA/3MPA with PFDT on surface

Abbreviations

11AUT 11-Amino-1-Undecanethiol Hydrochloride.

11MUA 11-Mercaptoundecanoic Acid.

3MPA 3-Mercaptopropionic Acid.

AFM Atomic Force Microscopy.

CV Cyclic Voltammogram.

HDPE High-density polyethylene.

PFDT 1H, 1H, 2H, 2H-Perfluorodecane Thiol.

QCM Quartz Crystal Microbalance.

SAM Self Assembled Monolayer.

SIMS Secondary Ion Mass Spectrometry.

SPM Scanning Probe Microscopy.

SPR Surface Plasmon Resonance.

STM Scanning Tunneling Microscopy.

TCP 1,2,3-Trichloropropane.

XPS X-ray Photoelectron Spectroscopy.

Chapter 1

Introduction

The dynamics of the bulk much depends on the very thin layer at the surface of the liquid, that we call interface. Understanding the interface requires realization of the intricate physics at the molecular scale. The interaction that occurs at such scale is very well described by the celebrated Van der Waals theory [1]. In light of this theory, Fowkes [2] introduced the idea of decomposing the surface tension or, equivalently, the surface energy, into two components, namely, the polar and the dispersive/nonpolar component. This promising theory initiated a string of investigations to quantify the interaction between two phases [3–6]. However, it was de Gennes's theory which introduced a more qualitative approach that re-defined the solid−liquid interaction. In his pioneering works, de Gennes [7] demonstrated that a liquid forms zero contact angle solid surface if the former has lower polarizability. Owing to all the aforementioned theories and others, several investigations have been pursued that shows effect of polar−polar and nonpolar−nonpolar interaction on solid−liquid combinations [8–11]. Additionally, this concept has been successfully extended for liquid−liquid combinations [12, 13].

Despite the extensive investigations, literature lacks any generalization either for liquid−vapor or for solid−liquid combinations. This thesis attempts to fill this void in understanding how the equilibrium surface tension of a binary liquid-vapor interface (where the liquid phase is of different substance than the vapor phase) or a solid-liquid interface is effected or modified by the individual polar and dispersive components of surface tension of the constituent phases. Henceforth, any reference to a liquid-vapor system shall refer to a binary system unless mentioned otherwise.

With the aim of maintaining individual chapters as stand alone documents, the liquid−vapor and solid−liquid cases are discussed in Chapter 2 and 3 each having their own elaborate introductions and conclusions. Parts of these chapters are adopted for preparing scientific papers that will shortly be submitted for journal publications. Despite Chapter 2 and 3 having sufficient elaboration on the relevant literature, this Introduction does touch upon the key ideas that the remaining of this thesis develops upon. A brief discussion of the forces that influence polar and dispersive components is presented in section 1.1, along with the relevant background and applications in sections 1.2.1 and 1.2.2, respectively, for the liquid-vapor combinations. Later in sections 1.3.1 and 1.3.2 the background and applications for solid-vapor interfaces have been discussed. Further, the self assembled monolayer (SAM) and x-ray photoelectron spectroscopy (XPS) are briefly discussed in sections 1.3.3 and 1.3.5 to highlight their essence in our study. Finally, this chapter is concluded with a concise overview of each of the chapters in section 1.4.

1.1 Polar-Polar and Nonpolar-Nonpolar Interaction

In pursuit of this investigation, an understanding of polar and nonpolar components of the surface tension or surface energy is essential. For this investigation, the description of the polar and dispersive components is more aligned with Fowkes model rather than that of Van Oss-Good model. This is because, the former is well suited for moderately polar phases whereas the latter for highly polar phases [14]. As most of the substances are organic with moderate polarity (even solid substrates are thiol functionalized surfaces), Fowkes decomposition of surface tension is more accurate.

Molecular origin of dispersive component:

Nonpolar component is linked to the dispersive forces which is dependent on the size of electron cloud of a molecule [15]. The electron cloud of molecules randomly fluctuates and temporarily concentrates the negative charge on one side or another, creating induced dipoles. This temporary distribution of charge increases with increasing number of electrons. The interactions between induced dipole-induced dipole results into Van der Waals' dispersive force, more famously know as London force [16]. And this force is responsible for the dispersive component of surface tension. As the dispersive component arises from the very existence of the electron cloud, it always assumes a finite value.

Molecular origin of polar component:

Although nonpolar forces are available between molecules as described above, polar force is not so common. They originate from the difference in eletronegativity between the bonded atoms of a molecules [1]. Consequently, polar components in polar molecules are a result of polar interactions that occur in molecules with a dipole moment [15]. Thus, polar components constitute of Van der Waal's dipole forces that are result of permanent dipole-dipole interactions (Keesom force) and permanent dipole - induced dipole interactions (Debye force) [16–19].

As narrated by Owens and Wendt [20], Rabel [21], Kaelble [22] and Wu [4] the surface tension of a substance arises due to imbalance of cohesive interactions between like molecules at the surface, which can be divided into polar forces and nonpolar forces. Thus, surface tension can be decomposed to polar and dispersive components. On the other hand, for interaction between two phases, cohesive forces between similar molecules along with adhesive forces between dissimilar molecules affects the surface tension. Since the Van der Waals forces contribute to the adhesive forces as well [15], the interfacial tension or the contact angle between two phases can be accounted by the polar–polar ($\gamma^{\mathrm{p}}_{1\mathrm{v}} - \gamma^{\mathrm{p}}_{2\mathrm{v}}$) and nonpolar–nonpolar ($\gamma^{\mathrm{d}}_{1\mathrm{v}} - \gamma^{\mathrm{d}}_{2\mathrm{v}}$) interaction.

Effect of dispersive component on contact angle

The Van der Waal's force of attraction between molecules are very weak. Hence, increasing dispersive component of a solid in contact with a completely nonpolar liquid will result into small decrease in contact angle. However, it may or may not show any substantial change in wettability when in contact with a polar liquid due to its weaker interaction [23].

Effect of polar component on contact angle

The effect of polar component on the contact angle can be described based on experimental data and results from literature. By varying the polar component of the solid, negligible change in interaction is observed with a completely nonpolar liquid. This is because polar component of solid interacts only with polar component of liquid [6, 8–11, 20–22]. However, if a polar liquid. i.e., water is considered then the contact angle will decrease with the increase of polar component of the solid. Essentially, increasing polar component increases the permanent dipole-permanent dipole interaction between the solid and liquid molecules, resulting into an increase in adhesion force at the solid interface [23]. Thus, wettability of the pair increases and contact angle decreases.

1.2 Liquid-Fluid Interface

1.2.1 Literature Review

Surface characterization using surface tension and interfacial tension has been studied extensively over the past few decades [24–28]. These earlier studies are briefly reviewed in Chapter 2. It has been suggested that this property is one of the key features to explain the molecular interaction that influences mass and energy transfer at surface or interface [29]. Necessarily, several investigations are performed, both experimental and molecular dynamics simulations, to measure surface tension of mixture of miscible fluids [30–32] and interfacial tension of immiscible fluids [27, 33–36]. In addition, polar and dispersive components of surface tension of one liquid are used to identify surface tensions of another liquid by considering the interfacial tension of the binary system [8, 37, 38]. Though these results provide sufficient evidence for surface characteristics of binary liquid systems, it fails to explain interaction happening on a liquid surface in the presence of saturated vapor medium. Thus, to expand the horizon of scientific field, experiments have been performed in miscible vapor medium of different concentrations and saturated medium of immiscible fluids or air saturated medium to characterize liquid−vapor system [39–42]. However, no such study is available, to the knowledge of the author, for saturated medium of miscible or partially miscible volatile liquids- a binary system which is susceptible to high mass transfer rate across surface. Hence, an investigation is conducted for miscible, immiscible and partially miscible liquid−vapor system to observe the interaction between them. Furthermore, the results are utilized to develop a generalized characterization of their interface by considering polar−polar and dispersive−dispersive interaction of the combination. To pursue this, a total of forty cases (ten polar−polar, eleven polar−non-polar, and nineteen non-polar − non-polar combinations - please refer to Table A.6 of Appendix for the details) are studied which further hypothesized the relation between all the liquid−vapor interface.

Now, surface characterization involving volatile liquids is very difficult due to high mass transfer rate at the surface (liquid in vapor medium) or interface (liquid in liquid medium) [43–45]. As measurement of surface tension is considered one of the most prevalent quantification to characterize a surface, several methods have been utilized to determine the surface tension of volatile liquids, such as maximum bubble pressure method, acoustic levitation method and fibre drop analysis method [43, 44, 46]. However, it is desired to measure surface tension using pendant drop method because of its precision and high degree of flexibility [47]. Essentially, this provides better accuracy than many other techniques [48–51], utilizing only small amount of liquid and measuring surface or interfacial tension even at high pressure [52–54]. Therefore, a method has been developed to measure the surface tension of a liquid in its own saturated medium to obtain an authenticate surface tension value. Consequently, the accuracy of the quantification is not compromised because the surface tension of a liquid in its own saturated medium differs by only 0.1mN/m compared to that in air medium [55]. This method is then modified further to investigate the liquid−fluid interface, i.e, a binary system (discussed in Chapter 2).

1.2.2 Applications

Liquid−vapor interfacial tension has wide range of applications starting from dictating heat and mass transfer between two phases across an interface [56]. It is important in several engineering, industrial and biological processes like modelling of distillation and adsorption, checking generation and stability of foams on addition of surfactants in foaming industries or effects of pulmonary surfactants on oxygenation process [47, 57, 58]. Moreover, Krishnan et. al utilized study of interfacial tension between water of blood plasma and air medium to compare plasma of four species, including human [59]. Besides that interfacial tension is considered to be the dominant parameter that controls the capillary trapping force that is utilized to trap fluids in the pore structures of reservoirs [60]. Additionally, this property dictates the flow process as well as controls the efficiency of capillary sealing for storage of carbon dioxide [61]. It has been also suggested that the knowledge of interfacial behavior is also necessary for recovery operation of enhanced carbon dioxide based oil [62]. Therefore, having an approximate idea of the interfacial tension using the presented generalization in this study, could save a huge portion of time that can be utilized in other areas of development.

1.3 Solid-Liquid Interface

1.3.1 Literature Review

Study of contact angle has been in practice for over couple of centuries [63, 64], which have been briefly discussed in Chapter 3. The importance of spreading phenomenon has influenced extensive research to understand the factors which dictates the equilibrium contact angle of a liquid on a solid surface [65–69] as this assists in determining the wetting characteristics of a liquid on a solid. However, this wetting characteristics, along with theoretical formulation, changes with characteristics of solid, liquid and condition of the surrounding medium [37, 63, 70, 71]. Considering only the solid characteristics, Wenzel [72] suggested that Young's [73] equation, which is further discussed in Chapter 3, cannot account for contact angle on rough surfaces. Moreover, Cassie and Baxter [74–76] suggested a similar theory for heterogeneous and porous substrates. According to them, Young's equation being only applicable for smooth, chemically homogeneous, inert, rigid, insoluble and non-reactive surfaces [73] cannot account for the change in surface characteristics of the non-ideal surface. It has also been suggested that the reason of this discrimination for rough and heterogeneous surfaces is the difficulty in assessment of the molecular interaction at the three-phase contact line [77]. In addition, liquid properties, such as viscosity, also has an effect on the equilibrium contact angle [78, 79]. Moreover, new parameters like surface temperature of liquids has an altering effect on equilibrium contact angle [80]. Even surrounding conditions like temperature and pressure also effects equilibrium contact angle [70, 81]. In the presence of all these influential parameters, de Gennes's hypothesis provided a constant parameter for most of the cases. He suggested that a liquid spreads completely on a solid if its polarizability is lower [7]. This theory curved the path to several investigations that confirmed that equilibrium contact angle has a dependency on polar−polar and dispersive−dispersive interaction between solid and liquid [9–11]. However, a generalization has not yet been reported which considers all possible solid and liquids (excluding specially fabricated species).

The investigation outlined in Chapter 3 provides a graphical relation, which can lay out a quick approximate idea about the contact angle of a solid liquid combination if polar and dispersive components are known or vice versa. For this investigation, substrates with a range of polarity was a necessity. Accordingly, SAM functionalized substrates are utilized and the fundamentals of the process is discussed in the following sections. Moreover, surface characterization using xps (discussed in upcoming section) was also performed to validate the contact angle measurements for solution concentration.

1.3.2 Applications

Wettability is an important parameter in many manufacturing processes where adherence as well as repulsion is desirable. The spreading of a drop on a smooth dry surface is important for processes like fuel injection, surface cooling, spray painting, as well as on aircraft wings [67, 82–84]. Spray painting or coating is an example where maximum adhesion is required, i.e low contact angle combination [85]. Another example like this is spraying pesticides on crop fields for better yield [86]. In comparison, there are processes where repulsion, i.e high contact angle is beneficial. For instance, while designing impermeable clothing the main focus is to design a material that has high contact angle with water [87]. Same characteristics is prudent for developing materials with anti-icing properties [88]. Therefore, as mentioned above, in development of materials contact angle usually has an influence, if not often. Therefore, having an approximate idea of the surface energy (summation of polar and dispersive components) from the generalization could prove to be beneficial.

1.3.3 Self Assembled Monolayer (SAM)

Self assembled monolayer (SAM) is an ultra-thin film that forms on a surface due to strong chemisorption from a solution on immersed solid substrates [89–91]. These are stable, closely packed, well-organized monolayers of chemicals, such as, thiols and disulfides [92–96]. Essentially, this particular solutions are chosen based on some important characteristic for functionalization purpose: 1) they must have functional group which interacts with the metal surface and 2) they should be able to be adsorbed and arranged on the surface without any external influence to form high density, unidirectional monolayers [97]. In combination with these solution, metal surfaces like gold, silver, copper or platinum could be utilized [98–105]. However, thiols are preferred over disulfides (unless thiols are reactive to the terminal group of a target liquid) [106] and gold is preferred over other metals because it is comparatively inert and does not have a stable oxide surface, resulting into negligible atmospheric contamination [89, 107]. Considering thiol SAM and gold substrate, combination used in this investigation, the supposedly two-dimensional monolayers are formed by covalent bond between sulphur (S) of thiol and gold molecule (Au), i.e. Au–S bond. After the thiol molecules are adsorbed on gold surface, they reorient themselves depending on the Van der Waals forces between themselves [89, 108–110]. Moreover, procedure for SAM preparation is quite simple compared to other surface treatment procedures as shown in Fig. 1.1. Further discussion on the SAM preparation is found in Chapter 3.

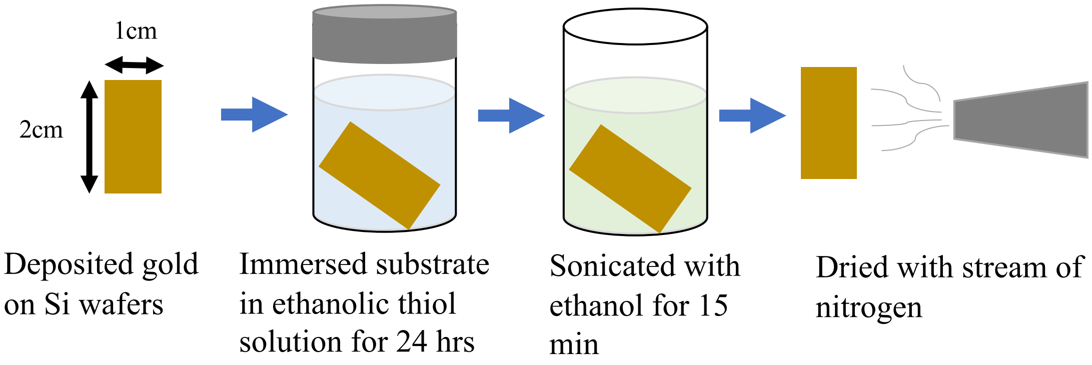

Figure 1.1: Schematic of the preparation method of SAM.

Apart from concentration of the thiol solution, the formation of SAM is dependent on type of solvent and temperature and time of immersion [89, 111–113]. Nevertheless, the scope of this investigation is not dependent on this factors as the conditions are constant for all the substrates. The functionalization procedure has become immensely popular due to its wide range of practical applications such as controlling surface properties, corrosion inhibition, patterning, fabrication of semiconductor devices, chemical sensor, biosensor etc [114–119]. In addition, it can be used to study the elemental phenomenon like single electron transfer mechanism or electron transfer that is dependent on distance [120, 121]. .

1.3.4 Mixed Self Assembled Monolayer (Mixed SAM)

There are three ways to prepare Mixed SAM [100, 108, 110, 122, 123]. They are:

- Mixing two different solution of thiols

- Backfilling method
- Using asymmetric disulfide derivatives

In this study, we have utilized the process of mixing two thiol solution to obtain mixed SAM. All these processes are dependent on favoured deposition of the most stable SAM. Furthermore, as suggested by Bain et. al [124], Laibinis et. al [100], Stranick et. al [122], and Lokanathan et. al [123], the surface composition is not same as the immersion solution mole fraction. As a result, it is important to characterize the surface using methods like Scanning Probe Microscopy (SPM) [125], which is a group of methods like Scanning Tunneling Microscopy (STM) [126] and Atomic Force Microscopy (AFM) [110]; Surface plasmon resonance (SPR) [127]; Quartz Crystal Microbalance (QCM) [128]; Cyclic Voltammogram (CV) [129], Secondary Ion Mass Spectrometry (SIMS) [130] and X-ray photoelectron spectroscopy (XPS) [124]. For this investigation XPS is used for surface characterization and its method of operation is described in next section.

1.3.5 X-ray photoelectron spectroscopy (XPS)

XPS is a type of spectroscopic technique that facilitates the quantification of surface composition, as well as the chemical and electronic state of the molecules on a surface. It was mainly developed by Siegbahn in 1960s [131, 132]. This method utilizes detection and measurement of the kinetic energy of electrons that are emitted from sample molecules within 5nm depth when bombarded with X-ray photon from a source [133, 134]. Conveniently, this kinetic energy of electron is equivalent to the binding energy of the electron to the atom, which are distinctive for individual elements but lacks molecular specification [135, 136]. However, its tendency to provide highly surface specific reading because the ejected electrons can move only a short range [135, 137] makes it a popular choice. Moreover, XPS technique is considered to be a chemical analysis technique that is very straight forward, can be used for all three phases and is

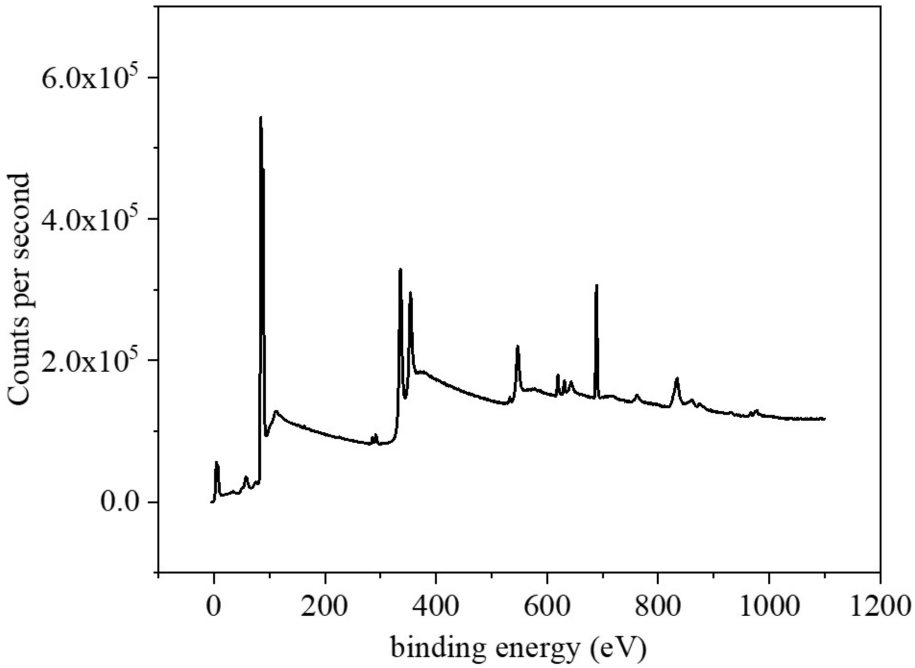

Figure 1.2: Sample of a survey scan from XPS measurement for 1H,1H,2H,2H-Perfluorodecanethiol (PFDT).

basically non-destructive [136]. A survey scan of 1H,1H,2H,2H-Perfluorodecanethiol (PFDT) which is obtained from XPS measurement is shown in Fig. 1.2.

1.4 Thesis Outline

The key question that we sought answer to in this thesis is how the polar and the dispersive components of the surface tension of two contacting phases influence the interfacial activity between liquid – solid or liquid – vapor. Essentially, it involves the study of saturation of medium, development of a protocol for measurement of interfacial tension, functionalization, surface characterization, and spreading. This extensive study has been categorically described in Chapter 2 and 3.

In Chapter 2, a relation is obtained to represent the interaction at the droplet interface of miscible, immiscible, and partially miscible liquid–fluid combination. To pursue this, experiments are conducted for a total of forty liquid and saturated vapor medium combinations to assess the polar–polar, polar–nonpolar and nonpolar–nonpolar interactions. In the process, a protocol has been developed to obtain accurate equilibrium surface tension, γ_{eq} for binary combinations, where mass transfer rate across interface is considerably high.

Chapter 3 constitutes an elaborate discussion for solid–liquid interaction quantified by the contact angle, and their dependence on the individual polar and dispersive components of the surface tension. Experiments are conducted on SAM functionalized substrates to conduct experiements on surface of various polarity. The process of functionaliztion and surface characterization is also described elaborately in this chapter. The findings from the proposed methodology are then applied to existing literature to confirm its accuracy.

Finally in Chapter 4, a summary of the key findings as well as the future scope of this study is discussed.

Chapter 2

Role of Polarity on Liquid-Fluid Interface

This chapter focuses on the dependency of equilibrium surface tension of a liquid in a saturated vapor medium of a different fluid on the polar and dispersive components of individual surface tension. In pursuit of this, the chapter starts with a small introduction, followed by the experimental section, and results and discussion. Finally, a conclusion is provided for the role of polarity on liquid−fluid interface.

2.1 Introduction

"A liquid spread completely if it is less polarizable than solid [7]." Polar-dispersive components of surface tension/surface energy, as well as the polarizability of the molecules is primarily governed by the inter-molecular interactions [16–19]. In accordance with this theory, for equilibrium configuration of drop on a solid surface, it is argued that the extend of interactions between polar−nonpolar, components of interfacial energies of solid and liquids dictate the final equilibrium contact angle [9–11]. Since 16th century, the theoretical concept of surface tension or energy is in practice, and J. A. von Segner [138] gets the credit to coin the term surface tension.

Seminal theories and attempts have been to made predict and comment on the interfacial tension. Benjamin Franklin [139], Ms. Pockles [140] and Lord Rayliegh's [141] experiments are a few noteworthy pioneering attempts to demonstrate the measurements of surface tension. But in our opinion, Berthelot's geometric mean rule of mixing [142], based on London theory of dispersion forces – the attractive forces between like and that between unlike molecules – is a basis of modern theories on predictions of interfacial tension. Based on Dupre's [143] work of adhesion, Berthelot's theory results into the relationship of surface or interfacial tension between two phases [142, 144, 145]:

$$\gamma_{12} = \gamma_{1\mathrm{v}} + \gamma_{2\mathrm{v}} - 2\sqrt{\gamma_{1\mathrm{v}}\gamma_{2\mathrm{v}}} \tag{2.1}$$

In the later years [1, 146], it was proven that this combining rule is unable to accurately quantify the strength of interaction between unlike molecules if the intermolecular potential difference between two phases is considerable.

In 1907, Antonow proposed Eq. 2.2, the simplest empirical relation for immiscible or partially miscible liquids suggesting their interfacial tension is equal to the individual surface tension of the liquid (in air or vapor medium), which has failed for a number of liquid-liquid cases but proved to be marginally accurate for solid-liquid combinations [75, 147, 148].

$$\gamma_{12} = |\gamma_{1\mathrm{v}} - \gamma_{2\mathrm{v}}| \tag{2.2}$$

Girifalco and Good [3] utilized Berthelot's theory and extended similar concept as Berthlot with an addition of constant ϕ. As depicted in Eq. 2.3, this theory suggests that, for two dispersed phases, geometric mean of free energy of cohesion between molecules of same component and the free energy of adhesion between molecules of different components must be considered for the quantification of interfacial tension

[3, 149].

$$\gamma_{12} = \gamma_{1\mathrm{v}} + \gamma_{2\mathrm{v}} - 2\phi\sqrt{\gamma_{1\mathrm{v}}\gamma_{2\mathrm{v}}} \tag{2.3}$$

Later Fowkes [2], for the first time, pinpointed the role of polar and dispersive components of two involved phases while quantifying the equivalent surface tension. The resultant equation was presenetd as:

$$\gamma_{12} = \gamma_{1\mathrm{v}} + \gamma_{2\mathrm{v}} - 2\sqrt{\gamma_{1\mathrm{v}}^{d}\gamma_{2\mathrm{v}}^{d}} \tag{2.4}$$

Here, γ^{d} and γ^{p} are dispersive and polar components of surface tensions. It is assumed that the polar and dispersive components are only two major contributors for total surface tension magnitude of $\gamma_{1\mathrm{v}}$ or $\gamma_{2\mathrm{v}}$. Though this expression is applicable for both similar and dissimilar phases, its validity is restricted to insoluble cases where at least one phase is completely nonpolar.

In 1971, Wu proved that though dispersive interaction can be represented by geometric mean relation, it is invalid for polar interactions. To accurately represent the dependency on polar and dispersive components, harmonic mean was proposed [4]:

$$\gamma_{12} = \gamma_{1\mathrm{v}} + \gamma_{2\mathrm{v}} - \frac{4\gamma_{1\mathrm{v}}^{d}\gamma_{2\mathrm{v}}^{d}}{\gamma_{1\mathrm{v}}^{d} + \gamma_{2\mathrm{v}}^{d}} - \frac{4\gamma_{1\mathrm{v}}^{p}\gamma_{2\mathrm{v}}^{p}}{\gamma_{1\mathrm{v}}^{p} + \gamma_{2\mathrm{v}}^{p}} \tag{2.5}$$

This expression has been validated for insoluble and partially soluble cases but it fails to account the large difference in polarizability as well as polar and dispersive components of the phases. These investigations works for solid-liquid or insoluble combinations. Similar conclusion cannot be portrayed for the miscible or immiscible liquid-fluid interface. Such interpretation can be be utilized to characterize the impact of the polarity of both the phases, drop and surrounding, on the equilibrium interfacial or surface tension γ_{eq}.

In around 1986, Van Oss, Good, and Chaudhury proposed that surface tension is indeed the summation of two components but not in terms of polar and dispersive components of surface tensions. Considering Lifshtiz van der Waals component (consisting of London, Keesom and Debye forces) and short range or Lewis acid-base component (consisting forces that only work within short range like hydrogen bond) [150] the following equation was proposed.

$$\gamma = \gamma^{LW} + \gamma^{SR} \tag{2.6}$$

where γ= surface tension of a phase, γ^{LW} is Lifshtiz or dispersive component and γ^{SR} is short range or polar component which is represented by product of electron donor (γ^-) and electron acceptor (γ^+) parameters: $\gamma^{SR} = 2\sqrt{\gamma^+\gamma^-}$. Based on this theory, the interfacial tension between two phases can be provided by:

$$\gamma_{12} = \gamma_{1\text{v}} + \gamma_{2\text{v}} - 2[(\sqrt{\gamma_{1\text{v}}^{LW}\gamma_{2\text{v}}^{LW}}) + (\sqrt{\gamma_{1\text{v}}^{+}\gamma_{2\text{v}}^{-}}) + (\sqrt{\gamma_{1\text{v}}^{-}\gamma_{2\text{v}}^{+}})] \tag{2.7}$$

This method is not limited to finding components of the dispersive phases only, provided at least three liquids with known components are used. Though these methods are extensively used for solid-liquid and liquid-liquid cases, but. cannot comment on the role of polar-dispersive components of the each involved phases on the interfacial tension.

Table 2.1: Established dependency of interfacial tension with advantages and disadvantages

Method	Equation	Advantage	Disadvantage
Berthelot's theory	Eq. 2.1	Basis of modern theories to investigate interfacial tension	Overestimates strength of interaction between unlike molecules
Antonow's theory	Eq. 2.2	Marginally accurate for solid-liquid combination	Failed for a number of liquid cases where either initial spreading is negative or highly positive
Girifalco and Good's theory	Eq. 2.3	Valid for both miscible and immiscible combinations	Valid if either or both phases are dispersive
Fowkes's theory	Eq. 2.4	Valid for both similar and dissimilar phases	Valid only for insoluble combination and atleast one phase should be completely nonpolar
Wu's theory	Eq. 2.5	Accurately quantifies both polar and dispersive interaction	Not validated for soluble cases and cannot account for large difference in polarizability, i.e, polarity of the phases
Van Oss, Good, and Chaudhury's theory	Eq. 2.7	Is not limited to dispersive phase	Atleast three liquids with known polar and dispersive components are required

These models are further described in Appendix A.3.

We acknowledge that there are numerous recent studies [12, 22, 151, 152] that focuses on studying the role of different components of each phase's surface tension on the resulting interfacial tension between two phases. We believe starting from Van der Waals [1, 144] to Wu and many more [2, 142, 147, 150, 153, 154] attempted to quantify the theoretical interfacial tension between two phases with the detailed knowledge of individual phase chemical composition in particular, based on the different quantifiable inter-molecular interaction contributing towards the individual surface tension. We strongly believe in the theory proposed by Fowkes, Gennes, and Wu where the polarity of each phase and interaction amongst themselves has been identified as a key component for the resultant interfacial tension between two phases. In the present study, a critical investigation is performed for a wide range of combinations, polar−polar, polar−nonpolar and nonpolar−nonpolar, to establish the role of polarity of surface tension components, of two involved phases, on the resultant equilibrated surface or interfacial tension. To specifically comment on polar component in total, forty cases (ten polar−polar, eleven polar−non-polar, and nineteen nonpolar− nonolar combinations - please refer to Table A.6 of Appendix for the details) are studied which further hypothesized the generalized interaction at the fluid-vapor interface.

2.2 Experimental Section

The Pendant drop method - a popular technique in the surface tension measurement (see Appendix A.2 for detail discussion) - employs the generation of a drop so that it is barely attached to the needle. All the surface tension values in this study were measured by pendant drop method using Drop Shape Analyser (DSA 100E, Kr$\ddot{u}$ss GmbH). Materials information and experimental procedure is further discussed in the following subsections.

2.2.1 Materials

Deionized water that is used for experimental, as well as cleaning purpose was produced in the lab using Milli-Q A10 (Millipore). Organic solvents such as ethanol, hexane, decane and hexadecane were purchased from Fischer Scientific with purity $\geq 95\%$ while others were from Millipore Sigma (purity $\geq 99\%$). Purity of all the chemicals are confirmed by experimental measurement of the surface tension of the liquids at 22 ± 2°C. Appreciating the sensitivity of surface tension to surface impurities (see Appendix A.5), adequate measures were taken to maintain a control environment and to minimize any possible contamination from the ambient. For cleaning procedure of the cuvette and flat tip needle (outer diameter= 1.827±0.2) isopropanol, deionized water and compressed air flow was utilized. To ensure visibility through cuvette after vapor saturation, the cuvette was further sterilized by benzomatic flame.

In Table. 2.2, surface tension of the pure liquids in air medium, from current experiments (γ_{exp}) as well as those from previous studies, are presented. Additionally, the constituent polar and dispersive components of the surface tension, as obtained from Fowkes' model in these respective studies, are tabulated. Fowkes model is more in line with our study, which is capable of providing results of high accuracy for nonpolar and moderately polar cases[14]. The agreement between the current experiments and those from previous studies precludes any concerns regarding the existence of any surface active impurities. Note, the tabulated surface tension from previous studies correspond to a temperature of 20°C, except for methanol and ethanol (25°) and pentan-1,5-diol (0°)C. The minute deviation of present measurements from the previous studies can be attributed to this temperature difference.

2.2.2 Methods

The complete experimental setup is shown in Fig. 2.1(a). Experiments were conducted by generating a pendant drop in a sealed cuvette, with a small opening to discharge the organic liquid. A small amount of organic liquid ($\approx$ 0.3mL to 0.5mL)

Table 2.2: Measured and literature values of surface tension of the liquids used for experiments

Name	γ_{exp} (mN/m) $\epsilon_{\max} = \pm 0.56$	γ	γ^{p} (mN/m) [Literature]	γ^{d}	Molecular formula	M_w (g/mol)
Polar molecules						
Water	72.36	72.80 [155]	51.00	21.80	H_2O	18
Methanol	22.22	22.00 [153]	6.05	15.95	CH_3OH	32
Ethanol	22.33	22.30 [153]	3.30	19.00	C_2H_5OH	46
Butanol	23.73	24.60 [156]	1.60	23.00	C_4H_9OH	74
Pentanol	24.83	25.60 [156]	1.40	24.20	$C_5H_{11}OH$	88
Pentane-1,5-diol	42.38	43.30 [157]	15.70	27.60	$C_5H_{10}(OH)_2$	104
Nonpolar molecules						
Pentane	16.00	16.10 [158]	0	16.10	C_5H_{12}	72
Hexane	18.73	18.49 [8]	0	18.49	C_6H_{14}	86
Heptane	20.09	20.30 [8]	0	20.30	C_7H_{16}	100
Octane	20.72	21.80 [8]	0	21.80	C_8H_{18}	114
Iso-octane	18.62	18.77 [159]	0	18.77	C_8H_{18}	114
Nonane	22.20	22.91 [8]	0	22.91	C_9H_{20}	128
Decane	22.92	23.90 [8]	0	23.90	$C_{10}H_{22}$	142
Dodecane	24.28	25.08 [8]	0	25.08	$C_{12}H_{26}$	170
Hexadecane	26.63	26.35 [8]	0	26.35	$C_{16}H_{34}$	226
Butyl acetate	24.54	24.85 [29]	0	24.85	$C_6H_{12}O_2$	116

was then discharged at the bottom of the cuvette and sealed completely. For liquids of low volatility, a sealed cuvette with the saturating fluid is kept for a maximum of three days before conducting the experiments. Saturation was confirmed in separate

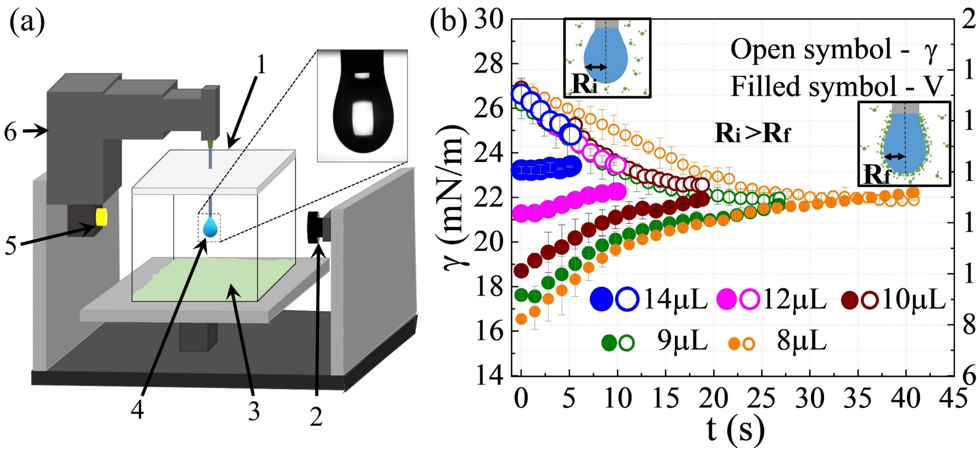

Figure 2.1: (a) Schematic of the experimental setup: 1. Sealed cuvette with saturated vapor, 2. Imager, 3. Liquid remains after saturation, 4. Pendant drop, 5. Illumination, 6. Flow controlling unit. Image of pendant drop in the inset is captured using the imager. (b) Surface tension as a function of measurement time and initial volume for hexadecane drop in saturated environment of pentane vapor. The open symbols represent surface tension, γ and the filled symbols represent the change in volume, V. This time evolution has been examined for five different initial volumes, V_o: 14 μL (blue), 11 μL (pink), 10 μL (maroon), 9 μL (green) and 8 μL (orange). At the time when drop dettaches from the needle, the volume for all last four cases are similar.

experiments, by observing no change in volume of pendant drop of same liquid as in the saturated environment.

As the ‘pendant’ drop hangs from the needle, the surface force just balances the gravitational pull so that any further increase to the drop volume would detach the droplet from the needle. The droplet remains in its mechanical equilibrium, iterative approximations are used to fit the droplet profile to obtain the radii of curvatures. The modified Young-Laplace equation is solved to estimate the surface tension for a liquid with known density difference with respect to surrounding medium [160]. Four trials for each combinations were performed to ensure reproducibility.

2.3 Results and Discussion

2.3.1 Accurate Quantification for the Interface with Mass Transfer

The pendant drop method often fails to estimate an accurate surface tension for liquid–vapor interfaces with very high mass transfer rate [45]. Such scenarios are commonly observed for highly volatile liquid drops or highly reactive surrounding media. In such cases, accurate fitting of the droplet profile/shape is a challenging task since it is essential for quantifying the radii of curvature and thus the correct surface tension. For example, if the pendant drop method is deployed for volatile liquids such as small chain alcohols and alkanes, the measurement becomes challenging, if not impossible in many cases. The difficulty arises due to inability to maintain the mechanical equilibrium which is triggered due to the rapid mass transfer at the interface either due to evaporation (drop to medium) or adsorption (medium to drop). Drop equilibrium is paramount for the the accurate quantification of surface tension but due to sudden increase or decrease in the drop volume, the drop shape disturbs the equilibrium. In the case of adsorption drop volume increases and detachment of droplet from the needle is unavoidable whereas in the case of evaporation the mechanical equilibrium is difficult to achieve. Therefore, a protocol is necessary prior to obtain the equilibrium surface tension measurements. Here we established such protocol for a methanol in air medium, as described in Appendix A.4. This protocol is further extended for systems where surrounding medium is other than air or saturated vapour of the same liquid as the drop.

For a volatile liquid in air medium, we start with a largest pendant drop volume, termed as initial volume (V_{o}) and we measured the instantaneous change in the surface tension until the volume decreases rapidly due to evaporation, imposing a difficulty to accurately contour the pendant drop shape. For such cases, saturating the surrounding medium with the vapor of the same liquid ensures accurate measurement of surface tension. Temporal variation of surface tension and volume of methanol, for both the cases – air medium and saturated medium of methanol – is provided in Appendix (Fig. A.2). It is evident that saturated medium is paramount for obtaining the equilibrium surface tension measurements.

For a binary system where mass transfer at the surface is very high due to rapid adsorption, the drop detaches from the needle. To ensure accurate measurement of γ_{eq}, the initial volume, V_{o}, of the drop is decreased gradually to delay the drop detachment, so to observe the maximum amount of interaction which would result in an steady-state value for the surface tension. In Fig. 2.1(b), the blue circles represent the case with largest V_o, i.e., $14\,\mu$L, for which the drop remains barely attached to the needle. Here open and filled circles represent the instantaneous surface tension and volume of drop, respectively. It is evident that the drop detaches from the needle within a few seconds, as the cuvette gets saturated, before reaching any steady state value.

Similar experiments have been carried out, but for different V_o, i.e., $12\,\mu$L (pink circles), $10\,\mu$L (maroon circles), $9\,\mu$L (green circles) and $8\,\mu$L (orange circles) to attain the equilibrium value for the surface tension. With reduced V_o, considerable delay of the drop detachment was observed, and a longer steady state period was achieved for an initial volume of $8\,\mu$L. This method of measuring surface tension in saturated vapor, with varied initial volume, not only provides results for immiscible combinations, but for miscible and partially miscible combinations as well. Hereafter, we will denote the value of the surface tension of pure liquid by γ_{o} and the equilibrium surface tension by γ_{eq}.

2.3.2 Polar-Dispersive components and Equilibrium Surface Tension

Polar Drop in Saturated Polar Medium

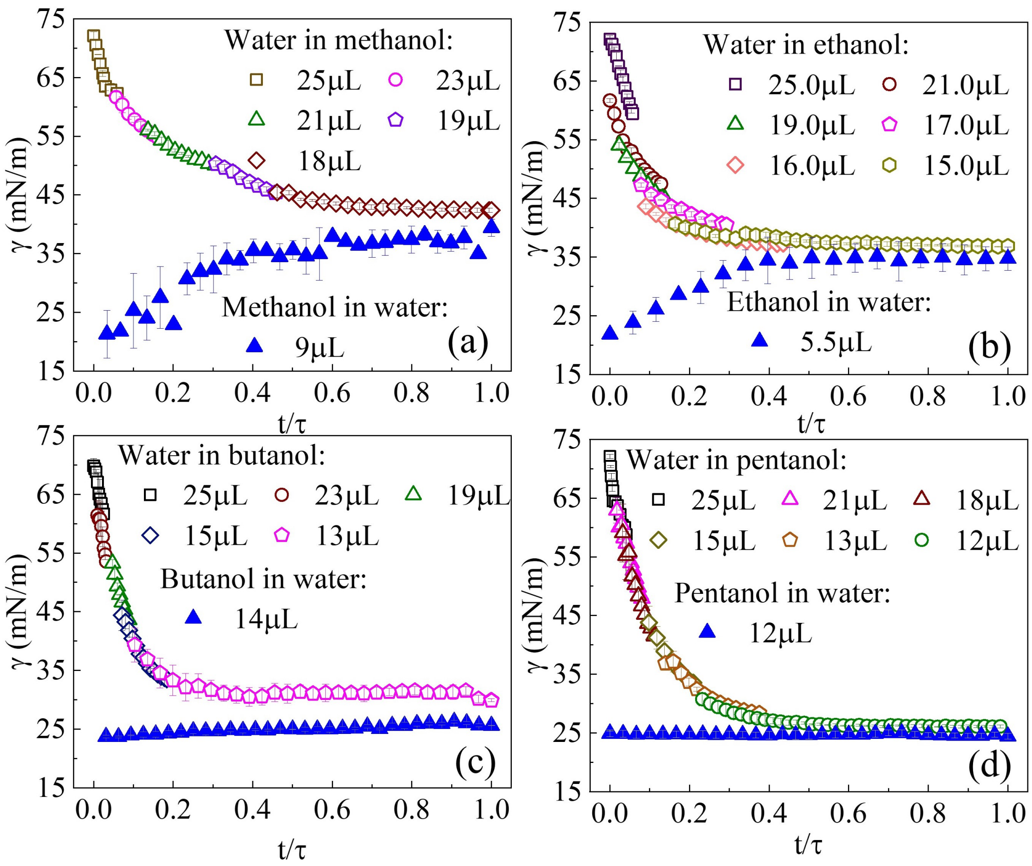

Figure 2.2: Temporal evolution of surface tension for different combinations of water and amphiphilic fluids: (a) water-methanol, (b) water-ethanol, (c) water-butanol, and (d) water-pentanol. Open symbols represent the cases where drop liquid was water with surrounding environment saturated with the vapor of amphiphilic liquids, whereas filled symbols denote the opposite cases, i.e, drops of amphiphilic liquids were surrounded by water-vapor saturated environment.

Experiments are conducted for water and amphiphilic chemicals, which cover both miscible (methanol and ethanol), slightly miscible (butanol) and immiscible (pentanol) combinations. Fig. 2.2 shows the attainment of equilibrium surface tension for combinations of water drop in four different small chain amphiphilic vapor and vice versa against dimensionless time (nondimensionalised by the final time, τ, for the completion of each set of experiment). Water is an anomalous liquid which has exceptionally high γ^{p} ($\approx$ 70%) whereas alcohols have considerably lower percentage of γ^{p} ($\approx$ 4–30%). Attributed to the presence of γ^{p} , these combinations are considered polar–polar interactions. Fig. 2.2 (a) shows the case where drops of different V_{o} of water were generated in saturated medium of methanol, until the point where a steady surface tension value, γ_{eq}, was achieved. To ensure the extent of interaction, another experiment is conducted with methanol drop in saturated water environment. Methanol being a highly volatile liquid evaporates in a matter of few seconds, which imposes a difficulty in reaching a steady value. So, to reach steady state surface tension as shown in Fig. 2.2 (a), the cuvette is saturated with both water and methanol to ensure negligible amount of evaporation takes place during this period of time. From the figure it is observed that the surface tension curves of water in saturated methanol and methanol in saturated water have converged. This suggests that surface tension is a function of polar and dispersive components of the liquid, as well as of the surrounding medium.

It has been suggested that interfacial activity is different for miscible and immiscible fluids because in the former the liquid has to be saturated before the surface is activated [161]. Furthermore, the degree of activity on surface for miscible liquids is greatly affected by the difference in solubility in bulk and in surface. This is dependent on the surface orientation of the vapor molecules, concentration of the vapor in the medium and facilitation of hydrogen bond for polar chemicals [161, 162]. Since in this study, we primarily investigate surface tension in saturated medium, the orientation of the molecules on the interface and ease of hydrogen bond formation between water and alcohol molecules can be deemed as dominating factor for the slight difference in converging γ_{eq} values (Appendix Table. A.6) as seen in Fig. 2.2 (a), (b) and (c).
The molecules of water and alcohols in the interface orient differently where the former arrange themselves so that their dipoles are aligned parallel to the surface

[163]. On the other hand, the alcohol molecules from the medium are adsorbed perpendicularly with its alkyl chain pointing away from the surface [161]. As a result, these orientations easily propagate formation of hydrogen bond between water and alcohols. For the other case with alcohol drops in water medium, the Langmuir monolayer is formed with the alkyl chain standing upright with its hydrocarbon chain pointing towards the interface, while the alcohol moiety is oriented towards the bulk liquid [164].

With the increase of carbon chain length from methanol (C_1) to pentanol (C_5), the -OH group moves further away from the surface of alcohol drop. As a consequence, hydrogen bond formation between water molecule and alcohol moiety becomes difficult. From Fig. 2.2, it is evident that with the increase in carbon chain length, the difference between the surface tension of pure fluid, γ_{o} and equilibrium surface tension, γ_{eq}, i.e. $\Delta\gamma$ increases. This is clearly seen in Fig. 2.2, where less surface activity is observed for butanol and pentanol drop in water medium compared to methanol and ethanol drop in water medium. In addition, the immiscibility of water-pentanol combination results into vapor accumulation on the drop surface [40]. Hence, with the decrease of miscibility, the γ_{eq} is equivalent to surface tension of the vapor as depicted in Fig. 2.2 (d).

Nonpolar Drop in Saturated Nonpolar Medium

Owing to the symmetry and low electronegativity difference between atoms of straight chain alkanes, the surface tension of these molecules has no polar component and $\gamma = \gamma^{\mathrm{d}}$ (Table 2.2). For a nonpolar drop in a nonpolar medium, it has been suggested that the Fowke's dispersive interaction (suggested by Fowkes [2] $(\gamma_d^d \gamma_m^d)^{1/2}$) increases with increasing molecular weight of either drop or volume and consequently an increase in the observed surface tension of the drop (Fig. 2.3). To evaluate this, experiments are performed with nonpolar-nonpolar combinations of heptane drop or medium in alkane (varying hydrocarbon chain length) medium or drop, respectively. When lower

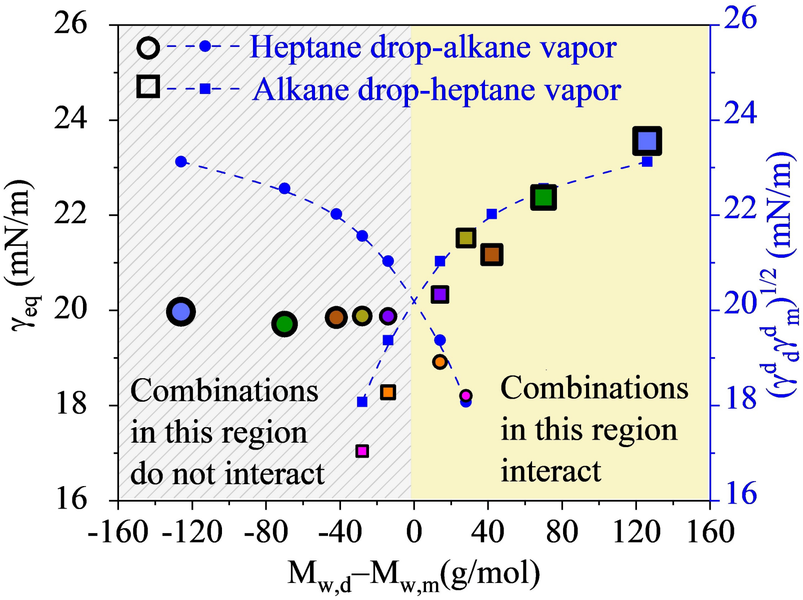

Figure 2.3: Experimental results of γ_{eq} for heptane-alkane combination as a function of difference between molecular weight of drop and medium $(M_{w,d} - M_{w,m})$ (open symbols). The right hand axis denotes Fowkes dispersive interaction $(\gamma^d_d \gamma^d_m)^{1/2}$ of liquid-vapor system depending on their molecular weight (filled symbol), with dotted line as guide to the eye. Individual γ^d are obtained from the experimental values by Jańczuk *et al.* [8]. The circles represent heptane drop in alkane vapor and the squares represent alkane drop in heptane vapor. The alkanes are: pentane (pink), hexane (orange), octane (purple), nonane (yellow), decane (brown), dodecane (green) and hexadecane (indigo).

molecular weight alkane medium is used with heptane drop, increasing surface tensions with increasing molecular weights are exhibited. This observation coincides well with Fowkes' statement and is also seen with alkane drops in a heptane medium for as long as the molecular weight of the alkane drop is higher compared to that of the heptane medium. The smaller alkane molecules have been shown to populate and decrease the surface tension of the higher molecular weight drop surface [165]. Interestingly, however, constant surface tensions with no drop surface activity are observed with heptane drops in alkane medium of higher molecular weights. This is counter to the above statement, and it can be concluded that surface activity occurs if $\gamma^d_m < \gamma^d_d$. Apart from that, Fig. 2.3 also exhibits that with increasing carbon number in either drop or vapor phase, γ_{eq} value increases.

Dependence on molecular weight was not observed for water-amphiphilic case. Hence, further analysis has been conducted using alcohol-alcohol combinations, which followed the same dependency as nonpolar-nonpolar combination (results shown in Appendix A.7). Probable cause for this difference can be contributed to the anomalous behavior of liquid water.

Polar–Nonpolar Combinations

Contrary to the surface tension dependence on molecular weight with the nonpolar drop and medium combinations, for polar–nonpolar cases, surface activity does not depend on $\gamma_m^d < \gamma_d^d$. Instead, experimental results show that activity occur on drop surface only if drop is polar and medium is nonpolar. For miscible combinations, the orientation of the molecules plays a huge role in promoting or hindering surface activity. When a polar drop is dispensed in a nonpolar medium, the polar molecules arrange themselves where the alkyl group is perpendicular to the surface and the terminal alcohol moiety is towards the bulk phase of the drop [164]. This allows for the adsorption of the nonpolar alkane molecules in the saturated vapor medium parallel to the surface [166] resulting to a decrease in the surface tension of drop [148, 165]. In this case, dependence of surface tension on the polar and dispersive components of both the liquid and the vapor can be further observed in Fig. 2.4 (c). For a nonpolar drop in a polar medium, the orientation of the alkane molecules in the drop is similar to the nonpolar medium of the previous case where the alkane molecules are parallel to the drop surface. The alcohol molecules in the saturated medium are then initially absorbed with their alkyl group entering perpendicularly to the drop surface. The molecules then rearrange with the alcohol moieties orientated towards the bulk of the drop. Similar findings are seen with nonpolar and polar liquid combinations [165]. Although alcohol molecules are absorbed, no change in surface tension of the drop which signifies no measurable surface activity. However, similar

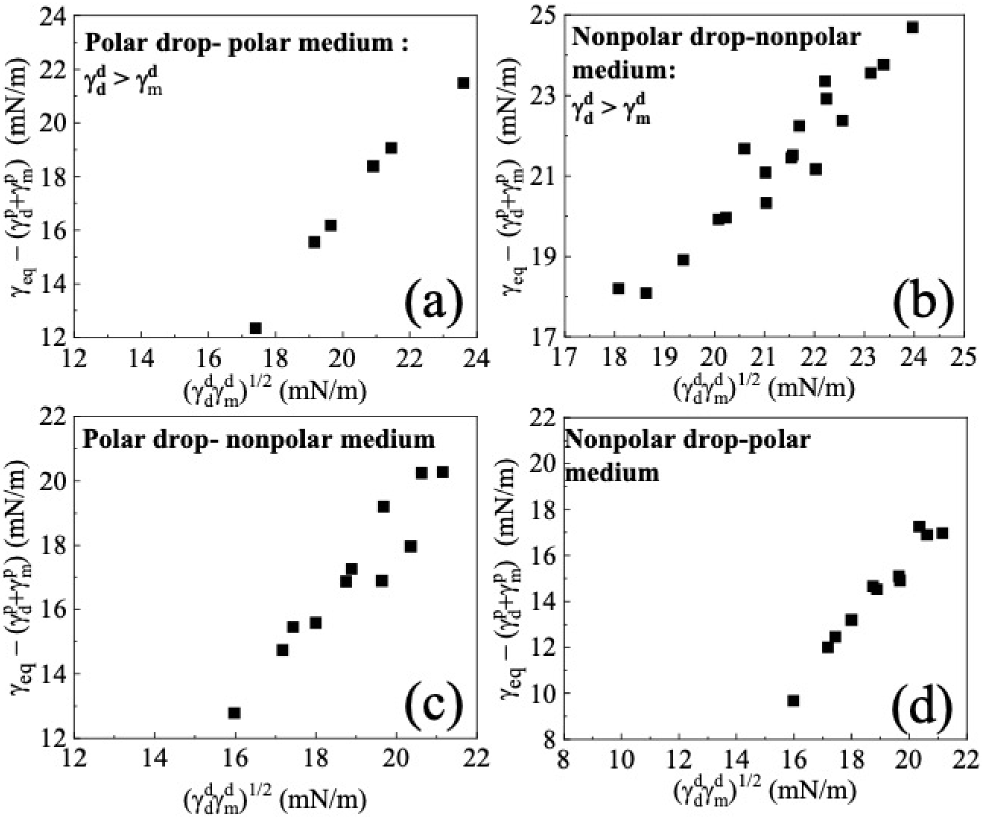

Figure 2.4: Role of γ_d^p and γ_m^p on γ_{eq} as a function of Fowkes dispersive interaction $(\gamma_d^d \gamma_m^d)^{1/2}$ for all types of combinations: (a) polar drop-polar medium, (b) nonpolar drop-nonpolar medium, (c) polar drop-nonpolar medium and (d) nonpolar drop-polar medium.

trend is observed for immiscible cases because they populate the surface in similar orientation as miscible molecules just before absorption.

Generalized Relation

A generalised relationship for γ_{eq} in terms of γ^{p} and γ^{d} is obtained for drop (polar or nonpolar) and medium (polar or nonpolar) combinations as depicted in Fig. 2.4. Fig. 2.4 (a) and (b) show polar–polar and nonpolar–nonpolar combinations, respectively, where the dispersive component of the drop is higher than that of the medium, i.e., $\gamma_d^d > \gamma_m^d$. For the latter figure, the y-axis label is kept identical to that of the former to manitain consistency even though $(\gamma_d^p + \gamma_m^p) = 0$. Evident from both figures, $\gamma_{eq} - (\gamma_d^p + \gamma_m^p)$ shows a linear correlation with the Fowkes dispersive interactions. In

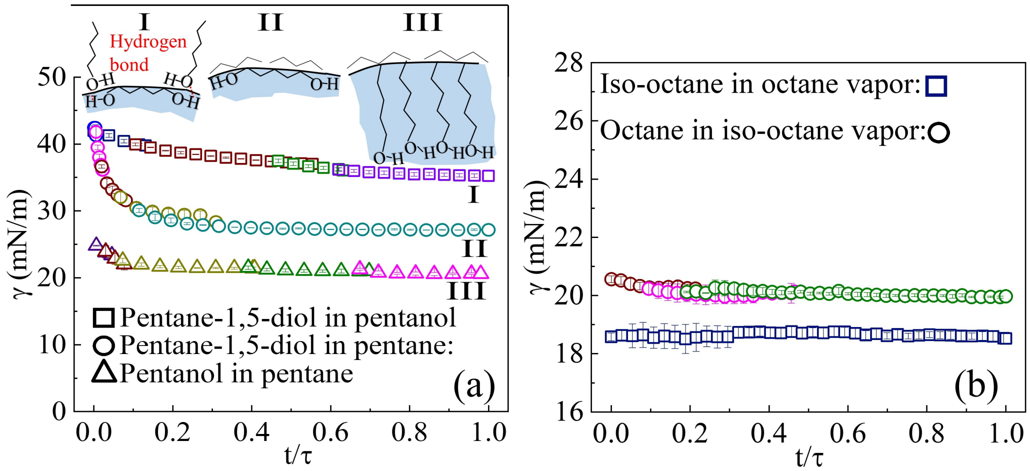

Figure 2.5: Temporal variation of the interaction between (a) polar-polar and polar-nonpolar fluids with fixed number of carbons: pentane-1,5-diol in pentanol (square) and pentane-1,5-diol in pentane (circle) and pentanol in pentane (triangle) (b) two structural isomers of C_8 alkanes: octane and iso-octane.

contrast to this, no surface activity is observed where $\gamma_d^d < \gamma_m^d$, which is also seen in Fig. 2.3. As discussed earlier, γ^p and γ^d is related to the polarizability of both the liquid and vapor, and the above observation shows that γ_{eq} is dependent on the polar and dispersive components of both the liquid and medium. This agrees well with Gennes. Fig. 2.4 (c) and (d) are for polar drop-nonpolar medium and nonpolar drop-polar medium respectively. Similar to Fig. 2.4 (a) and (b), a linear relationship is also observed between $\gamma_{eq} - (\gamma_d^p + \gamma_m^p)$ and Fowkes's dispersive interaction. Fig. 2.4 (c) further shows that if γ^p of the drop is present, it has an influence on the relationship between γ_{eq} and Fowkes's dispersive interaction. In contrast, Fig. 2.4 (d) shows nonpolar drop in polar medium. There is no visible surface activity, however, it is still included to show that all combinations have been explored.

2.3.3 Role of Molecular Orientation and Branching

The consequences associated with surface orientation is further analysed in this section. Fig. 2.5(a) represents a comparison between fluids with C_5 alkanes and alcohols.

The higher reduction of surface tension for pentane−1, 5−diol in saturated pentane vapor than in pentanol vapor is evident from this figure. As such, the γ_{eq} of the former combination (27.17 ± 0.14) is considerably lower than that of the latter (35.54 ± 0.29). It is observed that the dispersive components of pentane has interacted almost completely with dispersive component of pentane−1, 5−diol (dispersive component values in Table 2.2) that can be evidently seen with the large change in surface tension of the drop. This change can be attributed to contributing factors, such as surface ordering [161, 166]. In contrast, with the pentane−1, 5−diol in the presence of pentanol medium, the high polar component of surface tension of the drop has not resulted into a stronger polar-polar and dispersive-dispersive interaction. It is suggested that the -OH groups of the pentane−1, 5−diol anchors the molecule in a parallel position with the interface [167], which facilitates hydrogen bond formation between the alcohol moieties. Similar results can be observed with other alcohol-alcohol combinations (Appendix Fig. A.3). The absorption of pentanol or pentane results in low or high surface activity with pentane−1, 5−diol, respectively.

For an identical medium of saturated pentane vapor, Fig. 2.5 (a) further shows that $\Delta\gamma$ for pentane−1, 5−diol is considerably different than $\Delta\gamma$ for pentanol drop even though both pentanol and pentane-1,5-diol has same number of carbons. This difference can be attributed to the difference in orientation of the two alcohol molecules in pentane medium. Compared to the parallel positioning of pentane−1, 5−diol, pentanol alligns in a perpendicular fashion with −OH group oriented towards the bulk of the drop [164], which is also seen in alcohol drop−water medium case (Fig. 2.2). The difference in γ_{eq} values in Fig. 2.5 indicates that surface orientation has an impact on the nonpolar-nonpolar interaction, as well as confirming the effect of polar surface tension component on the nonpolar-nonpolar interaction.

Fig. 2.5 (b) shows the interaction between octane and iso-octane. Although both of these molecules are structural isomers of C_8 alkanes, they demonstrate non-identical initial surface tensions (γ_{o}), resulting into different dispersive component of surface

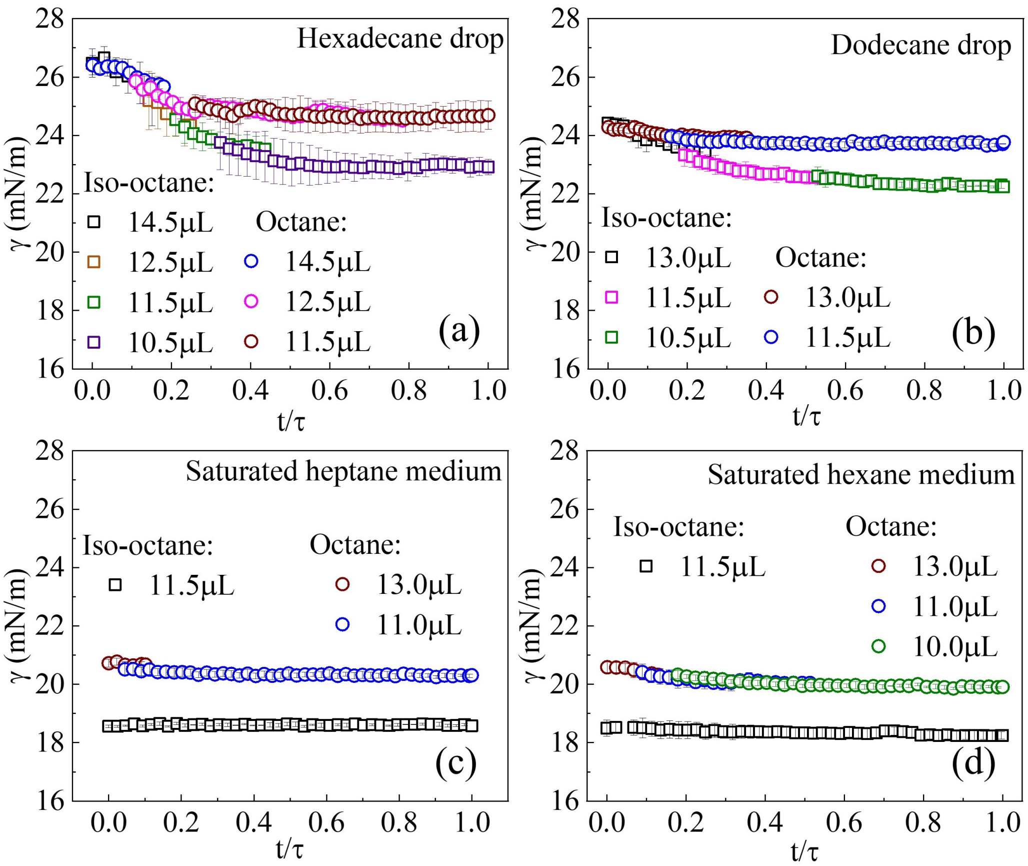

Figure 2.6: Temporal variation of surface tension for combinations of different linear alkanes and structural isomers of C_8 to portray the difference due to branching. Octane (circle) and iso-octane (square) with(a) hexadecane, (b) dodecane, (c) heptane, (d) hexane.

tension as seen in Table 2.2. The nonpolar-nonpolar surface tension interaction follows the same trend as in between two different nonpolar chemicals. From this figure, a decrease from γ_o to γ_{eq} for octane drop in saturated iso-octane vapor is observed while no visible change for iso-octane drop in saturted octane environment. Saturating the environment with branched isooctane vapor weakens the van der Waals interaction between linear octane molecules present at the interface [168], which results into the decrease in γ_o for first case. On the other hand, the weak intermolecular force in the latter case cannot be compensated by the stronger intermolecular forces of the few number of linear octane molecules at the interface.

To further investigate the effect of branching, similar experiments were performed with octane or iso-octane combined with four linear alkanes, i.e., hexane, heptane, dodecane and hexadecane, Fig. 2.6. Hexadecane drop in octane (open circles) and iso-octane (open squares) (Fig. 2.6(a)) shows that the measured initial surface tension of the drop is similar for both media. The latter case, however, exhibited a more profound decrease suggesting that there is more surface activity of the hexadecane drop in iso-octane compared to that in octane medium. Similar results can be seen further with the dodecane drop in both media (Fig. 2.6(b)). In cases wherein heptane or hexane drop in iso-octane or octane medium, or iso-octane or octane drop in hexadecane or dodecane medium, no surface activity is observed (figure shown in Appendix Fig. A.5 and A.6). This is in line with our previous findings where surface activity is observed if molecular weight of the medium is smaller than the molecular weight of the drop and $\gamma_m^d < \gamma_d^d$. Fig. 2.6(c) and (d) further shows that minimal and no surface activity is seen with octane and iso-octane drop, respectively, in heptane and hexane vapor. It is evident that though surface tension of octane drop changes in saturated vapor of heptane and hexane, no interaction is observed for iso-octane drop because of weak intermolecular forces between these branched molecules at the surface cannot be strengthened by the small number of linear alkanes that are present in the saturated vapor. Thus, it can be deduced from Fig. 2.6 that branched structure has an influence on nonpolar-nonpolar interaction.

2.4 Conclusion

The importance of polar and dispersive components of the surface tension on the γ_{eq} values is critically investigated for a wide range of liquids in saturated mediums of miscible, partially miscible and immiscible drop-vapor combinations. It has been shown that both the polar and dispersive components greatly influence the overall γ_{eq} of a drop in a medium. For nonpolar−nonpolar and polar−polar of drop-medium pairs, $\mathrm{M}_{\mathrm{w,d}}$ and $\mathrm{M}_{\mathrm{w,m}}$ are important parameters that determine if surface activity of the drop is or not observed. For instance, only when the $M_{w,d}$ is greater than $M_{w,m}$ surface activity can be seen. In addition, a linear correlation for these combinations is seen between Fowkes dispersive component with equilibrium surface tension, which is influenced by the polar and dispersive components of the surface tension of the drop and medium. For combination pairs with comparable molecular weights, surface activity is only observed with linear alkane drop in a branched alkane medium. In addition, for both cases where a higher M_w linear alkane drop in a lower M_w linear or branched medium, surface activity is seen more predominantly with the linear drop−branched medium combination. Interestingly, these observations are not seen with polar-nonpolar combinations. The drop needs to be polar and the medium nonpolar to exhibit surface activity and, is enhanced if the drop molecules are in the parallel orientation.

Chapter 3

Role of Polarity on Solid-Liquid Interface

Chapter 3 elaborately describes the study that has been conducted to quantify the solid−liquid interaction, and their dependence on the individual polarity of the surface tensions. Beginning with a small introduction, the chapter extends to experimental section, and results and discussion. The chapter ends with the conclusion that consists the observations of the study of solid−liquid interface.

3.1 Introduction

The determination of contact angle, which is a key parameter to quantify surface and interfacial interaction for solid and liquid, has frequently been utilized to ascertain fundamental properties of surface and interfaces [169]. It plays a vital role in many important processes like printing, oil recovery, liquid coating, spray quenching, etc. [170–173]. Such versatile applications induced an extensive study of its controlling parameters. One of the major contribution was from Gennes, who suggested that a liquid spreads completely on a solid if the polarizability of the former is lower [7]. Based on this theory, several demonstrations has been successfully verified which shows that the interactions between polar−nonpolar components of interfacial energies of solid and liquids influences the contact angle at equilibrium position [9–11]. To understand the dependency on polar and dispersive components, a brief introduction to its development is necessary.

In 1805, Young's qualitative description relating contact angle with surface tension of solid and liquids had provided a revolutionary guidance towards this path. He stated that the contact angle between a liquid and solid is the result of the mechanical equilibrium of each phase along the three phase contact line [73]. Though Galileo's observation of water drop not spreading over superhydrophobic cabbage leaf is considered to be the first representation of contact angle phenomenon [174], it is Young who coined the term [73]. Laplace developed similar theory mathematically around the same time as Young, but it was Gauss who combined these two theories in 1830 and developed a differential equation along with boundary conditions [175]. Later in 1937, Bangham and Razouk formulated the famous Young's equation that is presently in use [176] as shown below:

$$\gamma_{\mathrm{SV}} = \gamma_{\mathrm{SL}} + \gamma_{\mathrm{LV}} cos\theta \tag{3.1}$$

where γ_{SV} is surface energy of solid, γ_{LV} is surface tension of liquid, γ_{SL} and θ is interfacial tension and contact angle between solid and liquid respectively. Young's thermodynamic equation of contact angle is applicable for smooth, isotropic and rigid solid surfaces where an assumption of negligible liquid or vapor adsorption is valid [144, 149]. According to this theory, wetting is favored if surface energy of solid is high whereas surface tension of liquid and interfacial energy between solid and liquid is low. In later years, pioneering theories and attempts has been published by Berthelot [142], Antonow [147], Girifalco and Good [3] which relates interfacial tension of two phases with individual surface tension in air medium.

Consecutively, Zisman published the method to calculate the surface energy of solid by considering critical surface tension. According to this method, the intercept of cos $\theta = 1$ line and the extrapolated plot of cos θ versus γ_{LV} for a specific solid is known as the critical surface tension, γ_c which is assumed to be equal to the solid surface energy. This is a widely used relation which enables the measurement of solid surface energy by using a few liquids. In 1964, Fowkes introduced the concept of polar and dispersive interaction of two involved phases to represent the equilibrium surface tension [2]. The resultant equation was presented as:

$$\gamma_{\mathrm{SL}} = \gamma_{\mathrm{SV}} + \gamma_{\mathrm{LV}} - 2\sqrt{\gamma_{\mathrm{SV}}^{d}\gamma_{\mathrm{LV}}^{d}} \tag{3.2}$$

Here, γ_{SL} is interfacial tension between to constituents, whereas γ_{SV} and γ_{LV} are surface tension values in air medium of chemical 1 and 2, respectively. γ_{SV}^{d} and γ_{LV}^{d} are dispersive components of phase 1 and phase 2. Based on this theory, OWRK method is developed [6, 20–22] which is utilized in this study to calculate surface energy. This method will be discussed further in the following sections. OWRK method relates interfacial tension with interaction between polar and dispersive components, which combined with Young's equation provides relation between contact angle and polar−dispersive components. Although, role of polar−nonpolar components have been developed and studied extensively, no generalization is developed to the knowledge of the authors.

In this investigation, a generalized relationship between contact angle and role of polar−dispersive components has been developed graphically. To achieve this goal, functionalized gold substrates by Self Assembled Monolayer (SAM) has been utilized. The details of the chemicals used as SAM is provided in the succeeding section.

3.2 Experimental Section

3.2.1 Materials

This study utilizes gold substrates that are prepared by depositing gold (Au) on prime silicon wafers of diameter 100mm (Silicon Material Inc., USA). For the purpose of gold substrate functionalization, thiol samples are purchased from Milipore Sigma consisting of 1H,1H,2H,2H - Perfluorodecanethiol (97%, PFDT), 11-Amino-1-undecanethiol hydrochloride (97%, 11AUT), 3- Mercaptopropionic acid (≥99%, 3MPA) and 11-Mercaptoundecanoic acid (95%, 11MUA). The properties of these thiols are shown in Table 3.3. Anhydrous ethanol (Ethyl alcohol 200 proof in HDPE container) from Comercial Alcohols has been used to form the solution. Deionized water that is used for contact angle measurement, as well as cleaning purpose was produced in the lab using Milli-Q A10 (Millipore). Diiodomethane (99+% stabilized) is purchased form Fischer scientific.

Table 3.3: Chemical and physical properties of thiols at 25°C

Name	Chemical Formula	Molecular Weight (g/mol)	Form	Density (g/mL)
PFDT	$CF_3(CF_2)_7CH_2CH_2SH$	480.18	liquid	1.678
11AUT	$HSCH_2(CH_2)_9CH_2NH_2\cdot HCl$	239.85	solid	–
11MUA	$HS(CH_2)_{10}COOH$	218.36	solid	–
3MPA	$HSCH_2CH_2COOH$	106.14	liquid	1.218

3.2.2 Method

This study can be divided into four segments: preparation of gold substrates, functionalization of the substrates, surface characterization and contact angle measurement.

- The gold substrates are prepared by depositing 10nm of chromium followed by

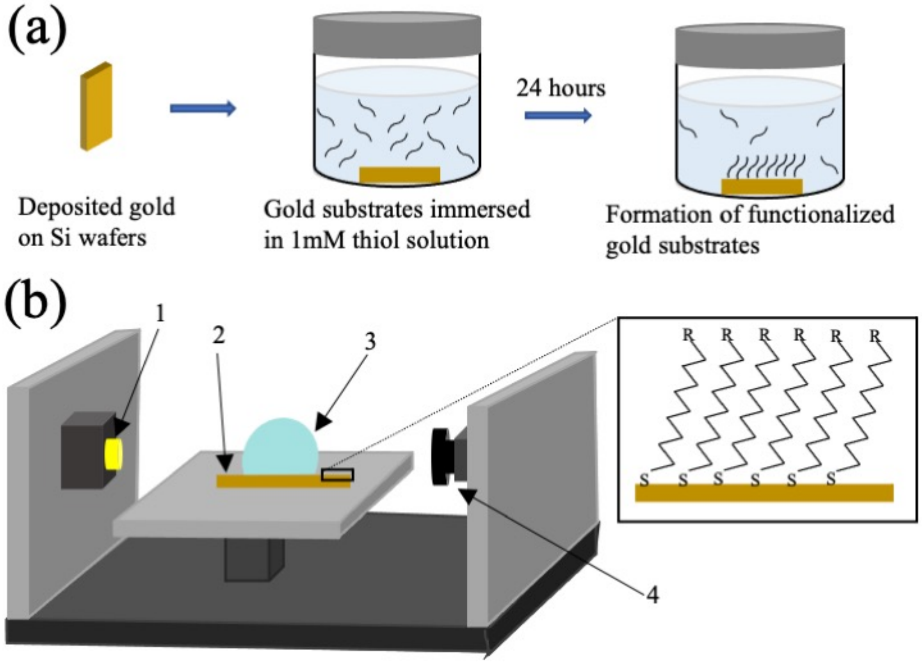

Figure 3.1: Schematic of (a) functionalization of the gold substrates (b) experimental setup for contact angle measurement: 1. Illumination, 2. Functionalized substrates, 3. Sessile drop of liquid, 4. Imager. The inset shows the functionalized substrate.

100nm of gold on prime silicon wafers.

- These freshly prepared substrates are then immersed in 1mM ethanolic solutions of the intended thiols for 24 hours.

- After the proposed time, equilibrium contact angle of water and diiodomethane sessile drops, resting on these functionalized substrates, are measured using a Mobile Surface Analyzer (MSA, KRÜSS GmbH) and a data analysis software. This software measures the contact angle by drawing a tangent to the two dimensional image of the drop at the three-phase contact point.The contact angles are then utilized to calculate the surface energy of the solid using OWRK method.

- Surface characterization of the functionalized substrates are performed using X-ray Photoelectron Spectroscopy (XPS) to compare the mole ratio of the thiols

These processes are briefly described in the following sections. Experimental setup for the functionalization process and the contact angle measurement is shown in Fig. 3.1.

Gold Substrate Preparation

Prime silicon wafers of diameter 100mm (Silicon Material Inc., USA) are coated with 10nm chromium (Cr) followed by 100nm gold (Au) using physical vapor deposition (PVD) method. This process deposits metal film of preferred thickness at a particular rate (23nm/min for Cr and 14.2nm/min for Au) using a load-locked, computer controlled, three inches planar magnetron sputtering system (Kurt J. Lesker, USA). The pressure inside the cryogenically pumped deposition chamber is maintained at pressure less than 1×10^{-7} torr, with Argon as the process gas. The Cr layer improves the adhesion of gold to silicon substrates [177]. Prior to the metal deposition, the silicon substrates are cleaned with piranha solution for 15 min which consists of a mixture of Sulfuric acid (H_2SO_4) and Hydrogen Peroxide (H_2O_2) in the ratio of 3:1. While mixing the aforementioned chemicals for piranha bath, extra precautions should be observed as the solution is prone to explosion. The precautions include careful addition of (H_2O_2) without exceeding 50% concentration, keeping the solution in open container to avoid gas generation resulting into pressurization and usage of glass lab-wares only. After piranha cleaning, the wafers are washed with DI water for five cycles in the dump rinser and dried with nitrogen in Semitool 870-S Spin Rinser dryer (Sitek Process, USA). Next, the gold substrates are cut into 1.0cm × 2.0cm chips using diamond blades of DAD 321 Dicing Saw (Disco Corporation, USA). This chips are then sonicated in ethanol for 15 minutes and dried with stream of 99.999% ultra pure nitrogen (Linde, Canada). The gold substrates are submerged in thiol solution soon after.

SAM functionalization on gold surface

For the SAM of all the pure thiols, the freshly prepared gold substrates are completely submerged in 1mM ethanolic solutions of alkanethiols at room temperature. Each substrate is soaked separately in small glass beakers for 24 hrs. This soaking time is optimum because the monolayers are absorbed onto clean gold substrates within 10 minutes of deposition and then slowly arrangers themselves to convenient orientations within few hours, depending on the van der Waal's interaction between them [89, 109, 110]. Similarly, the mixed SAM of PFDT-11AUT, PFDT-11MUA and PFDT-3MPA are formed by exposing the gold substrates in mixtures of variable composition of pure 1mM thiol solutions. The solutions were mixed by volume to ensure that the concentration of solution is maintained at 1mM. After 24 hrs of soaking time, all the substrates are sonicated and rinsed with anhydrous ethanol followed by drying with nitrogen stream. A detailed discussion of the molecular mechanism and effect of variable parameters on our chosen combinations are provided in Appendix A.12.

Surface Characterization by X-ray Photoelectron Spectroscopy (XPS)

In this study, composition of SAM monolayer deposited gold substrates are characterized from the survey spectra of major elemental peaks obtained by XPS. In XPS, the core electrons are knocked out, the binding energy of which helps determine the composition of the surface elements of the monolayers. The XPS measurements are performed using Kratos Axis Ultra (Kratos Ltd, UK) with monochromatic Al Kα source (hu = 1486.72 eV). The pressure in the analysis chamber of the equipment is about 5×10^{-10} torr and the electron energy analyzer works at pass energy of 20 eV to 160 eV to obtain core-level spectra and survey spectrum respectively. The equipment has glove box to allow loading of samples in controlled environment. CASAXPS software was used to analyze the atomic concentration from the peak areas. The samples were loaded for XPS measurement within a few hours of extracting them from the solution.

Contact angle measurement

Contact angle or wetting angle is an important indicator of a surface's wetting property, as well as of its surface energy. Appendix A.10 elucidates the definition, classification and some challenges associated with its proper (experimental) quantification. Contact angles of the functionalized substrates are measured to calculate the surface energy depending on variable SAM composition. Moreover, contact angle measurements are utilized to quantify the effect of percentage polarity of solid on solid-liquid interaction. The measurement involved recording images of 1μL sessile droplets on different substrates using fully automated Mobile Surface Analyzer (MSA, KRÜSS GmbH). This particular instrument is used because it utilizes liquid needle deposition, which has been proven to be more accurate than pendant drop deposition [178]. The resulting images are analysed by data analysis software to obtain contact angle measurements. The measurements were repeated four times for each SAM composition.

3.3 Results and Discussion

3.3.1 Surface energy of the functionalized substrates

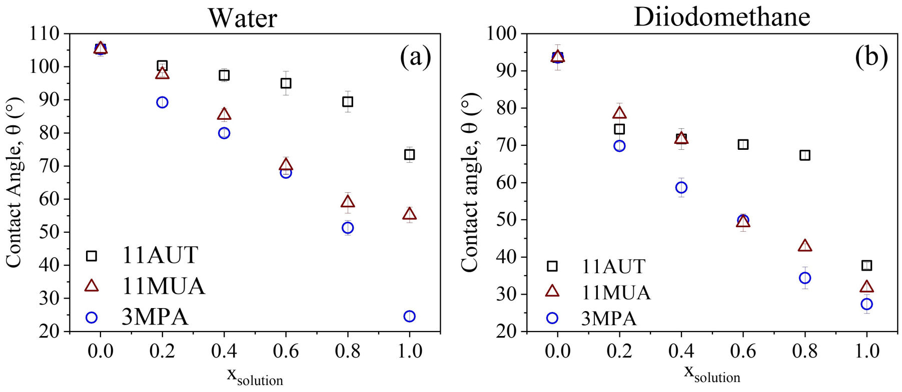

Figure 3.2: Static contact angle measurement of (a) water and (b) diiodomethane on the functionalised substrates.

The contact angle of water and diiodomethane as a function of mole fraction of solution used to functionalize the gold substrates are shown in Fig. 3.2(a) and (b) respectively. Here we have considered $x_{solution}$ and $x_{surface}$ to be the mole fraction of 11AUT/11MUA/3MPA in mixture with PFDT. In this figure, it is observed that the decrease in contact angle with increase in 11AUT mole fraction is less than anticipated considering the measured contact angle for 100% 11AUT SAM. Essentially, this indicates that the mole fraction of 11AUT on surface is lower than in solution, which will be further investigated in the next section. For the 11MUA SAM, the decrease in water contact angle in Fig. 3.2(a) with increase in mole fraction of the acids seems appropriate. However, considering the water contact angle for 100% 3MPA SAM, the decrease in contact angle value with increase in mole fraction of 3MPA is not consistent. Moreover, 3MPA is a small hydrocarbon chain acidic thiol (C_3) that is susceptible to form disorganised SAM layer on metal surfaces possibly resulting into interaction between the liquid and the metal [179]. This propensity should have enhanced the hydrophilic characteristics of these surfaces with 3MPA SAM more than that is seen in Fig. 3.2(a). These discrepancies will be further investigated in the surface characteristics section. In addition, the trend in contact angle of diiodomethane drop on the functionalized substrates as shown in Fig. 3.2(b) are almost consistent with the contact angles of water [Fig. 3.2(a)].

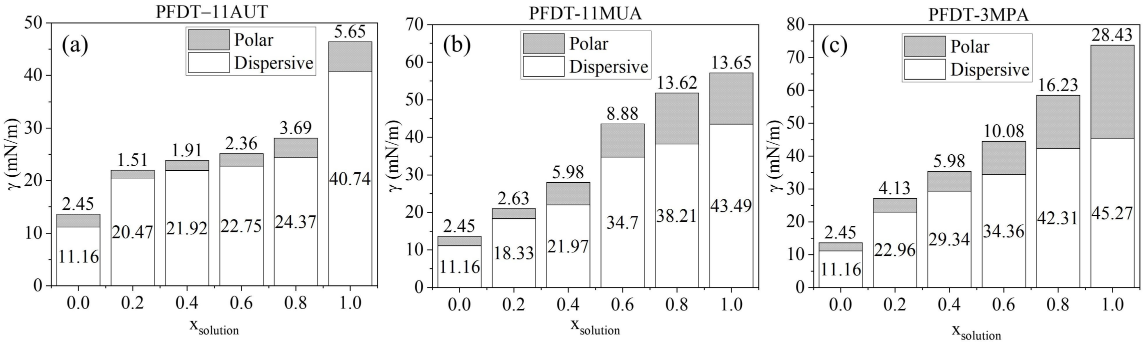

Figure 3.3: Surface energy of substrates functionalized by mixed SAM of (a) PFDT-11AUT, (b) PFDT-11MUA, and (c) PFDT-3MPA.

To determine the surface energy of the functionalized substrate (shown in Fig. 3.3), first the contact angles of highly polar (water) and completely nonpolar (diiodomethane) drops on the substrates are measured. Having the contact angles known, the Owens, Wendt, Rabel and Kaelble (OWRK) model [6, 20–22] is used to obtain the polar and the dispersive components of the surface tension. Initially, Owens and Wendt proposed the following equation [20] and solved it with two liquids of known polar and dispersive components:

$$\gamma_{\mathrm{SL}} = \gamma_{\mathrm{SV}} + \gamma_{\mathrm{LV}} - 2\left(\sqrt{\gamma_{\mathrm{SV}}^{D}\gamma_{\mathrm{LV}}^{D}} + \sqrt{\gamma_{\mathrm{SV}}^{P}\gamma_{\mathrm{LV}}^{P}}\right) \tag{3.3}$$

Here, γ_{SL} is solid-liquid interfacial tension, γ_{SV} and γ_{LV} represents surface tension in air medium of solid and liquid respectively. The superscripts p and d signifies polar and dispersive components of the appropriate surface tension. Later, Kaelble solved the equation for a number of combinations of two liquids and estimated the surface energy of a solid by averaging the obtained values [22]. Rabel took it to the final step by fitting a regression line using a number of data points in the plot of $\frac{\gamma_{\mathrm{LV}}(1+cos\ \theta)}{2\sqrt{\gamma_{\mathrm{LV}}^{d}}}$ versus $\sqrt{\frac{\gamma_{\mathrm{LV}}^{p}}{\gamma_{\mathrm{LV}}^{d}}}$. The equation of the regression line, in combination with Young's theory, is [21]:

$$\frac{\gamma_{\mathrm{LV}}(1 + cos\ \theta)}{2\sqrt{\gamma_{\mathrm{LV}}^{d}}} = \sqrt{\gamma_{\mathrm{SV}}^{p}}\sqrt{\frac{\gamma_{\mathrm{LV}}^{p}}{\gamma_{\mathrm{LV}}^{d}}} + \sqrt{\gamma_{\mathrm{SV}}^{d}} \tag{3.4}$$

Hence, the polar and the dispersive components of the surface energy is found from the gradient and the intercept, respectively. The OWRK model is generally favored over others due to its relative simplicity and better accuracy [6]. Other theoretical models that have been developed over the years are briefly discussed in Appendix A.11.

As observed from Fig. 3.3, the SAM functionalization resulted into solid substrates that exhibited increase in surface energy with increasing x_{solution}. The reason for utilizing this particular mixed SAM was to investigate whether functionalization process can result into constant dispersive component with changing polarity like corona treatment, plasma treatment, UV treatment, etc [23, 180, 181]. However, like earlier studies, it showed same increasing dispersive component along with increasing polarity for increase in surface energy [182]. Despite this limitation, these substrates are appropriate to provide a generalized relation between solid-liquid interaction and respective polar-dispersive components because the percentage polarity extends from 6.9% for PFDT−11AUT mixture with $x_{\text{solution}} = 0.2$ [Fig. 3.3(a)] to 38.6% for PFDT−3MPA mixture with $x_{\text{solution}} = 1$, see Fig. 3.3(c).

3.3.2 Surface Characteristics

Existence of mixed SAM on the gold substrates is confirmed using x-ray photoelectron spectroscopy. Here, Fig. 3.4 represents xps results for sixteen types of SAM monolayers (single or mixed) on gold surface. The peaks indicate the presence of the chemical component, the area of which is dependent on the number of monolayers consisting the particular element [183]. Fig. 3.4(a) focuses on fluorine by considering the binding energy of bombarded electron from F 1s orbital (688.65 eV) [184] for PFDT and 11AUT mixture. The bottom line (black) represents 100% PFDT SAM, whereas the top line (yellow) represents 100% 11AUT. In between the two extremities lies the variable mole fraction of the two chemicals as mentioned in the figure. It is observed that the peak height of F 1s decreases as the mole-fraction of PFDT decreases. Fig. 3.4(b) is quite different because it shows more than one peak for carbon depending on chemical bond. It has one peak for $-CF_3$ at binding energy of 291.3−293.4 eV [184, 185] and one for cumulative −CH and −CN because their peaks coincided with each other (-CH lies between 284eV-285.2eV depending on environmental condition; -CN 285.7eV) [184, 185]. Moreover, Fig. 3.4(b) shows the slow disappearance of $-CF_3$ peak whereas in Fig. 3.4(c) the appearance of the N 1s peak at 402.4 eV (399.5-402 eV [186]) is clearly visible as the composition of the mixture approaches 100% 11AUT. Similar behavior is observed for F 1s orbital in Fig. 3.4(d) and (g) for PFDT-11MUA and PFDT-3MPA mixtures respectively. 11AUT has amine functional group whereas 11MUA and 3MPA have carboxylic functional group. Hence, Fig. 3.4(e) and (h) shows another small peak for $-C = O$ [187, 188] at binding energy of 288.6 and 290.5

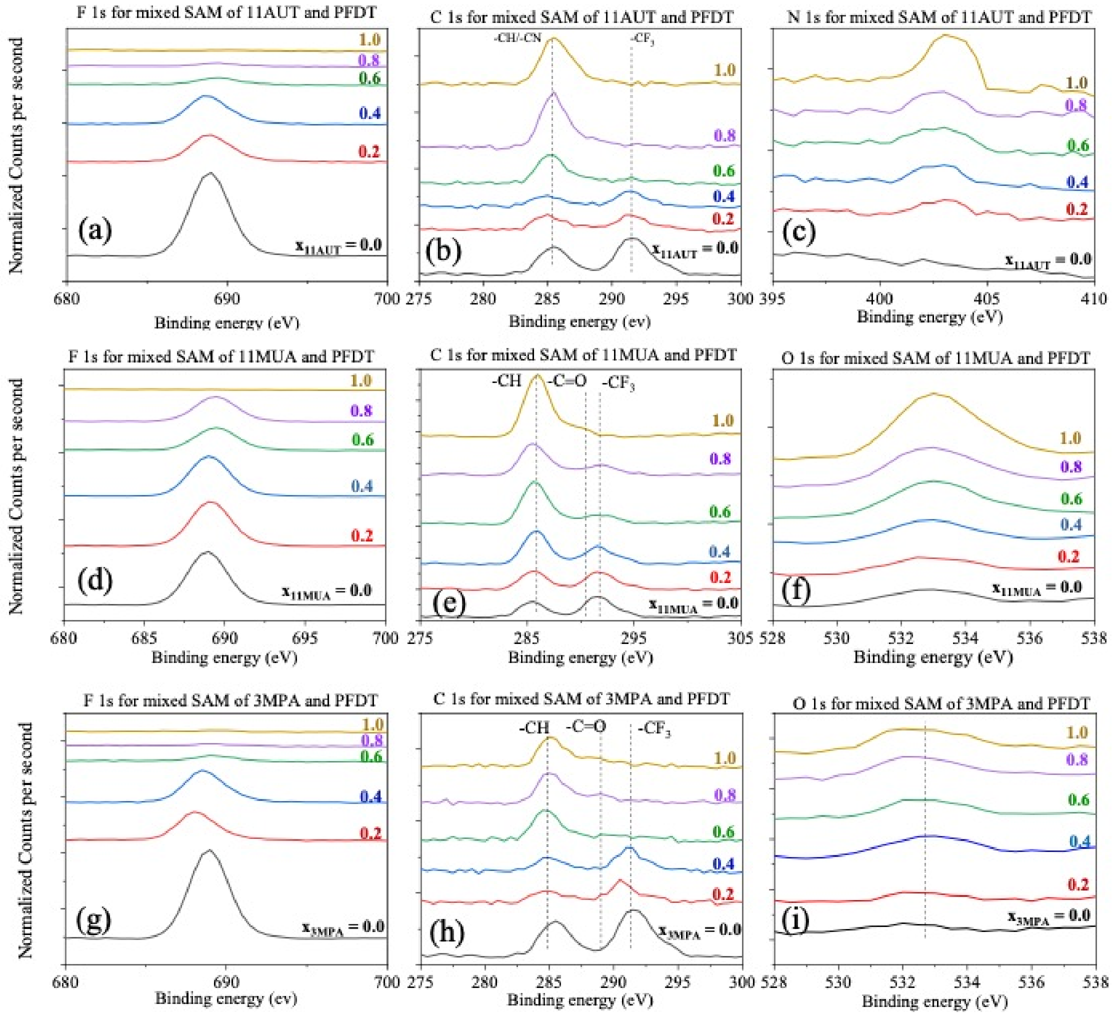

Figure 3.4: XPS of mixed thiol monolayers on gold surface showing dependency on molar ratio. Mixture of 11AUT and PFDT representing composition of (a)F 1s, (b)C 1s, (c)N 1s ; mixture of 11MUA and PFDT representing composition of (d)F 1s, (e)C 1s, (f)O 1s ; Mixture of 3MPA and PFDT representing composition of (g)F 1s, (h)C 1s, (i)O 1s.

eV for 3MPA and 11MUA respectively which is very small compared to the other carbon bonds. As surface mole fraction data using only carbon peaks is highly unreliable [189], the xps result for O 1s is considered as shown in Fig. 3.4(f) and (i) for variable 11MUA and 3MPA composition respectively. The change in peak at binding energy 532.8 eV [187] from 0 to 100% acid functional group further confirms the presence of varying composition. The intensity results obtained from survey spectra using CasaXps is further normalized to calculate the percentage atomic concentration of the individual elements to perceive the mole fraction of the constituents of the mixed SAM on the gold surface (calculation shown in Appendix A.13).

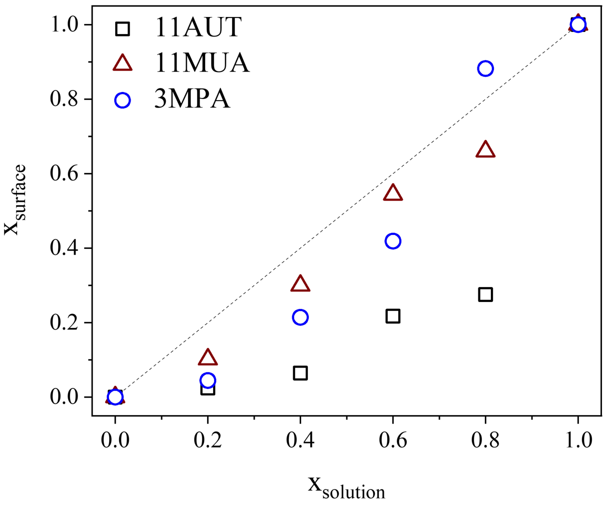

Figure 3.5: The surface molar ratio, $x_{surface}$ as a function of solution molar ratio, $x_{solution}$ where x represents mole fraction of 11AUT(square), 11MUA(triangle) and 3MPA(circle) SAM in mixed solution with PFDT.

Fig. 3.5 represents the relationship between surface composition of the $-NH_2$ functionality for 11AUT and $-COOH$ functionality for 11MUA and 3MPA on the binary mixed SAM and the solution mole fraction of the mentioned thiols in the mixture with PFDT. For mixture of 3MPA and PFDT, it is observed that the surface mole fraction of 3MPA is often less than that in solution. This effect can be attributed to the higher preference of PFDT molecules to be deposited on the gold surface because molecules with longer carbon chain is more likely to be adsorbed over molecules with shorter carbon chain. The main reason for the preference of adsorption is the enhanced Van der Waals interaction between SAM molecules with increase in carbon chain length [123, 190]. The slight increase in 3MPA mole fraction on surface, $x_{\text{surface}} = 0.88$ at $x_{\text{solution}} = 0.8$, can be attributed to the segregation effect that is observed for mixed SAM of different chain length [123, 190–192]. The segregation effect deposits more carboxyic acid group thiols on the surface due to their dominance over hydrogen bonding system with each other that ensures stability [193]. Furthermore, a similar lower x_{surface} observation can be made from Fig. 3.5 for mixed SAM of 11MUA and PFDT even though their chain length is similar (C_{11}). This effect can be attributed to the fact that PFDT has a lower solubility in ethanol compared to 11MUA [190]. The mixed SAM of 11AUT and PFDT shows the lowest surface coverage by 11AUT with decrease of PFDT mole fraction due to preference of protonation of aliphatic $-NH_2$ that leads to formation of bi-layers with free thiols [194, 195]. Moreover, this protonation of $-NH_2$ group results into a dipole repulsion between the molecules, which affects the deposition of amine terminated thiols on gold substrates [196]. Fig. 3.5 concludes that the mole fraction of mixed SAM on surface is different than mole fraction of the solution and the variation does not have any particular pattern [124].

3.3.3 Generalized Relation

A generalized relation representing the contact angle of a liquid on a solid surface and their polar/dispersive interaction in shown in Fig. 3.6, where, we have shown that all liquid-solid interaction will fall on the bounded arc.

To construct this figure, the contact angle of the liquid on the solid surfaces are obtained experimentally using portable surface analyzer (MSA, KRÜSS GmbH). Till to date, no experimental method has been established to directly measure the polar and dispersive components of surface energy or surface tension. However, several well

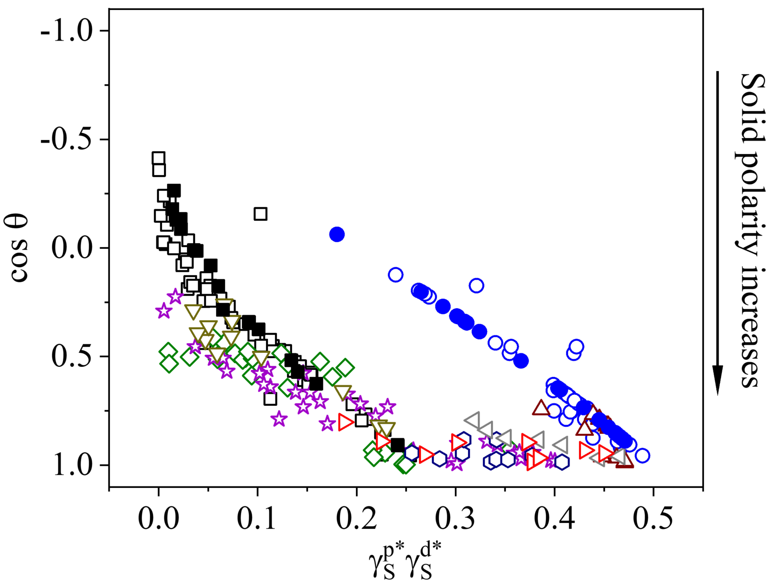

Figure 3.6: Contact angle as a function of polar and dispersive interaction of surface tension. Similar correlation between $\cos\theta$ and $\gamma_S^{p*}\gamma_S^{d*}$ is observed for current experiments (filled symbols) and previous studies (open symbols) [12–14, 197–207]. The symbols represents experimental data for water (■,□), diiodomethane(●, ○), $\alpha -$bromonaphthalein(△), formamide (◇), ethyele glycol (☆), glycerol (▽), TCP (⬡), bromobenzene (◁), bromoform (▷).

established theoretical models [2, 6, 20–22, 150, 208] can decompose surface tension into these constituent parts. In line with previous studies [12–14, 197–207], we adopt the well known OWRK method and utilizing our experimental data for the contact angles, polar and dispersive components of the surface tension are obtained because only two liquids are required for this process, provided their surface tension values are known prior.

To confirm the generalization, some already published results of nine different liquids are utilized [12–14, 197–207] along with our experimental results obtained using functionalized substrates. The names of the literature liquids are provided in the figure. Although the y-axis has a range from -1 to 1 (same as the range of cosine), the value of cos θ lie well within the range shown by the plot as maximum contact angle of a liquid on a smooth, clean substrate is around 120° (for water), provided the surface or the liquid is not specially engineered [209]. On the other hand, x-axis is defined as a product of non-dimensionalized polar and dispersive components of solid. Here, $\gamma_{\mathrm{S}}^{\mathrm{p}*} = \gamma_{\mathrm{S}}^{\mathrm{p}}/(\gamma_{\mathrm{S}}^{\mathrm{p}} + \gamma_{\mathrm{L}}^{\mathrm{p}})$ and $\gamma_{\mathrm{S}}^{\mathrm{d}*} = \gamma_{\mathrm{S}}^{\mathrm{d}}/(\gamma_{\mathrm{S}}^{\mathrm{d}} + \gamma_{\mathrm{L}}^{\mathrm{d}})$ which are chosen to represent the polar and dispersive components of solid surface as a ratio of the polar–polar and dispersive-dispersive interaction of solid and liquid. Components of solid surface energy is preferred because wetting is dependent on the nature of liquid provided the solid surface is smooth and clean [78, 153]. This characteristics is also noticeable in Fig. 3.6 where each liquid has their individual curve. Necessarily, both polar and dispersive interactions are considered because one as well as the other has an impact on polar liquid and polar solid interactions. Moreover, this plot is also applicable if either of the phase is completely nonpolar as in this case the polar component is nullified. The range of x-axis is chosen based on Gennes's theory where he suggests that a liquid with lower polarizability than a solid spreads completely on the solid surface [7]. As a result, after $\gamma_{\mathrm{S}}^{\mathrm{p}*}\gamma_{\mathrm{S}}^{\mathrm{d}*} = 0.5$ only a straight line parallel to x-axis (approximately at $\cos\theta = 1$) represents the high energy or engineered surfaces, which are special cases and are not shown in this study. This graph can also provide an estimation of the polarity of the surface if the liquid is known. As observed from Fig. 3.6, the polarity of the surface increases as value of $\cos\theta$ increases, depending on the liquid.

3.4 Conclusion

This study investigated and developed an extended graphical relation between liquid contact angle on a solid surface and polar–polar as well as dispersive–dispersive interaction between the two phases. It is observed that the generalization is applicable for a wide range of liquids and standard solid substrates. In addition, it is in agreement with Gennes's theory while also considering the maximum possible contact angles on a typical substrate [7, 209]. In the process, mixed SAM substrates are functionalized with combinations of 11AUT, 11MUA and 3MPA with PFDT. This particular mixture further confirmed that substrates of variable percentage polarity can be fabricated with this method. This generalization does not include specially engineered surfaces or liquids because their contact angle values will usually be very close to 0° or 180° which will result in to data points parallel and very close to either x or y axis of Fig. 3.6.

Chapter 4

Conclusion

4.1 Summary

This thesis addresses the fundamental aspect concerning the influence of intermolecular forces on the interaction between two phases. In this pursuit, interaction between solid–liquid and liquid–fluid has been investigated which is essentially represented by contact angle and equilibrium surface tension, respectively. This investigation shows that polar and dispersive components of surface tension of each phase influences interfacial activity since it has been suggested that polar–polar and nonpolar–nonpolar interactions at interface are result of intermolecular attraction or repulsion.

In Chapter 2, the dependency of γ_{eq} on the polar and the dispersive components of the surface tension of the constituent liquid and vapor phases is examined. Based on the experimental and literature results, individual trend of γ_{eq} as function of γ^{d} interaction is obtained for polar-polar, polar-nonpolar and nonpolar-nonpolar combinations. Evidently, our results suggested that molecular weight, M_{w} of both liquid and vapor has an impact on γ_{eq}, with the surface of drop becoming active only if $M_{\mathrm{w,drop}} > M_{\mathrm{w,medium}}$ for polar–polar and nonpolar–nonpolar cases. Surprisingly, surface activity for the polar–nonpolar case was only visible when the drop was polar and the vapor was nonpolar due to their molecular orientation at interface. This developed relation further demonstrated that if γ^{p} of the drop is present, it has an influence on the relationship between γ_{eq} and Fowkes's dispersive interaction. Additionally, the effect of orientation and branched structure was explored. These factors seem to have an positive impact on the interaction between dispersive components of surface tension of individul phases, resulting into lower equilibrium surface tension. Apart from maneuvering the difficulty of measuring the equilibrium surface tension in saturated medium, the challenge of the miscibility of the volatile vapor with the liquid has been conquered. This miscibility has initiated high mass transfer rate across the interface, which resulted into drop detachment from the needle before reaching an equilibrium value. Nevertheless, this challenge was subdued by developing a protocol.

Chapter 3 developed a graphical relation that shows dependency of liquid contact angle on a solid surface on polar−polar as well as dispersive−dispersive interaction between the two phases. This characterization includes experimental as well as literature data that also shows consistency with Gennes's well established theory. However, this investigation does not include specially engineered surfaces or liquids. This investigation further proved that functionalization by mixed SAM is capable of providing surfaces of variable percentage polarity.

To summarize, the contribution of this thesis to existing scientific literature are:

- Establishment of a generalized dependency of γ_{eq} on polar and dispersive components of surface tension of individual phases for all possible combinations: polar−polar, polar−nonpolar and nonpolar−nonpolar liquid-fluid.
- Obtained experimental γ_{eq} of miscible, partially miscible and immiscible liquid and saturated vapor combination.
- Development of a standard protocol to obtain γ_{eq} value for binary liquid−fluid combinations with high mass transfer rate across the drop surface.

- Confirmation of the fact that surface activity is only visible if molecular weight of drop is greater than the molecular weight of vapor for polar–polar and nonpolar–nonpolar combination

- Identification of the role of branching and orientation of molecules on favourable dispersive interaction.

- Establishment of a graphical relation between contact angle of a liquid drop on a solid surface and the polar and nonpolar components of the surface tension of each phase.

- Confirmation that mixed SAMs functionalized substrate are capable of providing substrates of variable percentage polarity.

4.2 Scope of the future work

In the previous chapters, experimental analyses have been reported, in light with relevant theories, on the interactions of the two phases (liquid–vapor or liquid–solid) at the interface. For studying the solid-liquid interface, substrates were functionalized to manipulate the percentage polarity. On the other hand, for liquid–fluid interface, forty different combinations were used to study the effect of individual polar and dispersive components. While doing so, combinations with variable miscibility were utilized.

These special characteristics of the interfaces has paved the way for some very interesting experimental, as well as theoretical possibilities, some of which are mentioned in this section. Some of the experimental scopes are:

- For the liquid-vapor combinations presented in Chapter 2, the interfacial tension (of the two phases) shows linear variation with the polar and dispersive components of the individual surface tensions. An interesting extension of this would be to examine whether similar relation is observed for liquid-liquid interfaces.

- The study of dependency of solid–fluid contact angle on polar and nonpolar interaction has been continued for decades. Nevertheless, with each investigation the scope of this field extends. The relation that is provided here is limited to standard solid and liquid combinations, disregarding any specially fabricated constituent (super-hydrophobic combinations) as their dependency scale is different. Investigation of this category could possibly result into a similar dependency as in this study, however, in a different range.

- As suggested by Cassie and Baxter [74–76], Young's equation is not valid for porous and heterogeneous substrates. Thus, a study can be pursued using these substrates to observe whether they portray the same dependency on polarity as the present investigation.

- Experimental investigation could be pursued for solid–fluid interfacial tension. It would be interesting to examine whether the solid–fluid interfacial activity shows a dependency on polarity of the individual constituent like the other combinations.
- This study experimentally investigated miscible liquid–fluid interfaces. These results can be further utilized to observe the effect of liquid–fluid interaction on the equilibrium contact angle of the liquid drop on a solid surface.

Apart from the experimental endeavours highlighted above, an in-depth understanding of the effect of polar and dispersive components on the interfacial tension, and on the interface as a whole, would require and extensive theoretical/computational investigation. It would be interesting to compare and combine theoretical models and experimental analysis to portray the effect of individual polarity on each type of binary interfaces, i.e., for liquid–fluid, solid–liquid and solid–fluid interfaces. It could be initiated by investigating the dependency of the solid–fluid combinations on the polar and dispersive interaction. Development of a theoretical framework to define the interactions of the interfaces, would be a major contribution in the field of interface science.

Bibliography

[1] J. N. Israelachvili, *Intermolecular and surface forces.* Academic press, 2015.

[2] F. M. Fowkes, "Attractive forces at interfaces," *Industrial & Engineering Chemistry*, vol. 56, no. 12, pp. 40–52, 1964.

[3] L. Girifalco and R. J. Good, "A theory for the estimation of surface and interfacial energies. i. derivation and application to interfacial tension," *The Journal of Physical Chemistry*, vol. 61, no. 7, pp. 904–909, 1957.

[4] S. Wu, "Calculation of interfacial tension in polymer systems," in *Journal of Polymer Science Part C: Polymer Symposia*, Wiley Online Library, vol. 34, 1971, pp. 19–30.

[5] C. Van Oss, R. Good, and M. Chaudhury, "Additive and nonadditive surface tension components and the interpretation of contact angles," *Langmuir*, vol. 4, no. 4, pp. 884–891, 1988.

[6] W. Owens, "Rabel and kaelble (owrk) method," *KRÜSS: Advancing your Surface Science [online]. KRÜSS GmbH— Borsteler Chaussee*, vol. 85, p. 22 453, 2020.

[7] P.-G. de Gennes, "Wetting: Statics and dynamics," *Reviews of modern physics*, vol. 57, no. 3, p. 827, 1985.

[8] B. Jańczuk *et al.*, "Determination of the components of the surface tension of some liquids from interfacial liquid-liquid tension measurements," *Journal of colloid and interface science*, vol. 157, no. 2, pp. 384–393, 1993.

[9] M. Jin, F. Thomsen, T. Skrivanek, and T. Willers, "Why test inks cannot tell the whole truth about surface free energy of solids," *Advances in Contact Angle, Wettability and Adhesion*, vol. 2, pp. 419–438, 2015.

[10] L. A. Belyaeva, P. M. van Deursen, K. I. Barbetsea, and G. F. Schneider, "Hydrophilicity of graphene in water through transparency to polar and dispersive interactions," *Advanced materials*, vol. 30, no. 6, p. 1 703 274, 2018.

[11] H. Brack, M Wyler, G Peter, and G. Scherer, "A contact angle investigation of the surface properties of selected proton-conducting radiation-grafted membranes," *Journal of Membrane Science*, vol. 214, no. 1, pp. 1–19, 2003.

[12] B. Jańczuk *et al.*, "The components of surface tension of liquids and their usefulness in determinations of surface free energy of solids," *Journal of colloid and interface science*, vol. 127, no. 1, pp. 59–66, 1989.

[13] B. Jańczuk and T. Białlopiotrowicz, “Surface free-energy components of liquids and low energy solids and contact angles,” *Journal of Colloid and Interface Science*, vol. 127, no. 1, pp. 189–204, 1989.

[14] S. M. Notley and M. Norgren, “Surface energy and wettability of spin-coated thin films of lignin isolated from wood,” *Langmuir*, vol. 26, no. 8, pp. 5484–5490, 2010.

[15] R. Chang, *Physical chemistry for the biosciences.* University Science Books, 2005.

[16] J. Kotz, P. Treichel, and G. Weaver, “Electron transfer reactions,” *Chemistry & Chemical Reactivity, Sixth Ed., Thomson Learning, Inc., Toronto, Canada*, 2006.

[17] D. A. McQuarrie and J. D. Simon, *Physical chemistry: a molecular approach.* University science books Sausalito, CA, 1997, vol. 1.

[18] R. H. Garrett and C. M. Grisham, *Biochemistry.* Brooks Cole, 2005.

[19] R. H. Petrucci, W. S. Harwood, and F. G. Herring, *General Chemistry: Principles and Modern Applications.* Prentice Hall, 2002.

[20] D. K. Owens and R. Wendt, “Estimation of the surface free energy of polymers,” *Journal of applied polymer science*, vol. 13, no. 8, pp. 1741–1747, 1969.

[21] W Rabel, “Einige aspekte der benetzungstheorie und ihre anwendung auf die untersuchung und veränderung der oberflächeneigenschaften von polymeren,” *Farbe und Lack*, vol. 77, no. 10, pp. 997–1005, 1971.

[22] D. Kaelble, “Dispersion-polar surface tension properties of organic solids,” *The Journal of Adhesion*, vol. 2, no. 2, pp. 66–81, 1970.

[23] A. D. Gilpin, B. R. Oakley, and R. G. Dillingham, “Water contact angle as a quantitative measure of total polyethylene surface energy,” *Journal of Adhesion Science and Technology*, vol. 29, no. 9, pp. 890–895, 2015.

[24] B. Comley, P. Harris, D. Bradshaw, and M. Harris, “Frother characterisation using dynamic surface tension measurements,” *International Journal of Mineral Processing*, vol. 64, no. 2-3, pp. 81–100, 2002.

[25] K. Loubière and G. Hébrard, “Influence of liquid surface tension (surfactants) on bubble formation at rigid and flexible orifices,” *Chemical Engineering and Processing: Process Intensification*, vol. 43, no. 11, pp. 1361–1369, 2004.

[26] R Miller, V. Fainerman, R Wüstneck, J Krägel, and D. Trukhin, “Characterisation of the initial period of protein adsorption by dynamic surface tension measurements using different drop techniques,” *Colloids and Surfaces A: Physicochemical and Engineering Aspects*, vol. 131, no. 1-3, pp. 225–230, 1998.

[27] A Goebel *et al.*, “Interfacial tension of the water/n-alkane interface,” *Langmuir*, vol. 13, no. 2, pp. 369–372, 1997.

[28] S. Harder, D. Zuck, and J. Wood, “Characterization of tablet surfaces by their critical surface-tension values,” *Journal of pharmaceutical sciences*, vol. 59, no. 12, pp. 1787–1792, 1970.

[29] A. A. Rafati and E. Ghasemian, “Experimental and theoretical study of surface tension of binary mixtures of (n-alkyl acetates+ heptane, benzene, and toluene),” *The Journal of Chemical Thermodynamics*, vol. 41, no. 3, pp. 386–391, 2009.

[30] G. Vazquez *et al.*, “Surface tension of alcohol water+ water from 20 to 50. degree. c,” *Journal of chemical and engineering data*, vol. 40, no. 3, pp. 611–614, 1995.

[31] Rolo *et al.*, “Surface tension of heptane, decane, hexadecane, eicosane, and some of their binary mixtures,” *Journal of Chemical & Engineering Data*, vol. 47, no. 6, pp. 1442–1445, 2002.

[32] J. Vijande, M. M. Pineiro, J. García, J. L. Valencia, and J. L. Legido, “Density and surface tension variation with temperature for heptane+ 1-alkanol,” *Journal of Chemical & Engineering Data*, vol. 51, no. 5, pp. 1778–1782, 2006.

[33] S. Zeppieri, J. Rodríguez, and A. López de Ramos, “Interfacial tension of alkane+ water systems,” *Journal of Chemical & Engineering Data*, vol. 46, no. 5, pp. 1086–1088, 2001.

[34] A. Alexander, “Interfacial tension, viscosity and potential changes produced by insoluble monolayers at the oil/water interface,” *Transactions of the Faraday Society*, vol. 37, pp. 117–121, 1941.

[35] J. D. Berry, M. J. Neeson, R. R. Dagastine, D. Y. Chan, and R. F. Tabor, “Measurement of surface and interfacial tension using pendant drop tensiometry,” *Journal of colloid and interface science*, vol. 454, pp. 226–237, 2015.

[36] C. Jian, Q. Liu, H. Zeng, and T. Tang, “A molecular dynamics study of the effect of asphaltenes on toluene/water interfacial tension: Surfactant or solute?” *Energy & fuels*, vol. 32, no. 3, pp. 3225–3231, 2018.

[37] D. Kwok, “The usefulness of the lifshitz–van der waals/acid–base approach for surface tension components and interfacial tensions,” *Colloids and Surfaces A: Physicochemical and Engineering Aspects*, vol. 156, no. 1-3, pp. 191–200, 1999.

[38] J. Alejandre and G. A. Chapela, “The surface tension of tip4p/2005 water model using the ewald sums for the dispersion interactions,” *The Journal of chemical physics*, vol. 132, no. 1, p. 014 701, 2010.

[39] A. Firooz *et al.*, “Surface tension and adsorption kinetics of amphiphiles in aqueous solutions: The role of carbon chain length and temperature,” *Journal of colloid and interface science*, vol. 370, no. 1, pp. 183–191, 2012.

[40] V. S. Chernyshev and M. Skliar, “Surface tension of water in the presence of perfluorocarbon vapors,” *Soft matter*, vol. 10, no. 12, pp. 1937–1943, 2014.

[41] F Hauxwell and R. Ottewill, “The adsorption of toluene vapor on water surfaces,” *Journal of Colloid and Interface Science*, vol. 28, no. 3-4, pp. 514–521, 1968.

[42] P. B. Duncan *et al.*, “Test of the epstein- plesset model for gas microparticle dissolution in aqueous media: Effect of surface tension and gas undersaturation in solution,” *Langmuir*, vol. 20, no. 7, pp. 2567–2578, 2004.

[43] Y. Bayazitoglu and G. F. Mitchell, “Experiments in acoustic levitation-surface tension measurements of deformed droplets,” *Journal of thermophysics and heat transfer*, vol. 9, no. 4, pp. 694–701, 1995.

[44] P. Feenstra, R. Judd, and D. Weaver, “A practical device for surface tension measurement in volatile fluids,” *HVAC&R Research*, vol. 7, no. 1, pp. 3–14, 2001.

[45] W. B. Tucker, “Surface tension by pendant drops,” Ph.D. dissertation, Massachusetts Institute of Technology, 1938.

[46] L. Gao and L. Zeng, “A remnant drop method for improving the uncertainty in surface tension measurements of volatile liquids using fibre drop analysis,” *Measurement Science and Technology*, vol. 14, no. 8, N50, 2003.

[47] H. Kahl, T. Wadewitz, and J. Winkelmann, “Surface tension of pure liquids and binary liquid mixtures,” *Journal of Chemical & Engineering Data*, vol. 48, no. 3, pp. 580–586, 2003.

[48] Y Rotenberg, L. Boruvka, and A. Neumann, “Determination of surface tension and contact angle from the shapes of axisymmetric fluid interfaces,” *Journal of colloid and interface science*, vol. 93, no. 1, pp. 169–183, 1983.

[49] S. Anastasiadis, J.-K. Chen, J. Koberstein, A. Siegel, J. Sohn, and J. Emerson, “The determination of interfacial tension by video image processing of pendant fluid drops,” *Journal of colloid and interface science*, vol. 119, no. 1, pp. 55–66, 1987.

[50] H. Girault, D. Schiffrin, and B. Smith, “The measurement of interfacial tension of pendant drops using a video image profile digitizer,” *Journal of colloid and interface science*, vol. 101, no. 1, pp. 257–266, 1984.

[51] P Cheng, D Li, L Boruvka, Y Rotenberg, and A. Neumann, “Automation of axisymmetric drop shape analysis for measurements of interfacial tensions and contact angles,” *Colloids and Surfaces*, vol. 43, no. 2, pp. 151–167, 1990.

[52] G Wiegand and E. Franck, “Interfacial tension between water and non-polar fluids up to 473 k and 2800 bar,” *Berichte der Bunsengesellschaft für physikalische Chemie*, vol. 98, no. 6, pp. 809–817, 1994.

[53] D. Dittmar, S Bijosono Oei, and R. Eggers, “Interfacial tension and density of ethanol in contact with carbon dioxide,” *Chemical engineering & technology*, vol. 25, no. 1, pp. 23–27, 2002.

[54] D Dittmar, R Eggers, H Kahl, and S Enders, “Measurement and modelling of the interfacial tension of triglyceride mixtures in contact with dense gases,” *Chemical Engineering Science*, vol. 57, no. 3, pp. 355–363, 2002.

[55] N. Pallas and B. Pethica, “The surface tension of water,” *Colloids and Surfaces*, vol. 6, no. 3, pp. 221–227, 1983.

[56] F. Jufu, L. Buqiang, and W. Zihao, “Estimation of fluid-fluid interfacial tensions of multicomponent mixtures,” *Chemical Engineering Science*, vol. 41, no. 10, pp. 2673–2679, 1986.

[57] I. Blute, R. J. Pugh, J. van de Pas, and I. Callaghan, “Industrial manufactured silica nanoparticle sols. 2: Surface tension, particle concentration, foam generation and stability,” *Colloids and Surfaces A: Physicochemical and Engineering Aspects*, vol. 337, no. 1-3, pp. 127–135, 2009.

[58] M. Ikegami, T. E. Weaver, S. N. Grant, and J. A. Whitsett, “Pulmonary surfactant surface tension influences alveolar capillary shape and oxygenation,” *American journal of respiratory cell and molecular biology*, vol. 41, no. 4, pp. 433–439, 2009.

[59] A. Krishnan, A. Wilson, J. Sturgeon, C. A. Siedlecki, and E. A. Vogler, “Liquid–vapor interfacial tension of blood plasma, serum and purified protein constituents thereof,” *Biomaterials*, vol. 26, no. 17, pp. 3445–3453, 2005.

[60] R. Gholami and N. Fakhari, “Support vector machine: Principles, parameters, and applications,” in *Handbook of Neural Computation*, Elsevier, 2017, pp. 515–535.

[61] C Chalbaud, M Robin, J. Lombard, F Martin, P Egermann, and H Bertin, “Interfacial tension measurements and wettability evaluation for geological co2 storage,” *Advances in water resources*, vol. 32, no. 1, pp. 98–109, 2009.

[62] N. Spycher and K. Pruess, “A phase-partitioning model for co 2–brine mixtures at elevated temperatures and pressures: Application to co 2-enhanced geothermal systems,” *Transport in porous media*, vol. 82, no. 1, pp. 173–196, 2010.

[63] G. Kumar and K. N. Prabhu, “Review of non-reactive and reactive wetting of liquids on surfaces,” *Advances in colloid and interface science*, vol. 133, no. 2, pp. 61–89, 2007.

[64] A. J. Milling, *Surface characterization methods: principles, techniques, and applications*. CRC Press, 1999, vol. 87.

[65] O. Voinov, “Hydrodynamics of wetting,” *Fluid dynamics*, vol. 11, no. 5, pp. 714–721, 1976.

[66] L. Tanner, “The spreading of silicone oil drops on horizontal surfaces,” *Journal of Physics D: Applied Physics*, vol. 12, no. 9, p. 1473, 1979.

[67] D. Bonn, J. Eggers, J. Indekeu, J. Meunier, and E. Rolley, “Wetting and spreading,” *Reviews of modern physics*, vol. 81, no. 2, p. 739, 2009.

[68] Y. Gu and D. Li, “Liquid drop spreading on solid surfaces at low impact speeds,” *Colloids and Surfaces A: Physicochemical and Engineering Aspects*, vol. 163, no. 2-3, pp. 239–245, 2000.

[69] M. Arif, A. Z. Al-Yaseri, A. Barifcani, M. Lebedev, and S. Iglauer, “Impact of pressure and temperature on co2–brine–mica contact angles and co2–brine interfacial tension: Implications for carbon geo-sequestration,” *Journal of colloid and interface science*, vol. 462, pp. 208–215, 2016.

[70] W. A. Zisman, “Relation of the equilibrium contact angle to liquid and solid constitution,” in, ACS Publications, 1964.

[71] T. Chau, W. Bruckard, P. Koh, and A. Nguyen, “A review of factors that affect contact angle and implications for flotation practice,” *Advances in colloid and interface science*, vol. 150, no. 2, pp. 106–115, 2009.

[72] R. N. Wenzel, “Resistance of solid surfaces to wetting by water,” *Industrial & Engineering Chemistry*, vol. 28, no. 8, pp. 988–994, 1936.

[73] T Young, “An assay on the cohesion of fluids. philos,” *Trans. R. Soc. London. 1805, 95*, vol. 65, 1805.

[74] A. Cassie and S Baxter, “Wettability of porous surfaces,” *Transactions of the Faraday society*, vol. 40, pp. 546–551, 1944.

[75] E. Carter and D. Jones, “An experimental test of the validity of antonow’s rule,” *Transactions of the Faraday Society*, vol. 30, pp. 1027–1038, 1934.

[76] S. Baxter and A. Cassie, “8—the water repellency of fabrics and a new water repellency test,” *Journal of the Textile Institute Transactions*, vol. 36, no. 4, T67–T90, 1945.

[77] A. Marmur, “Equilibrium contact angles: Theory and measurement,” *Colloids and Surfaces A: Physicochemical and Engineering Aspects*, vol. 116, no. 1-2, pp. 55–61, 1996.

[78] C. Van Oss, R. Giese, and W Wu, “On the degree to which the contact angle is affected by the adsorption onto a solid surface of vapor molecules originating from the liquid drop,” *Journal of dispersion science and technology*, vol. 19, no. 6-7, pp. 1221–1236, 1998.

[79] L. Chen and E. Bonaccurso, “Effects of surface wettability and liquid viscosity on the dynamic wetting of individual drops,” *Physical Review E*, vol. 90, no. 2, p. 022 401, 2014.

[80] F. Villa, M. Marengo, and J. De Coninck, “A new model to predict the influence of surface temperature on contact angle,” *Scientific reports*, vol. 8, no. 1, pp. 1–10, 2018.

[81] J.-W. Jung and J. Wan, “Supercritical co2 and ionic strength effects on wettability of silica surfaces: Equilibrium contact angle measurements,” *Energy & Fuels*, vol. 26, no. 9, pp. 6053–6059, 2012.

[82] N. K. Mishra, Y. Zhang, and A. Ratner, “Effect of chamber pressure on spreading and splashing of liquid drops upon impact on a dry smooth stationary surface,” *Experiments in fluids*, vol. 51, no. 2, pp. 483–491, 2011.

[83] L. Chen, G. K. Auernhammer, and E. Bonaccurso, “Short time wetting dynamics on soft surfaces,” *Soft Matter*, vol. 7, no. 19, pp. 9084–9089, 2011.

[84] J. C. Bird, S. Mandre, and H. A. Stone, “Short-time dynamics of partial wetting,” *Physical review letters*, vol. 100, no. 23, p. 234 501, 2008.

[85] A. L. Yarin, “Drop impact dynamics: Splashing, spreading, receding, bouncing…,” *Annu. Rev. Fluid Mech.*, vol. 38, pp. 159–192, 2006.

[86] V. Bergeron, D. Bonn, J. Y. Martin, and L. Vovelle, “Controlling droplet deposition with polymer additives,” *Nature*, vol. 405, no. 6788, pp. 772–775, 2000.

[87] G. Zhang, M. A. Quetzeri-Santiago, C. A. Stone, L. Botto, and J. R. Castrejón-Pita, “Droplet impact dynamics on textiles,” *Soft matter*, vol. 14, no. 40, pp. 8182–8190, 2018.

[88] J. Liu, C. Zhu, K. Liu, Y. Jiang, Y. Song, J. S. Francisco, X. C. Zeng, and J. Wang, “Distinct ice patterns on solid surfaces with various wettabilities,” *Proceedings of the National Academy of Sciences*, vol. 114, no. 43, pp. 11 285–11 290, 2017.

[89] C. D. Bain, E. B. Troughton, Y. T. Tao, J. Evall, G. M. Whitesides, and R. G. Nuzzo, “Formation of monolayer films by the spontaneous assembly of organic thiols from solution onto gold,” *Journal of the American Chemical Society*, vol. 111, no. 1, pp. 321–335, 1989.

[90] A. Muslihati, H. Basri, M. Z. Sahdan, K. M. Wibowo, N. Rosni, and M. Morsin, “The formation and organization of self-assembled monolayer (sam) for escherichia coli detection: A,” 2020.

[91] S Varatharajan, S. Berchmans, and V Yegnaraman, “Tailoring self-assembled monolayers at the electrochemical interface,” *Journal of Chemical Sciences*, vol. 121, no. 5, pp. 665–674, 2009.

[92] W Muller, H Ringsdorf, E Rump, G Wildburg, X Zhang, L Angermaier, W. Knoll, M Liley, and J Spinke, “Attempts to mimic docking processes of the immune system: Recognition-induced formation of protein multilayers,” *Science*, vol. 262, no. 5140, pp. 1706–1708, 1993.

[93] M. Mrksich, G. B. Sigal, and G. M. Whitesides, “Surface plasmon resonance permits in situ measurement of protein adsorption on self-assembled monolayers of alkanethiolates on gold,” *Langmuir*, vol. 11, no. 11, pp. 4383–4385, 1995.

[94] T. W. Schneider and D. A. Buttry, “Electrochemical quartz crystal microbalance studies of adsorption and desorption of self-assembled monolayers of alkyl thiols on gold,” *Journal of the American Chemical Society*, vol. 115, no. 26, pp. 12 391–12 397, 1993.

[95] K. Shimazu, I. Yagi, Y. Sato, and K. Uosaki, “In situ and dynamic monitoring of the self-assembling and redox processes of a ferrocenylundecanethiol monolayer by electrochemical quartz crystal microbalance,” *Langmuir*, vol. 8, no. 5, pp. 1385–1387, 1992.

[96] J. M. Brockman, A. G. Frutos, and R. M. Corn, “A multistep chemical modification procedure to create dna arrays on gold surfaces for the study of protein- dna interactions with surface plasmon resonance imaging,” *Journal of the American Chemical Society*, vol. 121, no. 35, pp. 8044–8051, 1999.

[97] A. Ulman, “Formation and structure of self-assembled monolayers,” *Chemical reviews*, vol. 96, no. 4, pp. 1533–1554, 1996.

[98] I. Taniguchi, K. Toyosawa, H. Yamaguchi, and K. Yasukouchi, “Reversible electrochemical reduction and oxidation of cytochrome c at a bis (4-pyridyl) disulphide-modified gold electrode,” *Journal of the Chemical Society, Chemical Communications*, no. 18, pp. 1032–1033, 1982.

[99] R. G. Nuzzo and D. L. Allara, “Adsorption of bifunctional organic disulfides on gold surfaces,” *Journal of the American Chemical Society*, vol. 105, no. 13, pp. 4481–4483, 1983.

[100] P. E. Laibinis, G. M. Whitesides, D. L. Allara, Y. T. Tao, A. N. Parikh, and R. G. Nuzzo, “Comparison of the structures and wetting properties of self-assembled monolayers of n-alkanethiols on the coinage metal surfaces, copper, silver, and gold,” *Journal of the American Chemical Society*, vol. 113, no. 19, pp. 7152–7167, 1991.

[101] M. M. Walczak, C. Chung, S. M. Stole, C. A. Widrig, and M. D. Porter, “Structure and interfacial properties of spontaneously adsorbed n-alkanethiolate monolayers on evaporated silver surfaces,” *Journal of the American Chemical society*, vol. 113, no. 7, pp. 2370–2378, 1991.

[102] D. Taneichi, R. Haneda, and K. Aramaki, “A novel modification of an alkanethiol self-assembled monolayer with alkylisocyanates to prepare protective films against copper corrosion,” *Corrosion science*, vol. 43, no. 8, pp. 1589–1600, 2001.

[103] J. C. Love, D. B. Wolfe, R. Haasch, M. L. Chabinyc, K. E. Paul, G. M. Whitesides, and R. G. Nuzzo, “Formation and structure of self-assembled monolayers of alkanethiolates on palladium,” *Journal of the American Chemical Society*, vol. 125, no. 9, pp. 2597–2609, 2003.

[104] Z. Li, S.-C. Chang, and R. S. Williams, “Self-assembly of alkanethiol molecules onto platinum and platinum oxide surfaces,” *Langmuir*, vol. 19, no. 17, pp. 6744–6749, 2003.

[105] D. Y. Petrovykh, H. Kimura-Suda, A. Opdahl, L. J. Richter, M. J. Tarlov, and L. J. Whitman, “Alkanethiols on platinum: Multicomponent self-assembled monolayers,” *Langmuir*, vol. 22, no. 6, pp. 2578–2587, 2006.

[106] C. D. Bain, H. A. Biebuyck, and G. M. Whitesides, "Comparison of self-assembled monolayers on gold: Coadsorption of thiols and disulfides," *Langmuir*, vol. 5, no. 3, pp. 723–727, 1989.

[107] G. A. Somorjai, *Chemistry in two dimensions: surfaces.* Cornell University Press, 1981.

[108] S. Stranick, S. Atre, A. Parikh, M. Wood, D. Allara, N Winograd, and P. Weiss, "Nanometer-scale phase separation in mixed composition self-assembled monolayers," *Nanotechnology*, vol. 7, no. 4, p. 438, 1996.

[109] C. D. Bain and G. M. Whitesides, "Modeling organic surfaces with self-assembled monolayers," *Angewandte Chemie*, vol. 101, no. 4, pp. 522–528, 1989.

[110] K. Tamada, M. Hara, H. Sasabe, and W. Knoll, "Surface phase behavior of n-alkanethiol self-assembled monolayers adsorbed on au (111): An atomic force microscope study," *Langmuir*, vol. 13, no. 6, pp. 1558–1566, 1997.

[111] F. Bensebaa, R. Voicu, L. Huron, T. H. Ellis, and E. Kruus, "Kinetics of formation of long-chain n-alkanethiolate monolayers on polycrystalline gold," *Langmuir*, vol. 13, no. 20, pp. 5335–5340, 1997.

[112] R. Yamada, H. Sakai, and K. Uosaki, "Solvent effect on the structure of the self-assembled monolayer of alkanethiol," *Chemistry letters*, vol. 28, no. 7, pp. 667–668, 1999.

[113] M. Kawasaki, T. Sato, T. Tanaka, and K. Takao, "Rapid self-assembly of alkanethiol monolayers on sputter-grown au (111)," *Langmuir*, vol. 16, no. 4, pp. 1719–1728, 2000.

[114] C. D. Bain and G. M. Whitesides, "Depth sensitivity of wetting: Monolayers of. omega.-mercapto ethers on gold," *Journal of the American Chemical Society*, vol. 110, no. 17, pp. 5897–5898, 1988.

[115] P. E. Laibinis and G. M. Whitesides, ". omega.-terminated alkanethiolate monolayers on surfaces of copper, silver, and gold have similar wettabilities," *Journal of the American Chemical Society*, vol. 114, no. 6, pp. 1990–1995, 1992.

[116] K. L. Prime and G. M. Whitesides, "Self-assembled organic monolayers: Model systems for studying adsorption of proteins at surfaces," *Science*, pp. 1164–1167, 1991.

[117] J. Sagiv, "Organized monolayers by adsorption. 1. formation and structure of oleophobic mixed monolayers on solid surfaces," *Journal of the American Chemical Society*, vol. 102, no. 1, pp. 92–98, 1980.

[118] C. Duan and M. E. Meyerhoff, "Separation-free sandwich enzyme immunoassays using microporous gold electrodes and self-assembled monolayer/immobilized capture antibodies," *Analytical Chemistry*, vol. 66, no. 9, pp. 1369–1377, 1994.

[119] C. Duschl, M. Liley, G. Corradin, and H. Vogel, “Biologically addressable monolayer structures formed by templates of sulfur-bearing molecules,” *Biophysical journal*, vol. 67, no. 3, pp. 1229–1237, 1994.

[120] D. Feldheim and C. Keating, “Self-assembly of single electron transistors and related devices,” *Chemical Society Reviews*, vol. 27, no. 1, pp. 1–12, 1998.

[121] A. M. Becka and C. J. Miller, “Electrochemistry at. omega.-hydroxy thiol coated electrodes. 4. comparison of the double layer at. omega.-hydroxy thiol and alkanethiol monolayer coated au electrodes,” *The Journal of Physical Chemistry*, vol. 97, no. 23, pp. 6233–6239, 1993.

[122] S. Stranick, A. Parikh, Y.-T. Tao, D. Allara, and P. Weiss, “Phase separation of mixed-composition self-assembled monolayers into nanometer scale molecular domains,” *The Journal of Physical Chemistry*, vol. 98, no. 31, pp. 7636–7646, 1994.

[123] A. R. Lokanathan, S. Zhang, V. R. Regina, M. A. Cole, R. Ogaki, M. Dong, F. Besenbacher, R. L. Meyer, and P. Kingshott, “Mixed poly (ethylene glycol) and oligo (ethylene glycol) layers on gold as nonfouling surfaces created by backfilling,” *Biointerphases*, vol. 6, no. 4, pp. 180–188, 2011.

[124] C. D. Bain and G. M. Whitesides, “Correlations between wettability and structure in monolayers of alkanethiols adsorbed on gold,” *Journal of the American Chemical Society*, vol. 110, no. 11, pp. 3665–3666, 1988.

[125] B. Pignataro, A Licciardello, S Cataldo, and G. Marletta, “Spm and tof-sims investigation of the physical and chemical modification induced by tip writing of self-assembled monolayers,” *Materials Science and Engineering: C*, vol. 23, no. 1-2, pp. 7–12, 2003.

[126] A.-A. Dhirani, R. W. Zehner, R. P. Hsung, P. Guyot-Sionnest, and L. R. Sita, “Self-assembly of conjugated molecular rods: A high-resolution stm study,” *Journal of the American Chemical Society*, vol. 118, no. 13, pp. 3319–3320, 1996.

[127] V. I. Silin, H. Wieder, J. T. Woodward, G. Valincius, A Offenhausser, and A. L. Plant, “The role of surface free energy on the formation of hybrid bilayer membranes,” *Journal of the American Chemical Society*, vol. 124, no. 49, pp. 14 676–14 683, 2002.

[128] P Ansorena, A Zuzuarregui, E Pérez-Lorenzo, M Mujika, and S Arana, “Comparative analysis of qcm and spr techniques for the optimization of immobilization sequences,” *Sensors and Actuators B: Chemical*, vol. 155, no. 2, pp. 667–672, 2011.

[129] J. Lee, B.-J. Jung, J.-I. Lee, H. Y. Chu, L.-M. Do, and H.-K. Shim, “Modification of an ito anode with a hole-transporting sam for improved oled device characteristics,” *Journal of Materials Chemistry*, vol. 12, no. 12, pp. 3494–3498, 2002.

[130] H Hantsche, "Comparison of basic principles of the surface-specific analytical methods: Aes/sam, esca (xps), sims, and iss with x-ray microanalysis, and some applications in research and industry," *Scanning*, vol. 11, no. 6, pp. 257–280, 1989.

[131] K. Siegbahn, "Esca: Atomic, molecular and solid state structure studies by means of electron spectroscopy; pres. to the royal society of sciences of uppsala, dec. 3rd, 1965," *Nova Acta Regiae Societatis Scientiarum Upsaliensis*, 1967.

[132] D. Briggs, *Handbook of X-ray and ultraviolet photoelectron spectroscopy.* Heyden, 1977.

[133] M. Benelmekki and A. Erbe, "Nanostructured thin films–background, preparation and relation to the technological revolution of the 21st century," in *Frontiers of Nanoscience*, vol. 14, Elsevier, 2019, pp. 1–34.

[134] X.-q. Li and W.-x. Zhang, "Sequestration of metal cations with zerovalent iron nanoparticles a study with high resolution x-ray photoelectron spectroscopy (hr-xps)," *The Journal of Physical Chemistry C*, vol. 111, no. 19, pp. 6939–6946, 2007.

[135] R. Ferrando, *Structure and properties of nanoalloys.* Elsevier, 2016.

[136] N. P. Cheremisinoff, *Condensed encyclopedia of polymer engineering terms.* Butterworth-Heinemann, 2001.

[137] U. Shanker, C. M. Hussain, and M. Rani, *Green Functionalized Nanomaterials for Environmental Applications.* Elsevier, 2021.

[138] Y. Pomeau, "Surface tension: From fundamental principles to applications in liquids and in solids," Ph.D. dissertation, Warsaw School of Statistical Physics, 2013.

[139] B. Franklin and W. Brownrigg, "Xliv. of the stilling of waves by means of oil. extracted from sundry letters between benjamin franklin, ll. dfrs william brownrigg, mdfrs and the reverend mr. farish," *Philosophical Transactions of the Royal Society of London*, no. 64, pp. 445–460, 1774.

[140] L. Rayleigh and A Pockels, "Surface tension," *Nature*, vol. 43, no. 1115, p. 437, 1891.

[141] L. Rayleigh *et al.*, "On the capillary phenomena of jets," *Proc. R. Soc. London*, vol. 29, no. 196-199, pp. 71–97, 1879.

[142] D. Berthelot, "Sur le mélange des gaz," *Compt. Rendus*, vol. 126, pp. 1703–1706, 1898.

[143] A Dupre, *Théorie mécanique de la chaleur (the mechanical theory of heat). gauthier-villan, paris*, 1869.

[144] K.-Y. Law and H. Zhao, *Surface wetting: characterization, contact angle, and fundamentals.* Springer International Publishing Basel, Switzerland, 2016.

[145] A. T. Tyowua, *Liquid Marbles: formation, characterization, and applications.* CRC Press, 2018.

[146] J Kestin and E. Mason, “Transport properties in gases (comparison between theory and experiment),” in *AIP Conference Proceedings*, American Institute of Physics, vol. 11, 1973, pp. 137–192.

[147] G. Antonow, “Sur la tension superficielle des solutions dans la zone critique,” *Journal de Chimie Physique*, vol. 5, pp. 364–371, 1907.

[148] R Loman and N. Zwikker, “The validity of antonow’s rule for the solid-liquid interface, and the consequent measurement of the surface-tension of solids,” *Physica*, vol. 1, no. 7-12, pp. 1181–1201, 1934.

[149] R. J. Good, “Contact angle, wetting, and adhesion: A critical review,” *Journal of adhesion science and technology*, vol. 6, no. 12, pp. 1269–1302, 1992.

[150] C. Van Oss, R. Good, and M. Chaudhury, “The role of van der waals forces and hydrogen bonds in “hydrophobic interactions” between biopolymers and low energy surfaces,” *Journal of colloid and Interface Science*, vol. 111, no. 2, pp. 378–390, 1986.

[151] J. Bradley, “Determining the dispersive and polar contributions to the surface tension of water-based printing ink as a function of surfactant surface excess,” *Journal of Physics D: Applied Physics*, vol. 38, no. 12, p. 2045, 2005.

[152] M. Wang, X. Xu, Y. Ge, P. Dong, R. Baines, P. M. Ajayan, M. Ye, and J. Shen, “Surface tension components ratio: An efficient parameter for direct liquid phase exfoliation,” *ACS applied materials & interfaces*, vol. 9, no. 10, pp. 9168–9175, 2017.

[153] W. R. Good, “A comparison of contact angle interpretations,” *Journal of Colloid and Interface Science*, vol. 44, no. 1, pp. 63–71, 1973.

[154] J. Spelt and A. Neumann, “Solid surface tension: The equation of state approach and the theory of surface tension components. theoretical and conceptual considerations,” *Langmuir*, vol. 3, no. 4, pp. 588–591, 1987.

[155] C. Van Oss, “Acid—base interfacial interactions in aqueous media,” *Colloids and Surfaces A: Physicochemical and Engineering Aspects*, vol. 78, pp. 1–49, 1993.

[156] M. Saito and A. Yabe, “Dispersion and polar force components of surface tension of oily soils,” *Textile Research Journal*, vol. 54, no. 1, pp. 18–22, 1984.

[157] K. Gebhardt, *Grundlagen der physikalischen Chemie von Grenzflächen und Methoden zur Bestimmung grenzflächenenergetischer Probleme.* IGB, 1982.

[158] D. Kwok, Y Lee, and A. Neumann, “Evaluation of the lifshitz- van der waals/acid-base approach to determine interfacial tensions. 2. interfacial tensions of liquid-liquid systems,” *Langmuir*, vol. 14, no. 9, pp. 2548–2553, 1998.

[159] J. J. Jasper, “The surface tension of pure liquid compounds,” *Journal of physical and chemical reference data*, vol. 1, no. 4, pp. 841–1010, 1972.

[160] J. Andreas, E. Hauser, and W. Tucker, “Boundary tension by pendant drops1,” *The Journal of Physical Chemistry*, vol. 42, no. 8, pp. 1001–1019, 2002.

[161] B. Chen *et al.*, "Vapor- liquid interfacial properties of mutually saturated water/1-butanol solutions," *Journal of the American Chemical Society*, vol. 124, no. 41, pp. 12 232–12 237, 2002.

[162] W. D. Harkins, E. C. Davies, and G. L. Clark, "The orientation of molecules in the surfaces of liquids, the energy relations at surfaces, solubility, adsorption, emulsification, molecular association, and the effect of acids and bases on interfacial tension. 1 (surface energy vi.)," *Journal of the American Chemical Society*, vol. 39, no. 4, pp. 541–596, 1917.

[163] R. M. Townsend, J. Gryko, and S. A. Rice, "Structure of the liquid–anapor interface of water," *The Journal of chemical physics*, vol. 82, no. 9, pp. 4391–4392, 1985.

[164] C. Stanners, Q Du, R. Chin, P Cremer, G. A. Somorjai, and Y.-R. Shen, "Polar ordering at the liquid-vapor interface of n-alcohols (c1-c8)," *Chemical physics letters*, vol. 232, no. 4, pp. 407–413, 1995.

[165] D Papaioannou and C Panayiotou, "Surface tension of binary liquid mixtures," *Journal of colloid and interface science*, vol. 130, no. 2, pp. 432–438, 1989.

[166] B. Chen, J. I. Siepmann, K. J. Oh, and M. L. Klein, "Simulating vapor–liquid nucleation of n-alkanes," *The Journal of chemical physics*, vol. 116, no. 10, pp. 4317–4329, 2002.

[167] A Aspée and E. Lissi, "Interfacial free energies and surface areas of cycloalkanols and α, ω-alkanediols at the air-water interface," *Journal of colloid and interface science*, vol. 205, no. 2, pp. 482–488, 1998.

[168] T. Klein, J. Cui, A. Kalantar, J. Chen, M. H. Rausch, T. M. Koller, and A. P. Froba, "Viscosity and surface tension of branched alkanes 2-methylnonane and 4-methylnonane," *Journal of Chemical & Engineering Data*, vol. 63, no. 8, pp. 2833–2839, 2018.

[169] C. Timmons and W. Zisman, "The effect of liquid structure on contact angle hysteresis," *Journal of Colloid and Interface Science*, vol. 22, no. 2, pp. 165–171, 1966.

[170] Y. Son, C. Kim, D. H. Yang, and D. J. Ahn, "Spreading of an inkjet droplet on a solid surface with a controlled contact angle at low weber and reynolds numbers," *Langmuir*, vol. 24, no. 6, pp. 2900–2907, 2008.

[171] N. R. Morrow, "The effects of surface roughness on contact: Angle with special reference to petroleum recovery," *Journal of Canadian Petroleum Technology*, vol. 14, no. 04, 1975.

[172] M. Sakai, T. Yanagisawa, A. Nakajima, Y. Kameshima, and K. Okada, "Effect of surface structure on the sustainability of an air layer on superhydrophobic coatings in a water- ethanol mixture," *Langmuir*, vol. 25, no. 1, pp. 13–16, 2009.

[173] S. H. Wang, Z. Y. Cai, M. Z. Li, and Y. W. Lan, "Numerical analysis of the multi-point stretch forming process of aircraft outer skin part," in *Advanced Materials Research*, Trans Tech Publ, vol. 154, 2011, pp. 1068–1072.

[174] G. Galileo, *Discorso...: intorno alle cose, che stanno in sù l'acqua, ò che in quella si muouono*. C. Giunti.

[175] R. Finn, "Capillary surface interfaces," *Notices of the AMS*, vol. 46, no. 7, pp. 770–781, 1999.

[176] D. H. Bangham and R. I. Razouk, "Adsorption and the wettability of solid surfaces," *Trans. Faraday Soc.*, vol. 33, pp. 1459–1463, 0 1937.

[177] M. D. Porter, T. B. Bright, D. L. Allara, and C. E. Chidsey, "Spontaneously organized molecular assemblies. 4. structural characterization of n-alkyl thiol monolayers on gold by optical ellipsometry, infrared spectroscopy, and electrochemistry," *Journal of the American Chemical Society*, vol. 109, no. 12, pp. 3559–3568, 1987.

[178] A. Ahmed, R. Sanedrin, T. Willers, and P. R. Waghmare, "The effect of dynamic wetting pressure on contact angle measurements," *Journal of Colloid and Interface Science*, vol. 608, pp. 1086–1093, 2022.

[179] D. A. Pearlman and P. A. Kollman, "Evaluating the assumptions underlying force field development and application using free energy conformational maps for nucleosides," *Journal of the American Chemical Society*, vol. 113, no. 19, pp. 7167–7177, 1991.

[180] J. Gassan, V. S. Gutowski, and A. K. Bledzki, "About the surface characteristics of natural fibres," *Macromolecular materials and engineering*, vol. 283, no. 1, pp. 132–139, 2000.

[181] J. Hah, M. Sulkis, M. Kang, Z. Sun, J. Kim, K.-S. Moon, M. O. Reese, and C. P. Wong, "Surface modification of backsheets using coupling agents for roll-to-roll processed thin-film solar photovoltaic (pv) module packaging application," *ACS Applied Materials & Interfaces*, vol. 13, no. 1, pp. 1682–1692, 2020.

[182] X. Bulliard, A. Benayad, S.-G. Ihn, S. Yun, J.-H. Park, W. Choi, Y. S. Choi, and Y. Kim, "Autocatalytic effect of amine-terminated precursors in mixed self-assembled monolayers," *RSC advances*, vol. 3, no. 4, pp. 1112–1118, 2013.

[183] J. Kovac, "Surface characterization of polymers by xps and sims techniques," *Mater. tehnol*, vol. 45, pp. 191–197, 2011.

[184] Y. Cheng, A. Barras, S. Lu, W. Xu, S. Szunerits, and R. Boukherroub, "Fabrication of superhydrophobic/superoleophilic functionalized reduced graphene oxide/polydopamine/pfdt membrane for efficient oil/water separation," *Separation and Purification Technology*, vol. 236, p. 116 240, 2020.

[185] Y. Ge and J. E. Whitten, "Interfacial electronic properties of thiophene and sexithiophene adsorbed on a fluorinated alkanethiol monolayer," *The Journal of Physical Chemistry C*, vol. 112, no. 4, pp. 1174–1182, 2008.

[186] S. Ravi, S. Zhang, Y.-R. Lee, K.-K. Kang, J.-M. Kim, J.-W. Ahn, and W.-S. Ahn, "Edta-functionalized kcc-1 and kit-6 mesoporous silicas for nd3+ ion recovery from aqueous solutions," *Journal of Industrial and Engineering Chemistry*, vol. 67, pp. 210–218, 2018.

[187] C.-a. Tao, J. Wang, S. Qin, Y. Lv, Y. Long, H. Zhu, and Z. Jiang, "Fabrication of ph-sensitive graphene oxide–drug supramolecular hydrogels as controlled release systems," *Journal of Materials Chemistry*, vol. 22, no. 47, pp. 24 856–24 861, 2012.

[188] M. Zatoń, B. Prélot, N. Donzel, J. Rozière, and D. J. Jones, "Migration of ce and mn ions in pemfc and its impact on pfsa membrane degradation," *Journal of The Electrochemical Society*, vol. 165, no. 6, F3281, 2018.

[189] G. Greczynski and L. Hultman, "C 1s peak of adventitious carbon aligns to the vacuum level: Dire consequences for material's bonding assignment by photoelectron spectroscopy," *ChemPhysChem*, vol. 18, no. 12, p. 1507, 2017.

[190] C.-Y. Chen, K.-Y. Wu, Y.-C. Chao, H.-W. Zan, H.-F. Meng, and Y.-T. Tao, "Concomitant tuning of metal work function and wetting property with mixed self-assembled monolayers," *Organic Electronics*, vol. 12, no. 1, pp. 148–153, 2011.

[191] T. Kakiuchi, M. Iida, N. Gon, D. Hobara, S.-i. Imabayashi, and K. Niki, "Miscibility of adsorbed 1-undecanethiol and 11-mercaptoundecanoic acid species in binary self-assembled monolayers on au (111)," *Langmuir*, vol. 17, no. 5, pp. 1599–1603, 2001.

[192] D. Hobara, M. Ota, S.-i. Imabayashi, K. Niki, and T. Kakiuchi, "Phase separation of binary self-assembled thiol monolayers composed of 1-hexadecanethiol and 3-mercaptopropionic acid on au (111) studied by scanning tunneling microscopy and cyclic voltammetry," *Journal of electroanalytical chemistry*, vol. 444, no. 1, pp. 113–119, 1998.

[193] O. V. Bueno, J. Benítez, and M. A. San-Miguel, "Understanding segregation processes in sams formed by mixtures of hydroxylated and non-hydroxylated fatty acids," *RSC advances*, vol. 9, no. 67, pp. 39 252–39 263, 2019.

[194] M. B. Haddada, J. Blanchard, S. Casale, J.-M. Krafft, A. Vallée, C. Méthivier, and S. Boujday, "Optimizing the immobilization of gold nanoparticles on functionalized silicon surfaces: Amine-vs thiol-terminated silane," *Gold Bulletin*, vol. 46, no. 4, pp. 335–341, 2013.

[195] H. Wang, S. Chen, L. Li, and S. Jiang, "Improved method for the preparation of carboxylic acid and amine terminated self-assembled monolayers of alkanethiolates," *Langmuir*, vol. 21, no. 7, pp. 2633–2636, 2005.

[196] Y. Yokota, T. Yamada, and M. Kawai, "Ion-pair formation between ferrocene-terminated self-assembled monolayers and counteranions studied by force measurements," *The Journal of Physical Chemistry C*, vol. 115, no. 14, pp. 6775–6781, 2011.

[197] N. Rathod and S. G. Hatzikiriakos, "The effect of surface energy of boron nitride on polymer processability," *Polymer Engineering & Science*, vol. 44, no. 8, pp. 1543–1550, 2004.

[198] B Saha, E Liu, S. Tor, N. Khun, D. Hardt, and J. Chun, "Anti-sticking behavior of dlc-coated silicon micro-molds," *Journal of micromechanics and microengineering*, vol. 19, no. 10, p. 105 025, 2009.

[199] M. Annamalai, K. Gopinadhan, S. A. Han, S. Saha, H. J. Park, E. B. Cho, B. Kumar, A. Patra, S.-W. Kim, and T Venkatesan, "Surface energy and wettability of van der waals structures," *Nanoscale*, vol. 8, no. 10, pp. 5764–5770, 2016.

[200] B Jańczuk *et al.*, "Wettability and surface tension of fluorite," *Colloids and Surfaces A: Physicochemical and Engineering Aspects*, vol. 75, pp. 163–168, 1993.

[201] G. Levitin, C. Timmons, and D. W. Hess, "Photoresist and etch residue removal: Effect of surface energy and interfacial tension," *Journal of the Electrochemical Society*, vol. 153, no. 7, G712, 2006.

[202] A. Carré, "Polar interactions at liquid/polymer interfaces," *Journal of Adhesion Science and Technology*, vol. 21, no. 10, pp. 961–981, 2007.

[203] D. Papakonstantinou, E. Amanatides, D. Mataras, V. Ioannidis, and P. Nikolopoulos, "Improved surface energy analysis for plasma treated pet films," *Plasma Processes and Polymers*, vol. 4, no. S1, S1057–S1062, 2007.

[204] A. Michiardi, C. Aparicio, B. D. Ratner, J. A. Planell, and J. Gil, "The influence of surface energy on competitive protein adsorption on oxidized niti surfaces," *Biomaterials*, vol. 28, no. 4, pp. 586–594, 2007.

[205] A. Kozbial, Z. Li, C. Conaway, R. McGinley, S. Dhingra, V. Vahdat, F. Zhou, B. D'Urso, H. Liu, and L. Li, "Study on the surface energy of graphene by contact angle measurements," *Langmuir*, vol. 30, no. 28, pp. 8598–8606, 2014.

[206] L. Gargallo, B. Miranda, A. Leiva, H. Rıos, F. González-Nilo, and D. Radić, "Surface characterization of poly (4-vinylpyridine) quaternized with tetradecyl bromide: Effect of the degree of quaternization," *Journal of colloid and interface science*, vol. 271, no. 1, pp. 181–186, 2004.

[207] T. Senturk Parreidt, M. Schmid, and C. Hauser, "Validation of a novel technique and evaluation of the surface free energy of food," *Foods*, vol. 6, no. 4, p. 31, 2017.

[208] A. Neumann, R. Good, C. Hope, and M Sejpal, "An equation-of-state approach to determine surface tensions of low-energy solids from contact angles," *Journal of colloid and interface science*, vol. 49, no. 2, pp. 291–304, 1974.

[209] M. F. Montemor, *Smart composite coatings and membranes: Transport, structural, environmental and energy applications*. Elsevier, 2015.

[210] P.-G. De Gennes, F. Brochard-Wyart, D. Quéré, *et al.*, *Capillarity and wetting phenomena: drops, bubbles, pearls, waves*. Springer, 2004, vol. 336.

[211] J. W. Bush, "Surface tension module," *URL http://web. mit. edu/1.63/www/Lecnotes/Surfacetension*, 2004.

[212] J. Yang, J. Wu, and S. Bi, "Surface tension measurements by pendant drop method of 10 pure long-chain alkanes and alcohols for temperatures up to 573.15 k," *Journal of Chemical & Engineering Data*, 2021.

[213] J. N. Israelachvili, *Intermolecular and surface forces.* Academic press, 2011.

[214] C. E. Stauffer, "The measurement of surface tension by the pendant drop technique," *The journal of physical chemistry*, vol. 69, no. 6, pp. 1933–1938, 1965.

[215] F. Bashforth and J. C. Adams, *An attempt to test the theories of capillary action by comparing the theoretical and measured forms of drops of fluid.* University Press, 1883.

[216] J Juuza, "The pendant drop method of surface tension measurement: Equation interpolating the shape factor tables for several selected planes," *Czechoslovak Journal of Physics*, vol. 47, no. 3, pp. 351–357, 1997.

[217] E. Y. Arashiro and N. R. Demarquette, "Use of the pendant drop method to measure interfacial tension between molten polymers," *Materials Research*, vol. 2, pp. 23–32, 1999.

[218] *Drop shape analyzer-dsa100e.*

[219] N. J. Alvarez, L. M. Walker, and S. L. Anna, "A non-gradient based algorithm for the determination of surface tension from a pendant drop: Application to low bond number drop shapes," *Journal of colloid and interface science*, vol. 333, no. 2, pp. 557–562, 2009.

[220] M. K. Chaudhury, *Short-range and long-range forces in colloidal and macroscopic systems.* State University of New York at Buffalo, 1984.

[221] S. Das, J. H. Snoeijer, and D. Lohse, "Effect of impurities in description of surface nanobubbles," *Physical Review E*, vol. 82, no. 5, p. 056 310, 2010.

[222] P. R. Waghmare, S. Das, and S. K. Mitra, "Drop deposition on under-liquid low energy surfaces," *Soft Matter*, vol. 9, no. 31, pp. 7437–7447, 2013.

[223] Y. Liu, R. Ganti, H. G. Burton, X. Zhang, W. Wang, and D. Frenkel, "Microscopic marangoni flows cannot be predicted on the basis of pressure gradients," *Physical review letters*, vol. 119, no. 22, p. 224 502, 2017.

[224] X. Wang, M. Liu, D. Jing, A. Mohamad, and O. Prezhdo, "Net unidirectional fluid transport in locally heated nanochannel by thermo-osmosis," *Nano Letters*, vol. 20, no. 12, pp. 8965–8971, 2020.

[225] I. Benouaguef, N. Musunuri, E. C. Amah, D. Blackmore, I. S. Fischer, and P. Singh, "Solutocapillary marangoni flow induced in a waterbody by a solute source," *Journal of Fluid Mechanics*, vol. 922, 2021.

[226] J. K. Park, J. Ryu, B. C. Koo, S. Lee, and K. H. Kang, "How the change of contact angle occurs for an evaporating droplet: Effect of impurity and attached water films," *Soft Matter*, vol. 8, no. 47, pp. 11 889–11 896, 2012.

[227] M. Miyama, Y. Yang, T. Yasuda, T. Okuno, and H. K. Yasuda, "Static and dynamic contact angles of water on polymeric surfaces," *Langmuir*, vol. 13, no. 20, pp. 5494–5503, 1997.

[228] Y. Yuan and T. R. Lee, "Contact angle and wetting properties," in *Surface science techniques*, Springer, 2013, pp. 3–34.

[229] O. Carrier and D. Bonn, "Contact angles and the surface free energy of solids," in *Droplet Wetting and Evaporation*, Elsevier, 2015, pp. 15–23.

[230] T. Pratap and K. Patra, "Micro–nano surface texturing, characterization, and their impact on biointerfaces," in *Advanced Machining and Finishing*, Elsevier, 2021, pp. 577–610.

[231] A. Adamson, *Physical Chemistry of Surfaces, 5th Ed.* Wiley, New York., 1990.

[232] P. R. Waghmare and S. K. Mitra, "Contact angle hysteresis of microbead suspensions," *Langmuir*, vol. 26, no. 22, pp. 17 082–17 089, 2010.

[233] D. Kwok, A Leung, C. Lam, A Li, R Wu, and A. Neumann, "Low-rate dynamic contact angles on poly (methyl methacrylate) and the determination of solid surface tensions," *Journal of colloid and interface science*, vol. 206, no. 1, pp. 44–51, 1998.

[234] W. Chen, A. Y. Fadeev, M. C. Hsieh, D. Öner, J. Youngblood, and T. J. McCarthy, "Ultrahydrophobic and ultralyophobic surfaces: Some comments and examples," *Langmuir*, vol. 15, no. 10, pp. 3395–3399, 1999.

[235] H. Eral, D. t Mannetje, and J. M. Oh, "Contact angle hysteresis: A review of fundamentals and applications," *Colloid and polymer science*, vol. 291, no. 2, pp. 247–260, 2013.

[236] C. W. Extrand, "Model for contact angles and hysteresis on rough and ultraphobic surfaces," *Langmuir*, vol. 18, no. 21, pp. 7991–7999, 2002.

[237] C. Jie-Rong and T Wakida, "Studies on the surface free energy and surface structure of ptfe film treated with low temperature plasma," *Journal of applied polymer science*, vol. 63, no. 13, pp. 1733–1739, 1997.

[238] S. Wu, "Polar and nonpolar interactions in adhesion," *The Journal of Adhesion*, vol. 5, no. 1, pp. 39–55, 1973.

[239] J Schultz, C Cazeneuve, M. Shanahan, and J. Donnet, "Fibre surface energy characterization," *The Journal of Adhesion*, vol. 12, no. 3, pp. 221–231, 1981.

[240] M. Boeckl and D. Graham, "Self-assembled monolayers: Advantages of pure alkanethiols," *Material matters*, vol. 1, no. 2, pp. 3–5, 2006.

[241] L. H. Dubois, B. R. Zegarski, and R. G. Nuzzo, "Fundamental studies of microscopic wetting on organic surfaces. 2. interaction of secondary adsorbates with chemically textured organic monolayers," *Journal of the American chemical Society*, vol. 112, no. 2, pp. 570–579, 1990.

[242] S. Watcharinyanon, "Structure of self-assembled monolayers on gold studied by nexafs and photoelectron spectroscopy," Ph.D. dissertation, Karlstads universitet, 2008.

Appendix A:

A.1 Literature review

A literature overview of the solid−liquid and liquid−vapor interface has been tabulated chronologically in Table A.4.

Table A.4: Literature overview in chronological order

Year	Author	Key contribution
1612	Galileo	Recognized the wetting phenomena for the very first time [174].
1751	J. A. von Segner	Introduced theoretical concept of surface tension [138].
1774	Benjamin Franklin	Observed reduction of surface tension which resulted into wave-calming effect of oil [139].
1805	Young	Developed theory to measure contact angle of a liquid on a solid using individual surface tension [73].
1879	Lord Rayleigh	Introduced theoretical framework to measure surface tension by jet-vibration [141].
1891	Ms. Agnes Pockles	Invented a small device to measure surface tension [140].
1898	Berthelot	Published geometric mean rule of mixing based on which the theories of measurement of interfacial tension are standing [142].
1907	Antonow	Established simplest empirical relation between interfacial tension and individual surface tensions [147].
1936	Wenzel	Suggested that Young's equation is not valid for rough surfaces [72].

Continued on next page

Table A.4 – continued from previous page

Year	Author	Key contribution
1941	Alexander	Experimentally measured interfacial tension of immicible liquids using ring method [34].
1944	Cassie and Baxter	Established that Young's equation is not valid for porous surfaces [74].
1957	Girifalco and Good	Suggested mathematical theory that relates interfacial tension between two phases and the individual surface tension of those phases. [3].
1964	Fowkes	Pinpointed role of polar and nonpolar components of individual surface tension on the interfacial tension, provided at least one phase is completely nonpolar[2].
1964	Zisman	Published the method to calculate surface energy of solid using critical surface tension [70].
1969-1971	Owens and Wendt, Rabel, Kaelble	Developed mathematical formula that suggests that interfacial tension between a solid and a liquid is dependant on individual surface tension as well as polar and nonpolar components of the individual surface tension [6, 20–22].
1971	Wu	Proposed harmonic mean equation to represent polar–polar interaction between two phases [4].
1985	de Gennes	Suggested that a liquid spreads completely on a solid if the polarizability of the former is lower [7].
1986	Van Oss, Good, and Chaudhury	Introduced new definition for the components of surface tension: Lifshitz van der Waals and short range components. This is accurately applicable for inorganic combinations [150].
1989	Jańczuk *et al.*	Utilized liquid surface tension values and polar-nonpolar components to measure surface energy of solid [12].

Continued on next page

Table A.4 – continued from previous page

Year	Author	Key contribution
1993	Jańczuk *et al.*	Utilized surface tension values and polar-nonpolar components of one liquid to measure surface tension of another liquid [200].
1995	Vazquez *et al.*	Experimentally measured interfacial tension of miscible liquids [30].
1997	Goebel *et al.*	Computationally measured interfacial tension values of immiscible liquids [27].
2002	Rolo *et al.*	Compared surface tension values of miscible liquids, that are obtained experimentally and computationally [31].
2002	Chen *et al.*	Computationally measured surface tension of a liquid in saturated miscible vapor [161].
2004	Duncan *et al.*	Experimentally measured surface tension value of a liquid in saturated immiscible vapor [42].
2012	Firooz *et al.*	Experimentally measured surface tension value of a liquid in miscible vapor of variable concentrations [39].

A.2 Pendant Drop Method for Surface Tension Measurement

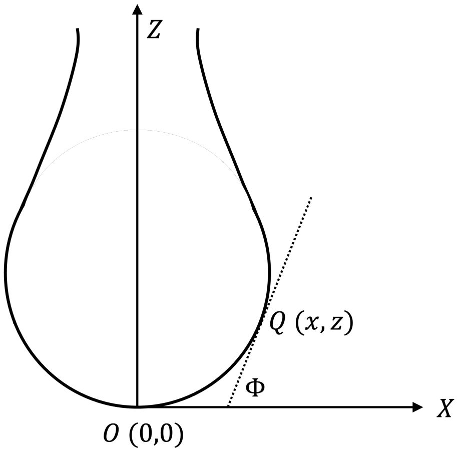

Figure A.1: Schematic representation of the contour of a pendant drop. *O* is the lowest point (apex) of the drop, and *Q (x,z)* sits on an arbitrary location on the surface.

The surface tension of the liquid-fluid combinations reported in this study were measured by DSA 100E (KR*Ü*SS GmbH) utilizing the integrated image analysis software, ADVANCE. To measure the surface tension, first a pendant drop is generated in a controlled environment. The image acquisition unit of DSA 100E records the time-evolution of the drop shape and subsequently measures the surface tension, γ using the pendant drop technique. Once γ attains a steady state value (i.e., $d\gamma/dt \rightarrow 0$), it is considered to be the equilibrium surface tension, γ_{eq}. The pendant drop method of surface tension measurement is elaborated in subsequent sections.

Pendant drop method: The interfacial curvature of a drop or bubble is a manifestation of the pressure imbalance, ΔP between the inner and the outer phases, i.e., the liquid and the vapor phases [210, 211]. The curvature of the interface can be related to ΔP through the well known Young-Laplace equation:

$$\Delta P = \gamma \left(\frac{1}{R_1} + \frac{1}{R_2} \right) \tag{A.1}$$

where, R_1 and R_2 are the principal radii of curvature.

Figure A.1 schematically represents a pendant drop of pear-like shape. To describe the curvature of such a drop, we consider the apex of the drop, O $(x = 0, z = z_{\min})$ and an arbitrary point on the drop surface, Q (x, z). The axial symmetry of the drop allows to re-write (A.1) at O as:

$$\Delta P_{\mathrm{O}} = \frac{2\gamma}{R_o} \tag{A.2}$$

where, $R_0 = R_1 = R_2$. At Q (x, z), however, the original form of (A.1) retains, i.e.,

$$\Delta P_{\mathrm{Q}} = \gamma \left(\frac{1}{R_{\mathrm{Q}1}} + \frac{1}{R_{\mathrm{Q}2}} \right) \tag{A.3}$$

where, $R_{\mathrm{Q}1}$ and $R_{\mathrm{Q}2}$ are the principal radii of curvature at Q.

The difference of ΔP at points O and Q, i.e., $\Delta P_{\mathrm{O}} - \Delta P_{\mathrm{Q}}$ can also be realized from the hydro-mechanical equilibrium [212],

$$\Delta P_{\mathrm{O}} - \Delta P_{\mathrm{Q}} = \Delta \rho g z \tag{A.4}$$

where, $\Delta\rho$ is the density difference between the two phases, g is the gravitational acceleration, and $z = z_{\mathrm{Q}} - z_{\mathrm{O}}$. Combining (A.2), (A.3) and (A.4), one obtains:

$$\gamma \left(\frac{1}{R_{\mathrm{Q}1}} + \frac{1}{R_{\mathrm{Q}2}} \right) = \frac{2\gamma}{R_0} - \Delta \rho g z \tag{A.5}$$

The curvature at Q can be analytically expressed through differential geometry as [210, 213]:

$$\frac{1}{R_{\mathrm{Q}1}} = \frac{\eta_{xx}}{(1 + \eta_x^2)^{3/2}} = \frac{d\Phi}{ds}$$

and,

$$\frac{1}{R_{\mathrm{Q}2}} = \frac{\eta_x}{x\,(1 + \eta_x^2)^{1/2}} = \frac{\sin\Phi}{x}$$

where, Φ is the angle intersected by a tangent drawn at Q with the horizontal axis, x (see Fig. A.1), η defines the curved surface, the subscripts refer to the derivatives. With the above expressions for $R_{\mathrm{Q}1}$ and $R_{\mathrm{Q}2}$, (A.5) reduces to:

$$\frac{d\phi}{ds} = \frac{2}{R_0} - \frac{\Delta \rho g z}{\gamma} - \frac{\sin\Phi}{x} \tag{A.6}$$

Non-dimensionalizing (A.6) such that, $x = Xl_c, z = Zl_c, S = sl_c$ and, $R_0 = \xi l_c$, the Bashforth and Adams equation [214–217] is retrieved:

$$\frac{d\Phi}{dS} = \frac{2}{\xi} - Z - \frac{\sin\Phi}{X} \tag{A.7}$$

Here, $\xi = R_0 / \sqrt{\frac{\gamma}{\Delta\rho g}}$ is the shape parameter of the drop, and l_c is the capillary length, i.e., $l_c = \sqrt{\gamma/(\Delta\rho g)}$. By iterative techniques, ξ is varied to best-fit the pendant drop profile acquired through an image acquisition unit.

Uncertainties and the counter-measures:

Similar to any experimental method, it is not unusual that the pendant drop surface tension measurement technique that has been employed in this study, has its uncertainties. Despite confirming controlled and systematic experimentation, errors or uncertainties may arise from a number of sources, and are elaborated below along with their counter-measures.

Experimental uncertainties:

Dispensing an accurate volume of pendant drop for surface tension measurement is not barred of uncertainties. To properly address this, we have used computer controlled drop dispensing feature of DSA 100E [218] which ensures a resolution of $0.1\,\mu L$ with glass syringe.

The reproducibility of the data has been confirmed through repeated measurements and for each data points, the average of at-least four measurements has been reported in this study.

Instrumentation/data analysis error:

1. Proper focus: High quality and properly focused images of the pendant drop are essential so that the principal radii can be accurately measured [35, 219]. The Drop Shape Analyzer (DSA 100E, KR$\ddot{U}$SS GmbH) acquires the drop profile at 60 fps using CF04 camera (1920 × 1200 pixels) and its integrated image analysis software (ADVANCE) employs the measurement recipe at every time step to measure the surface tension of a pendant drop with a resolution of 0.01mN/m [218].

2. Droplet size: The size of the pendant drop should be small enough to ensure that surface tension dominates inertia. As a result, drops size should be maintained such that the Bond number, Bo (defined in Eq. A.8) is maintained below unity, i.e., $Bo < 1$. However, droplets with $Bo \to 0$ should be avoided in surface tension measurements since they might result into fitting problems [35, 219]. For the present study, the Bo is maintained within the range of $0.5 - 0.7$.

$$\mathrm{Bo} = \frac{\Delta\rho g R_o^2}{\gamma} \tag{A.8}$$

3. Noise factors: Unwanted vibrations and air current [35] from the surroundings may often lead to an angular variation of the drop from the plane of symmetry resulting in inaccuracies in the measurements. To mitigate such uncertainties, the drop shape analyser was placed on an anti-vibration table, and the drop was generated in a sealed cuvette.

4. Uncertainties in liquid density: The accuracy of density difference ($\Delta\rho$) of the drop liquid, ρ_l and the surrounding vapor, ρ_v, effects the measurement of surface tension.

The surface tension data can be regarded as of higher precision if the Worthington number, W_o is closer to unity [35]. For a droplet of volume V and needle diameter ϕ, W_o is defined in Eq. A.9 and scales from 0 to 1.

$$\mathrm{W_o} = \frac{\Delta\rho g V}{\pi\gamma\phi} \tag{A.9}$$

As shown in Table A.5, W_o obtained from current experiments advocates for higher precision of our measurements.

Table A.5: Measurement of W_o for water-methanol (polar-polar), ethanol-pentane (polar-non polar) and hexadecane-pentane (non polar - non polar).

properties	water–methanol	ethanol–pentane	hexadecane–pentane
$\rho_l(kg/m^3)$	997	789	769
$\rho_v(kg/m^3)$	0.215	3.0	3.0
$V(\mu L)$	24	11	14
$\gamma(mN/m)$	42.25	18.76	21.68
W_o	0.97	0.79	0.85

A.3 Theoretical Models for Prediction of Interfacial Tension

Few key models for the prediction of interfacial tension of binary phases from their individual surface tensions are briefly discussed in subsequent sections.

A.3.1 Berthelot's combining rule

Berthelot's mixing [142] suggests work of adhesion, W_{12} between two phases is solely based on London theory of dispersion forces and it can be accurately quantified by the geometric mean of work of cohesion in phase 1 (W_{11}) and phase 2 (W_{22}) as:

$$W_{12} = \sqrt{W_{11}W_{22}} \tag{A.10}$$

Here, $W_{11}= 2\gamma_{1\mathrm{v}}$ and $W_{22}= 2\gamma_{2\mathrm{v}}$, with $\gamma_{1\mathrm{v}}$ and $\gamma_{2\mathrm{v}}$ denoting the surface tension of the individual phases. Later, Dupre defined that the amount of reversible work required for the separation of an interface to form two new surfaces is dependent on the interfacial tension, γ_{12} of the two contacting phases [143].

$$W_{12} = \gamma_{1\mathrm{v}} + \gamma_{2\mathrm{v}} - \gamma_{12} \tag{A.11}$$

Combining Eqs. (A.10) and (A.11) one obtains [142, 144, 145]:

$$\gamma_{12} = \gamma_{1\mathrm{v}} + \gamma_{2\mathrm{v}} - 2\sqrt{\gamma_{1\mathrm{v}}\gamma_{2\mathrm{v}}} \tag{A.12}$$

A.3.2 Antonow's rule

Antonow proposed that surface free energy is the result of the broken bond at surface, which must be balanced by the formation of new bonds between two contacting, immiscible phases. This resulted into the development of the following simple empirical relation, as shown in Eq. A.13 [75, 147, 148].

$$\gamma_{12} = |\gamma_{1\mathrm{v}} - \gamma_{2\mathrm{v}}| \tag{A.13}$$

A.3.3 Good and Girifalco's rule

Girifalco and Good [3] utilized Berthelot's mixing rule and extended similar concept as Berthelot which accurately relates the interfacial tension of two contacting phases (consisting of similar molecules) to their individual surface tension [142]. However, for cases where predominant forces are different between the contacting phases, a considerable deviation occurs from the estimated interfacial interaction. To address this, Girifalco and Good introduced a factor ϕ in Eq. (A.12) as:

$$\gamma_{12} = \gamma_{1\mathrm{v}} + \gamma_{2\mathrm{v}} - 2\phi\sqrt{\gamma_{1\mathrm{v}}\gamma_{2\mathrm{v}}} \tag{A.14}$$

Girifalco and Good defined ϕ as the ratio of the adhesive and the cohesive energy for the two contacting phases. The value of ϕ varies depending on the predominant forces in the individual phases, which has been evaluated elsewhere [3]. If the forces are of different types, $\phi < 1$, whereas it can assume values larger than unity for some cases where interactions between the phases are very strong.

A.3.4 Fowkes' rule

Fowkes [2], for the first time, decomposed the surface tension of two involved phases into polar and dispersive components. He proposed that polar (permanent dipole-permanent dipole and permanent dipole-induced dipole) and dispersive components (induced dipole- induced dipole) are the only parameters that influence surface tension $\gamma_{1\mathrm{v}}$ or $\gamma_{2\mathrm{v}}$.

While proposing the relation for interfacial tension, Fowkes utilized similar method as Good and Girifalco. In his theory, the geometric mean has been specifically applied to the dispersive interaction, provided at least one phase is completely nonpolar. Expressed mathematically,

$$\gamma_{12} = \gamma_{1\mathrm{v}} + \gamma_{2\mathrm{v}} - 2\sqrt{\gamma_{1\mathrm{v}}^{d}\gamma_{2\mathrm{v}}^{d}} \tag{A.15}$$

where, γ^{d} and γ^{p} are dispersive and polar components of surface tensions and $\gamma^{\mathrm{d}}+\gamma^{\mathrm{p}} = \gamma$.

A.3.5 Wu's rule

The inter-molecular forces responsible for polar-polar interaction are permanent dipole-permanent dipole and permanent dipole- induced dipole, out of which permanent dipole-permanent dipole plays the key role [15]. Wu proved by empirical methodology that even though induced dipole-induced dipole interaction can be accurately quantified by geometric mean relation, it cannot accurately represent polar interactions. Hence, the harmonic mean was proposed [4]:

$$\gamma_{12} = \gamma_{1\mathrm{v}} + \gamma_{2\mathrm{v}} - \frac{4\gamma_{1\mathrm{v}}^{d}\gamma_{2\mathrm{v}}^{d}}{\gamma_{1\mathrm{v}}^{d} + \gamma_{2\mathrm{v}}^{d}} - \frac{4\gamma_{1\mathrm{v}}^{p}\gamma_{2\mathrm{v}}^{p}}{\gamma_{1\mathrm{v}}^{p} + \gamma_{2\mathrm{v}}^{p}} \tag{A.16}$$

This expression has been validated for insoluble cases, provided the polarizabilities are nearly equal.

A.3.6 Van Oss's rule

In around 1984, Chaudhury proposed that all the van der waal's interaction are additive and can be represented accurately by a single quantity [220]. Thus, to accurately quantify polar interactions such as that in acid-base (where applicable), the electron acceptor and electron donor approach has been used [145]. In this theory, surface tension has been decomposed to Lifshtiz van der Waals component (consisting of London, Keesom and Debye forces) and short range or Lewis acid-base component [150].

$$\gamma = \gamma^{LW} + \gamma^{SR} \tag{A.17}$$

where γ= surface tension of a phase, γ^{LW} is Lifshtiz or dispersive component and γ^{SR} is short range or polar component which is represented by product of electron donor (γ^{-}) and electron acceptor (γ^{+}) parameters: $\gamma^{SR} = 2\sqrt{\gamma^{+}\gamma^{-}}$.

While deveoping this theory, Van Oss, Good, and Chaudhury pinpointed the asymmetrical interaction between Lewis acid-base groups. This difference arises because electron-donor and electron-acceptor parameters vary for a given phase, which has an impact on the interfacial interaction. Thus to accommodate all the variables, interaction between electron acceptor of phase 1 (γ_{1v}^{+}) and electron donor of phase 2 (γ_{2v}^{-}) as well as interaction between electron donor of phase 1 (γ_{1v}^{-}) and electron acceptor of phase 2 (γ_{2v}^{+}) are considered separately. Based on these, the interfacial tension between two phases can be provided by:

$$\gamma_{12} = \gamma_{1v} + \gamma_{2v} - 2[(\sqrt{\gamma_{1v}^{LW}\gamma_{2v}^{LW}}) + (\sqrt{\gamma_{1v}^{+}\gamma_{2v}^{-}}) + (\sqrt{\gamma_{1v}^{-}\gamma_{2v}^{+}})] \tag{A.18}$$

This method is well established for cases where the interactions between two phases are not limited to the Van der Waals forces.

A.4 Surface Tension in Air Medium

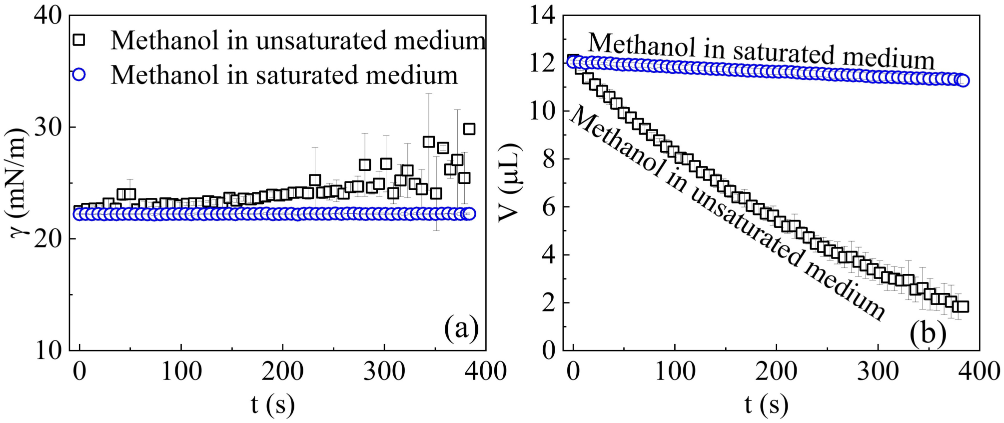

Figure A.2: Temporal variation of (a) surface tension, γ and (b) Volume, V for methanol in saturated methanol vapor (blue circle) and methanol in unsaturated air medium (black square).

Surface tension measurement of volatile liquids in air medium is very difficult due to high mass transfer rate at the surface. As seen from Fig. A.2 (a), the surface tension of methanol in unsaturated air medium (black square) does not reach an equilibrium value due to rapid decrease of pendant drop volume in Fig. A.2 (b). To mitigate this problem, the environment is saturated with methanol vapor to obtain an equilibrium mass transfer across the surface. Thus, an equilibrium result of the surface tension of methanol is obtained (blue circle).

A.5 Impact of Impurities on Surface Tension:

Surface active impurities are known to have effects on the interfacial properties, more specifically on the surface tension. Depending on the experimental procedure or objective of the study, these may exist at the interface either as impurities from the ambient, or as inherent impurity of the solvent itself. And in most cases, surface tension is decreased due to their presence [221, 222]. Furthermore, the concentration gradients of surface active impurities at the surface results in gradients of surface tension across the liquid-vapor interface causing soluto-capillary flows [223–225]. Therefore, for any experimental study concerning surface tension and contact angles, it is essential to conduct measurements in a controlled environment to avoid any possible contamination of the liquids as well as to minimize impurities from ambient. Additionally, observing the dynamic behaviour of surface tension is crucial [221].

To minimize the above mentioned uncertainties, all measurements reported in this study were carried out in a controlled environment. The variation of surface tension over time was measured until a plateau was reached. Since the impurities inherent in the solvent were not known, average of repeated measurements [226] (with a maximum deviation of $\pm 0.5\,mN/m$) was compared to available literature of pure liquids which shows good agreement. This confirms that any impurity that may have existed were not surface active and hence precludes any concern.

A.6 Equilibrium Surface Tension of Binary Combinations

Several experiments are conducted to obtain a generalised relations between γ_{eq} and polar and dispersive components of surface tensioon of both the liquid and the medium. The temperature was maintained at $22 \pm 2°\text{C}$ and repeated three-four times. The combinations used are: polar–polar, polar–nonpolar and nonpolar–nonpolar. The experimental results are provided in Table. A.6.

Table A.6: Experimental results of equilibrium surface tension, γ_{eq} for polar-polar, polar-nonpolar and nonpolar-nonpolar combinations along with their miscibility.

Chemical 1	Chemical 2	$\gamma_{\text{eq,(drop−medium)}}$ (mN/m) $\gamma_{\text{eq,(1−2)}}$	 $\gamma_{\text{eq,(2−1)}}$	Solubility (g/L)
		Polar-polar		
Water	Methanol	42.25 ± 0.39	39.41 ± 1.94	miscible
Water	Ethanol	36.81 ± 0.57	34.73 ± 2.51	miscible
Water	Butanol	29.82 ± 0.23	25.67 ± 0.26	immiscible
Water	Pentanol	26.16 ± 0.34	24.67 ± 0.41	immiscible
Ethanol	Methanol	21.71 ± 0.05	22.23 ± 0.12	miscible
Butanol	Methanol	23.21 ± 0.04	22.25 ± 0.20	miscible
Pentanol	Methanol	23.63 ± 0.03	22.23 ± 0.16	miscible
Butanol	Ethanol	23.29 ± 0.08	22.60 ± 0.27	miscible
Pentanol	Ethanol	23.77 ± 0.03	22.21 ± 0.02	miscible
Pentane-1,5-diol	Pentanol	35.24 ± 0.30	–	miscible
		Polar-nonpolar		
Methanol	Pentane	18.83 ± 0.23	15.74 ± 0.10	immiscible
Ethanol	Pentane	18.76 ± 0.29	15.76 ± 0.09	miscible
Pentanol	Pentane	20.60 ± 0.31	16.01 ± 0.17	miscible
Methanol	Hexane	20.79 ± 0.08	18.05 ± 0.01	immiscible

Continued on next page

Table A.6 – continued from previous page

Chemical 1	Chemical 2	$\gamma_{\mathrm{eq,(drop-medium)}}$ (mN/m)		Solubility (g/L)
		$\gamma_{\mathrm{eq,(1-2)}}$	$\gamma_{\mathrm{eq,(2-1)}}$	
Ethanol	Hexane	20.17 ± 0.08	17.97 ± 0.12	miscible
Butanol	Hexane	21.84 ± 0.09	18.49 ± 0.15	miscible
Pentanol	Hexane	21.67 ± 0.38	18.37 ± 0.14	miscible
Methanol	Heptane	21.64 ± 0.35	19.25 ± 0.08	immiscible
Ethanol	Heptane	20.19 ± 0.21	18.40 ± 0.48	miscible
Ethanol	Octane	21.26 ± 0.26	20.56 ± 0.05	miscible
Ethanol	Iso-octane	20.56 ± 0.25	17.84 ± 0.18	miscible
		Nonpolar-nonpolar		
Pentane	Heptane	21.26 ± 0.26	18.21 ± 0.05	miscible
Pentane	Hexadecane	15.51 ± 0.50	21.68 ± 0.18	miscible
Hexane	Heptane	18.28 ± 0.26	18.92 ± 0.18	miscible
Hexane	Octane	18.37 ± 0.28	19.93 ± 0.48	miscible
Hexane	Iso-octane	18.25 ± 0.16	18.10 ± 0.18	miscible
Hexane	Decane	18.03 ± 0.52	21.09 ± 0.18	miscible
Hexane	Dodecane	18.12 ± 0.11	21.45 ± 0.18	miscible
Heptane	Octane	19.88 ± 0.17	20.33 ± 0.17	miscible
Heptane	Iso-octane	19.18 ± 0.18	18.58 ± 0.05	miscible
Heptane	Nonane	19.88 ± 0.19	21.52 ± 0.12	miscible
Heptane	Decane	19.85 ± 0.13	21.17 ± 0.15	miscible
Heptane	Dodecane	19.71 ± 0.58	22.38 ± 0.07	miscible
Heptane	Hexadecane	19.58 ± 0.67	23.56 ± 0.33	miscible
Heptane	Butyl acetate	19.66 ± 0.11	23.36 ± 0.26	miscible
Octane	Iso-octane	19.96 ± 0.02	18.53 ± 0.22	miscible
Octane	Dodecane	23.77 ± 0.06	20.30 ± 0.16	miscible

Continued on next page

Table A.6 – continued from previous page

Chemical 1	Chemical 2	$\gamma_{\mathrm{eq,(drop-medium)}}$ (mN/m)		Solubility (g/L)
		$\gamma_{\mathrm{eq,(1-2)}}$	$\gamma_{\mathrm{eq,(2-1)}}$	
Octane	Hexadecane	20.84 ± 0.13	24.70 ± 0.49	miscible
Iso-octane	Dodecane	18.26 ± 0.45	22.24 ± 0.01	miscible
Iso-octane	Hexadecane	18.24 ± 0.26	22.92 ± 0.27	miscible

A.7 Dependence of Equilibrium Surface Tension on Molecular Weight, Polar and Dispersive Components

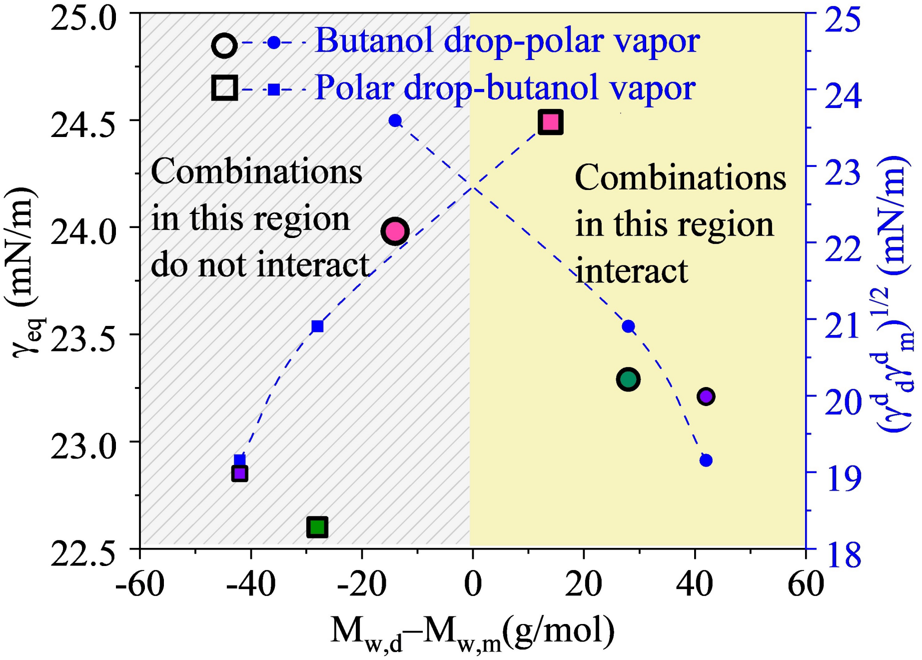

Figure A.3: Experimental results of γ_{eq} for butanol-polar amphiphile as a function of difference between molecular weight of drop and medium ($M_{w(d)} - M_{w(m)}$) (open symbols). The right hand axis denotes interaction of γ^d of liquid-vapor system depending on their molecular weight (filled symbol). Individual γ^d are obtained from the experimental values by Jańczuk *et al.* [8]. The circles represents butanol drop in alcohol vapor and the squares represent alcohol drop in butanol vapor. The alcohols are: pentanol (pink), ethanol (green) and methanol (purple).

A.8 Dependence of Equilibrium Surface Tension on Fowkes Interaction

Fowkes interactions does not consider the influence of polar components of surface tension on the dispersive-dispersive interaction. For (a) polar-polar combinations, $(\gamma_d^p \gamma_m^p)^{1/2} \neq 0$, while for (b) nonpolar-nonpolar combination $(\gamma_d^p \gamma_m^p)^{1/2} = 0$. Both of these cases correctly portrays the presence of γ^p in either of the fluids. On the contrary, (c) polar-nonpolar combination fails to represent the presence of polar surface tension component of the drop, which has influence on the overall interaction at surface. Thus, the experimental results for γ_{eq} fails to follow a trend for this case. The nonpolar drop- polar medium combination does not portray any activity on surface and the experimental γ_{eq} represents the surface tension of the drop, which also fails to portray a trend with Fowkes polar interaction.

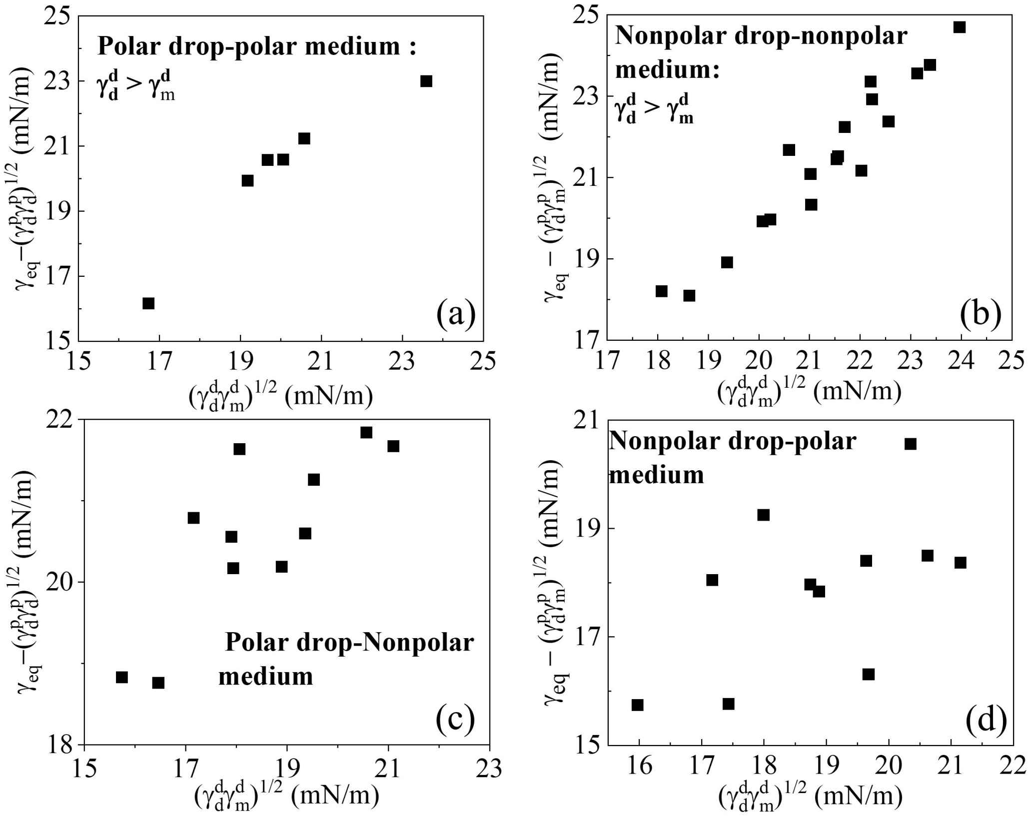

Figure A.4: Role of γ^p on γ_{eq} $[(\gamma_{eq} - (\gamma_d^p \gamma_m^p)^{1/2}]$ as a function of γ^d interaction suggested by Fowkes [2] $(\gamma_d^d \gamma_m^d)^{1/2}$ for all types of combinations: (a) polar drop-polar medium, (b) nonpolar drop-nonpolar medium, (c) polar drop-nonpolar medium and (d) nonpolar drop-polar medium.

A.9 Comparison of Equilibrium Surface Tension between Linear and Branched Structures

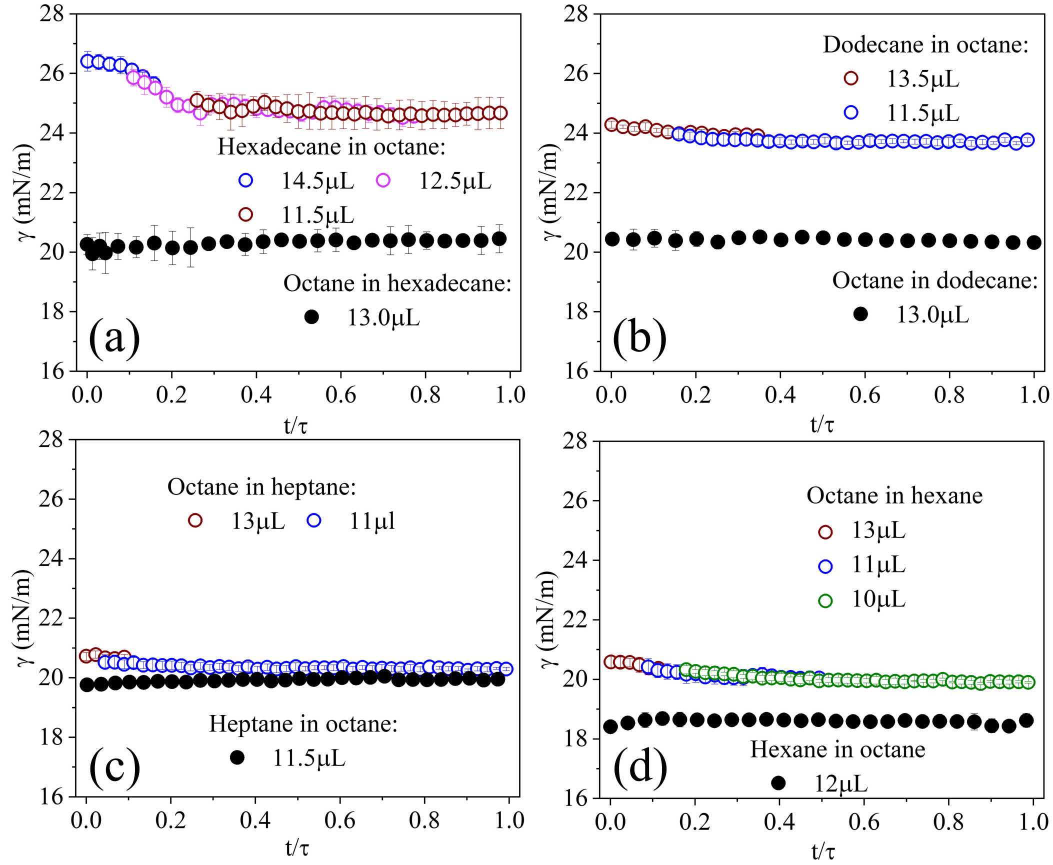

Figure A.5: Temporal variation of surface tension for combinations of octane with different linear alkanes. (a) Hexadecane drop in saturated octane vapor (open circle) and octane drop in saturated hexadecane vapor (filled circle); (b) Dodecane drop in saturated octane vapor (open circle) and octane drop in saturated dodecane vapor (filled circle); (c) Heptane drop in saturated octane vapor (filled circle) and octane drop in saturated heptane vapor (open circle); (d) Hexane drop in saturated octane vapor (filled circle) and octane drop in saturated hexane vapor (open circle).

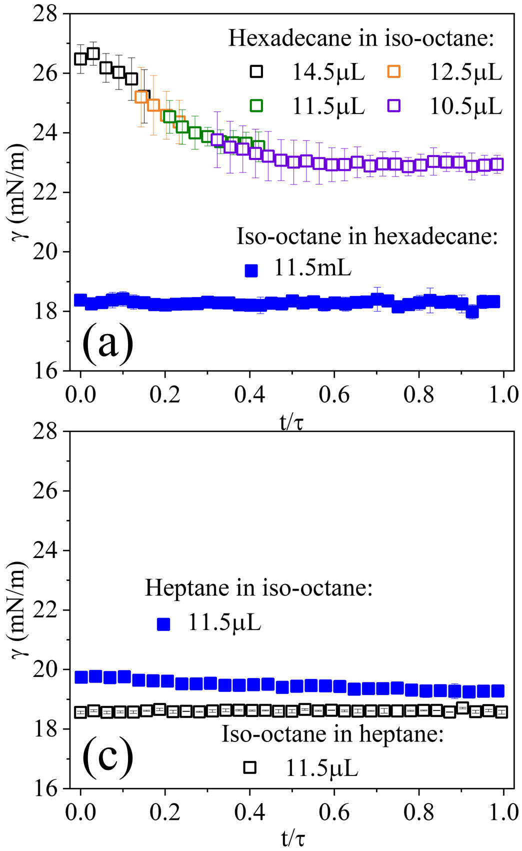

Figure A.6: Temporal variation of surface tension for combinations of iso-octane with different linear alkanes. (a) Hexadecane drop in saturated iso-octane vapor (open square) and iso-octane drop in saturated hexadecane vapor (filled square); (b) Dodecane drop in saturated iso-octane vapor (open square) and iso-octane drop in saturated dodecane vapor (filled square); (c) Heptane drop in saturated iso-octane vapor (filled square) and iso-octane drop in saturated heptane vapor (open square); (d) Hexane drop in saturated iso-octane vapor (filled square) and iso-octane drop in saturated hexane vapor (open square).

A.10 Contact Angles

Contact angle represents the wetting behaviour of a sessile drop on a solid substrate. This is the angle that forms at the triple point (measured inside the liquid phase) where the liquid and vapor phases meet the solid substrate, see Fig. A.7. The equilibrium contact angle is associated with the mechanical equilibrium of the interfacial forces acting at the triple point. As shown in Fig. A.7 (a),

$$\gamma_{\mathrm{lv}}\cos\theta = \gamma_{\mathrm{sv}} - \gamma_{\mathrm{sl}} \tag{A.19}$$

Here, γ_{lv}, γ_{sv} and γ_{sl} denote, respectively, the interfacial tension at the liquid-vapor, solid-vapor and solid-liquid interfaces, θ is the static contatc angle, or the Young‘s contact angle, and (A.19) is known as the Young‘s equation.

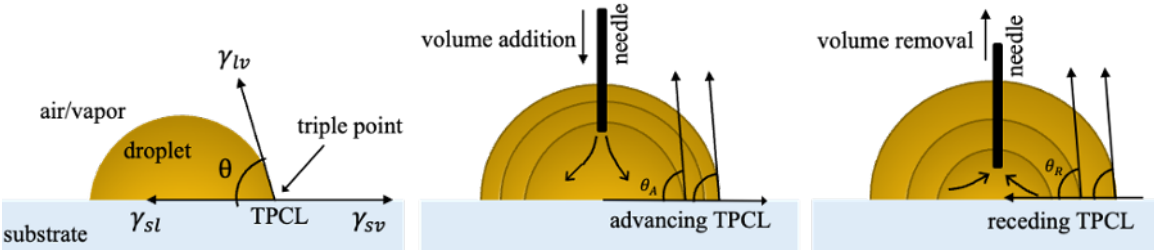

Figure A.7: Schematic representation of contact angles fromed by a liquid drop on a substrate, (a) static contact angle (b) advancing contact angle, and (c) receding contact angle. TPCL denote the three phase contact line.

The young's static contact angle, however, does not sufficiently characterize a substrate's wetting property. Rather, a number of meta-stable states are often observed depending on whether the liquid is expanding (wetting) or contracting (de-wetting) on the substrate. If the three phase contact line is in motion relative to the surface, the contact angle is characterized as dynamic contact angle [227, 228]. Based on wetting or de-wetting, dynamic contact angles are characterized as advancing and receding contact angles.

Advancing and receding contact anlges: During wetting process, the contact area of a droplet with the solid substrate (the base area of the drop) increases. Stated differently, and as in Fig. A.7 (b), when the volume of a droplet resting on a substrate is increased, the three-phase contact line advances to the dry surface [227]. The contact angle measured under such condition is referred to as the advancing contact angle, θ_A. This of often preferred to the static contact angle, as θ_A is measured at a surface just wetted in the dynamic wetting process and thus the effects of localized inhomogeneities of the substrate and any possible effect of evaporation are minimized. Conversely, during de-wetting process, or when liquid is continuously withdrawn from a sessile drop, the three phase contact line recedes. The contact angle measured during this process is called receding contact angle, θ_R as seen in Fig. A.7 (c). The advancing contact angle approaches a maximum, and the receding contact angle approaches a minimum [228], and between these two limits, there exist contact angles of the numerous meta-stable states [228, 229].

Contact angle hysteresis and experimental difficulties in measuring the Young's contact angle:

Although contact angle is a simple and easily quantifiable parameter to indicate the wettability of a surface, it has measurement uncertainty associated with the meta-states of the drop. Such uncertainty is characterized by the contact angle hysteresis [230] which refers to the difference between the advancing and the receding angles, i.e., $\theta_H = \theta_A - \theta_R$. For a perfectly smooth surface, no such discrepancy is expected [227].

In practice, however, contact angle hysteresis is a very common phenomenon [231, 232] and the equilibrium contact angle measurements are barely devoid of variations [232, 233]. The reason lies in, but not limited to, the surface roughness, surface chemical heterogeneity, adsorption and desorption, swelling and penetration, surface deformation, surface-configuration and molecular level topogray, charge of surface molecules. [234–236]. Experimentally methods of contact angle measurement usually deploys optical techniques with a viewing magnification scale much higher than the surface asperities and molecular level topography [77]. As such, deviations from the 'true' or Young's contact angle are unavoidable, and hence are often referred to as the apparent contact angle.

In this thesis, in line with numerous experimental studies in the literature [12–14, 197–207], by 'contact angle' we refer to the 'apparent contact angle' which is reasonably adequate to serve the objectives of our study without any loss of generality. However, appropriate care has been taken to ensure that the external effects are minimized. For example, the contact angle measurements were done in a controlled environment and on pristine substrates. Moreover, the process with which the substrates were prepared (piranha cleaning, physical vapor deposition and smooth functionalization) eliminates the micro-scale roughness. Also, some of the samples were randomly discharged using an ionizer, but no significant change was observed in the results. To smear out the variation of the contact angle due to any possible evaporative flux or localized surface imperfections, multiple measurements were taken and the average of these values are reported.

A.11 Theoretical models for measuring surface energy of a solid

There are various theoretical models, other than OWRK, that have been developed over time to quantify the relation between contact angle and different parameters of surface tension, which are described briefly in this portion:

Zisman's method: This method utilizes the concept of critical surface tension to measure the surface energy of a solid. The successful development of this method is based on the spreading pressure, S_{sl} which is given by: [70].

$$S_{SL} = W_{SL} - W_{LL} \tag{A.20}$$

Here, W_{SL}= work of adhesion between solid and liquids and W_{LL}= work of cohesion between liquid molecules. Elaborately, a liquid spreads completely on a solid if the work of cohesion between the individual phases is less than the work of adhesion between two phases [1], i.e, S_{SL} is positive for complete wetting of a solid by a liquid. So, a liquid just spreads on a solid, with $\theta = 0$ if the forces of adhesion is equal to forces of cohesion [73, 142, 143]. That means the limiting value of S_{SL} is equal to zero at $\cos\theta = 1$. The surface tension of a liquid that provides $S_{SL} = 0$ with a solid is known as the critical surface tension, γ_c of that solid [70]. This γ_c is equal to the surface energy of the solid.
To obtain the γ_c, the contact angle measurements of a number of liquids are plotted on a $\cos\theta$ versus γ_{LV} graph for a specific solid. According to Zisman's, the intercept of this graph at $\cos\theta = 1$ gives γ_c, i.e., surface energy of the solid. This method is limited to cases where both the solid and the liquid are completely dispersive, which is not very feasible.

Neumann's equation of state: Neumann, Good, Hope, and Sejpal developed this method to estimate the surface energy of a solid with ease. This equation was developed empirically by considering thermodynamic stability and utilizing a large amount of contact angle data with different solid-liquid combinations. Hence, it is proper to assume that this relation is valid for all possible systems. With a constant $\beta = 0.0001247$, that has been determined empirically, the equation is:

$$\gamma_{SL} = \gamma_{SV} + \gamma_{LV} - 2\sqrt{\gamma_{SV}\gamma_{LV}}e^{-\beta((\gamma_{LV}-\gamma_{SV}))^2} \tag{A.21}$$

In combination with Young's equation, this equation can be modified to:

$$cos\theta = -1 + 2\sqrt{\frac{\gamma_{SV}}{\gamma_{LV}}}e^{-\beta((\gamma_{LV}-\gamma_{SV}))^2} \tag{A.22}$$

From Eq. A.22, the surface tension or surface energy can be determined for an unknown liquid or solid, respectively. This equation does not consider the type of interaction between two phases, which implies that the decomposition of surface tension into polar and dispersive components is not necessary. On the contrary, it only needs contact angle data of only one combination to estimate the unknown surface energy/surface tension. Due to the absence of the effect of type of interaction, it is only valid for combinations where at least one phase is completely dispersive.

Fowkes' method: Although Fowkes' method [2], in combination with Young's equation [73] and Dupre's adhesion theory [143], relates contact angle with polar and dispersive components of the surface tension, it is not as much popular because the geometric mean for polar components are not present in Fowkes' mathematical model itself. In fact, Owens and Wendt, Rabel, Kaelble proposed that the interaction between polar components can be explained by geometric mean [20–22]. However, there is slight difference between the two methods. OWRK uses linear regression model to calculate the components simultaneously. On the contrary, Fowkes method estimates surface energy in two steps. First of all, a complete dispersive interaction with a purely nonpolar liquid is utilized to calculate the dispersive component of surface energy. The combination of Fowkes' relation (Eq. A.15) and Young's equation (Eq. A.19) to determine the dispersive component is as follows [12]:

$$\sqrt{\gamma_{\mathrm{SV}}^{d}} = \frac{\sqrt{\gamma_{\mathrm{LV}}^{d}}(1 + cos\theta)}{2} \tag{A.23}$$

Here, γ_{SV}^{d} is dispersive component of solid surface energy and γ_{LV}^{d} is dispersive component of liquid surface tension. Secondly, a polar liquid is used to estimate polar component using the following relation, which is derived elsewhere [12]:

$$\gamma_{\mathrm{LV}}(1 + cos\theta) = 2\sqrt{\gamma_{\mathrm{SV}}^{d}\gamma_{\mathrm{LV}}^{d}} + 2\sqrt{\gamma_{\mathrm{SV}}^{p}\gamma_{\mathrm{LV}}^{p}} \tag{A.24}$$

Hence, the surface energy of the solid is calculated by $\gamma_{\mathrm{SV}}^{d} + \gamma_{\mathrm{SV}}^{p} = \gamma_{\mathrm{SV}}$.

Extended Fowkes' method: This method introduces another component of surface tension besides polar and dispersive, a component due to formation of hydrogen bond. This component is known as the hydrogen bridge fraction, which is used to further modify Eq. A.15 as follows [237]:

$$\gamma_{\mathrm{SL}} = \gamma_{\mathrm{SV}} + \gamma_{\mathrm{LV}} - 2\sqrt{\gamma_{\mathrm{SV}}^{d}\gamma_{\mathrm{LV}}^{d}} - 2\sqrt{\gamma_{\mathrm{SV}}^{p}\gamma_{\mathrm{LV}}^{p}} - 2\sqrt{\gamma_{\mathrm{SV}}^{h}\gamma_{\mathrm{LV}}^{h}} \tag{A.25}$$

where, γ_{SV}^{h} and γ_{LV}^{h} are hydrogen bond bridge fractions of surface tension for solid and liquid and $\gamma^{\mathrm{d}} + \gamma^{\mathrm{p}} + \gamma^{\mathrm{h}} = \gamma$.

Following the footsteps of the Fowkes' method, this calculation utilizes three liquids to calculate surface energy of solid in three steps. The first step is the same as before (Eq. A.23), where a completely nonpolar liquid is used to estimate the dispersive component of the surface energy of solid. In the second step, a liquid is chosen such that the hydrogen bridge fraction is zero ($\gamma_{\mathrm{LV}}^{h} = 0$), resulting into same relation as in Eq. A.24. For the final step, the contact angle of a third liquid of known polar, dispersive and hydrogen bridge fractions on the solid surface is measured. Although this theory provides a more accurate quantification for cases where hydrogen bond is applicable, it is not as popular as the other methods because it requires at least three liquids.

Wu's method: As mentioned in an earlier section, Wu utilized harmonic mean to quantify polar and dispersive interactions between two phases [4]. Theoretically, contact angle measurements of only two liquids of known polar and dispersive components of surface tension are sufficient to provide surface energy of a solid, provided at least one of the liquids is polar. Combining Wu's relation (Eq. A.16) and Young's equation (Eq. A.19) gives:

$$\gamma_{\mathrm{LV}}(cos\theta + 1) - \frac{4\gamma_{\mathrm{SV}}^{d}\gamma_{\mathrm{LV}}^{d}}{\gamma_{\mathrm{SV}}^{d} + \gamma_{\mathrm{LV}}^{d}} - \frac{4\gamma_{\mathrm{SV}}^{p}\gamma_{\mathrm{LV}}^{p}}{\gamma_{\mathrm{SV}}^{p} + \gamma_{\mathrm{LV}}^{p}} = 0 \tag{A.26}$$

By substituting the appropriate values of the two liquids, the polar and dispersive components of the solid surface energy can be obtained by solving two quadratic equations [238]. However, this imposes a probability of obtaining two values for each surface tension components, where only one represents the actual parameters. It is not a problem if one of the values has a negative sign as neither surface energy nor its components can be negative. The problem arises when all the estimates are positive. In that case, measurements with two other liquids can simplify this predicament by choosing the results that agree well with all the cases. The degree of accuracy that Wu's method does not justify the difficulties faced by using four liquids [6].

Schultz method: Schultz, Cazeneuve, Shanahan, and Donnet developed this method in 1981, which is still in use today to characterize surfaces of high-surface energy using contact angle measurement [239]. Measurement of contact angle on a high-energy solid is extremely difficult as all liquids spreads completely on them. To quantify the surface energy of such surfaces, a slight modification of the test environment proved to be the solution. Rather than performing the experiments in air medium, a surrounding immiscible liquid medium is used. This method modifies Young's equation (Eq. A.19) in terms of solid-liquid medium interfacial tension ($\gamma_{\mathrm{SL_m}}$), solid-liquid drop interfacial tension ($\gamma_{\mathrm{SL_d}}$), liquid drop-liquid medium interfacial tension ($\gamma_{\mathrm{L_dL_m}}$) and contact angle of liquid drop on solid surface (θ), where the subscripts S, $\mathrm{L_d}$ and $\mathrm{L_m}$ represents solid phase, liquid drop phase and liquid medium phase respectively [239].

$$\gamma_{\mathrm{SL_m}} = \gamma_{\mathrm{SL_d}} + \gamma_{\mathrm{L_dL_m}}\cos\theta \tag{A.27}$$

On the other hand, Fowkes' method [2] and OWRK method [20–22] are also modified for this special case, resulting into two equations:

$$\gamma_{\mathrm{SL_d}} = \gamma_{\mathrm{SV}} + \gamma_{\mathrm{L_dV}} - 2\sqrt{\gamma_{\mathrm{SV}}^{d}\gamma_{\mathrm{L_dV}}^{d}} - 2\sqrt{\gamma_{\mathrm{SV}}^{p}\gamma_{\mathrm{L_dV}}^{p}} \tag{A.28}$$

$$\gamma_{\mathrm{SL_m}} = \gamma_{\mathrm{SV}} + \gamma_{\mathrm{L_mV}} - 2\sqrt{\gamma_{\mathrm{SV}}^{d}\gamma_{\mathrm{L_mV}}^{d}} - 2\sqrt{\gamma_{\mathrm{SV}}^{p}\gamma_{\mathrm{L_mV}}^{p}} \tag{A.29}$$

Schultz method can be used in two ways as shown in Fig. A.8:

- single liquid drop (usually water) in variable liquid medium
- variable liquid drops in single liquid (usually water) medium

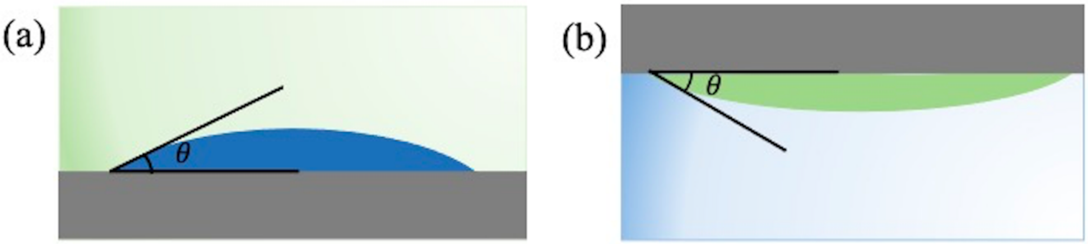

Figure A.8: Schematic for Schultz method: (a) water drop in variable liquid medium (b) variable drops in water medium

In the first method, a single liquid drop is generated in a range of completely nonpolar liquid medium to remove the $\gamma^p_{\mathrm{L_m v}}$ term. Based on this, the substitution of Eq. A.28 and Eq. A.29 in Eq. A.27 gives:

$$\gamma_{\mathrm{L_d v}} - \gamma_{\mathrm{L_m v}} + \gamma_{\mathrm{L_d L_m}}\cos\theta = 2\sqrt{\gamma^d_{\mathrm{SV}}}\left(\sqrt{\gamma^d_{\mathrm{L_d v}}} - \sqrt{\gamma^d_{\mathrm{L_m v}}}\right) + 2\sqrt{\gamma^p_{\mathrm{SV}}\gamma^p_{\mathrm{L_d v}}} \tag{A.30}$$

Thus, using contact angle data for a range of dispersive liquid can be utilized to plot graph of $(\gamma_{\mathrm{L_d v}} - \gamma_{\mathrm{L_m v}} + \gamma_{\mathrm{L_d L_m}}\cos\theta)$ versus $\left(\sqrt{\gamma^d_{\mathrm{L_d v}}} - \sqrt{\gamma^d_{\mathrm{L_m v}}}\right)$, and the linear regression line provides γ^d_{SV} and γ^p_{SV} from the gradient and the intercept, respectively.
Similarly, for the second case, drops of variable dispersive liquids are generated in polar water medium to remove $\gamma^p_{\mathrm{L_d v}}$. This results into:

$$\gamma_{\mathrm{L_d v}} - \gamma_{\mathrm{L_m v}} + \gamma_{\mathrm{L_d L_m}}\cos\theta = 2\sqrt{\gamma^d_{\mathrm{SV}}}\left(\sqrt{\gamma^d_{\mathrm{L_d v}}} - \sqrt{\gamma^d_{\mathrm{L_m v}}}\right) + 2\sqrt{\gamma^p_{\mathrm{SV}}\gamma^p_{\mathrm{L_m v}}} \tag{A.31}$$

As before, the γ^d_{SV} and γ^p_{SV} are obtained from the gradient and the intercept of the linear regression line. The second method is usually preferred because a larger value of contact angle is observed that can be measured more accurately.

Van Oss method: As mentioned in an earlier section, this method considers that the dispersive component alone is accountable for all types of Van der Waals force, whereas the polar part represents the interaction between electron-donors and electron-acceptors [150, 220]. Hence, the contact angle data can be used to quantify the type of interactions by combining this relation and Young's theory [73], which results into:

$$\gamma_{\mathrm{LV}}(cos\theta + 1) = 2\left[\left(\sqrt{\gamma^{LW}_{\mathrm{1v}}\gamma^{LW}_{\mathrm{2v}}}\right) + \left(\sqrt{\gamma^{+}_{\mathrm{1v}}\gamma^{-}_{\mathrm{2v}}}\right) + \left(\sqrt{\gamma^{-}_{\mathrm{1v}}\gamma^{+}_{\mathrm{2v}}}\right)\right] \tag{A.32}$$

This method is usually preferred for highly polar surface, where interaction between electron-donor and electron-acceptor are prominent [14, 150]. However, it is rarely used as it requires at least three liquids of known polar and dispersive components to measure the surface energy of a surface. Out of these three liquids, at least two must have $\gamma^{+} > 0$ and $\gamma^{-} > 0$ and the other must have $\gamma^{+} = \gamma^{-}$. For the latter case, water is preferred as it has neutral value in LEWIS scale.

A.12 Functionalization by Self-Assembled Mono layers

The formation of SAM is divided into two steps [97]. First of all, the thiol head group consists sulfhydryl (–SH) moiety that forms covalent bond with gold (Au) surface,i.e. Au–S bond that allows them to be randomly adsorbed to the surface. Secondly, the thiols that are randomly adsorbed on the surface reorients themselves to form densely packed monolayer depending on the extent of Van der Waals forces between the lateral molecules [89, 108–110]. This interaction between adsorbed monolayers increases with increase in length of alkane chain, that extends from the surface with different tail groups at the end [89]. Therefore, the formation of stable and well organized SAM is an optimization between head group-substrate bond and inter-molecular interaction between parallel molecules.

Effect of head group

The interaction between solid surface and the functional head group of the chemical is considered as the driving force for the formation of SAM [97, 240]. For thiol SAM on gold surface, the energy corresponding to S−Au is very high [241] which encourages the interaction between gold and thiol molecules, resulting into the maximum possible adsorption. Considering the present investigation, all the molecules used consists of same head group, i.e, sulfhydryl (–SH) moiety. As a result, the interaction between the head-group and the gold surface does not contribute to the preference of adsorption in mixed SAM of PFDT- 11AUT, PFDT-11MUA, or PFDT-3MPA.

Effect of tail group

Characteristic of tail group also plays a role in case of mixed SAM [194, 195], the effect of which is observed for PFDT-11AUT. In case of 11AUT, the self assembled molecules do not limit themselves to monolayer due to the protonation of $-NH_2$. This results into formation of double layers with free thiols [194, 195]. Moreover, due to attainment of positive charge by the $-NH_2$ group, a repulsion force acts between the molecules of 11AUT. This further affects the adsorption of thiols with amine tail group on gold substrates [196]. To sum up, PFDT adsorption on the gold surface increases.

Effect of chain length

Due to head-group of all chemicals being similar, the inter-molecular forces between the lateral molecules has become more important to ensure increased surface coverage [240, 242]. This interaction is dependent on the van der Waals forces between the adjacent molecules, which increases with increasing chain length of the alkane part. The effect of increasing chain length is observed only for mixed SAM of PFDT-3MPA as all the other chemicals have same alkane chain length (C_{11}). A preference for adsorption of PFDT is observed for this combination, as represented by XPS data.

Effect of solvent

The effect on mixed SAM is only considerable when the chain length of the two constituents are similar [190]. For mixed SAM of PFDT-11MUA, it has been observed that adsorption of PFDT on gold surface is more compared to that of 11MUA. This could be attributed to the fact that PFDT is less soluble in ethanol, the solvent used to form solution, than 11MUA. Hence, it is more convenient to remove PFDT from the solution.

A.13 Molar ratio of functionalized substrates

Molar ratio of the functionalized substrates are calculated with the help of XPS measurement. First of all, the peak areas of respective chemical components are normalized using RSF values (Relative Sensitivity Factors). These normalized areas are then utilized to calculate the mole fractions of the mixed SAMs on the functionalized substrates. It has been observed that it is different than the mole fraction of mixed SAMs in the solution.

Table A.7: Normalized areas of mixed SAMs

$x_{solution}$	Integrated Area (F1s peak)	RSF F1s	Normalized Area (F1s)	Integrated Area (N1s/O1s peak)	RSF N1s/O1s	Normalized Area (N1s/O1s)
PFDT–3MPA						
0	486776.60	1	486776.60	5.00E-7	0.733	6.82E-08
0.2	155817.00	1	155817.00	5338.58	0.733	7283.19
0.4	179661.00	1	179661.00	35915.72	0.733	48998.26
0.6	160160.00	1	160160.00	84529.81	0.733	115320.34
0.8	11172.00	1	11172.00	15901.01	0.733	21693.05
1.0	0	1	0	28416.90	0.733	38767.94
PFDT–11MUA						
0	486776.60	1	486776.60	5.00E-7	0.733	6.82E-08
0.2	367983.96	1	367983.96	30513.03	0.733	41627.60
0.4	407876.68	1	407876.68	127908.39	0.733	174499.85
0.6	211057.12	1	211057.12	184467.07	0.733	251660.39
0.8	235520.66	1	235520.66	1288056.46	0.733	1757239.37
1.0	0	1	0	98268.00	0.733	134062.76
PFDT–11AUT						
0	486776.60	1	486776.60	5.00E-7	0.733	6.82E-08
0.2	169553.00	1	169553.00	2115.77	0.499	4240.01
0.4	173480.00	1	173480.00	5963.84	0.499	11951.59
0.6	41093.70	1	41093.70	5698.90	0.499	11420.63
0.8	16720.80	1	16720.80	3167.96	0.499	6348.61
1.0	0	1	0	4979.64	0.499	9979.24

Table A.8: Mole fraction of mixed SAMs on functionalized substrates

$x_{solution}$	Normalized Area (F1s)	Normalized Area (N1s/O1s)	Fraction of F1s	Fraction of O1s/N1s
		PFDT–3MPA		
0	486776.60	6.82E-08	1	1.401E-13
0.2	155817.00	7283.19	0.955	0.045
0.4	179661.00	48998.26	0.786	0.214
0.6	160160.00	115320.34	0.581	0.419
0.8	11172.00	21693.05	0.340	0.660
1.0	0	38767.94	0	1
		PFDT–11MUA		
0	486776.60	6.82E-08	1	1.401E-13
0.2	367983.96	41627.60	0.898	0.102
0.4	407876.68	174499.85	0.700	0.300
0.6	211057.12	251660.39	0.456	0.544
0.8	235520.66	1757239.37	0.118	0.882
1.0	0	134062.76	0	1
		PFDT–11AUT		
0	486776.60	6.82E-08	1	1.401E-13
0.2	169553.00	4240.01	0.975	0.024
0.4	173480.00	11951.59	0.936	0.064
0.6	41093.70	11420.63	0.783	0.217
0.8	16720.80	6348.61	0.725	0.275
1.0	0	9979.24	0	1